EXCITED STATE STUDIES OF PYRIMIDINE BASES AND RADIOSENSITIZING DRUGS BY LASER FLASH PHOTOLYSIS

A thesis submitted for the degree of Doctor of Philosophy

by

Anthony William Parker

Department of Chemistry,
University of Warwick

November, 1985

To my parents and Roya

They are ill discoverers that think there is no land, when they can see nothing but sea.

Francis Bacon (1561-1626)

Advancement of Learning, II, vii, 5.

ACKNOWLEDGEMENTS

I wish to express my sincere gratitude to my supervisor, Professor Terence J. Kemp, for his continued advice and encouragement throughout the course of this study.

My thanks are also due to Dr. Peter Wardman of the Gray Laboratory of the Cancer Research Campaign, Mount Vernon Hospital, Northwood, Middlesex, for his many contributing discussions, and to his wife, Ursula, for her kind hospitality during my visits to Mount Vernon.

I also thank the technical staff of the Department of Chemistry, University of Warwick, especially those from the electronic and mechanical workshops and Haydn Beaton for his help with some of the syntheses and purifications.

I am indebted to the S.E.R.C. and the Cancer Research Campaign for the financial support enabling this study to be made.

My thanks are extended to Mrs. Paula Keilthy, for her efficient typing of this thesis.

Finally, I wish to thank the people to whom this work is dedicated, my parents for all the help they have given me over the years of my education, and my fianceé, Roya, for all her encouragement.

ABSTRACT

The mechanism whereby radiosensitizing drugs act in the radiotherapeutic treatment of cancer is yet to be fully elucidated. The prevailing current view (the so-called charge sequestration model) is that cancer cell death is initiated by charge separation induced by the ionising radiation, yielding radical anions (of thymine) and cations (of guanine) in the DNA polymer chain. The radiosensitizer, by virtue of its electron-affinic properties, removes the electron from the (thymine) radical anion, thereby preventing charge recombination and allowing the radical cation to 'fix' the damage *via* secondary reactions. To date, most efforts to verify this model have involved the observation of various DNA radical ions by electron spin resonance and pulse radiolysis techniques. However, excited states of DNA or the drug, as well as radical ions, may be involved in the sensitizing action, and there have been a variety of laser flash photolysis studies of reaction between the excited radiosensitizer and ground state nucleic acid bases. The main body of this thesis (Chapter 3) has been to determine, using 249 nm laser flash photolysis, whether reaction in solution occurs between triplet excited nucleic acid bases (in particular thymine and uracil) and (ground state) radiosensitizing drugs. (Such a study has only recently been made feasible by the development of powerful ultraviolet pulsed lasers which are able to produce measurable concentrations of these triplet states in solution; even so, monitoring systems are extended to their limits of detection.)

The triplet states of thymine and uracil (in acetonitrile) were quenched by a variety of electron acceptor molecules, including radiosensitizing drugs. The quenching kinetics correlated with the electron affinities of the electron acceptors according to the Weller equation for excited state electron transfer. This constitutes positive evidence that triplet DNA bases can produce the radical cations which are presumed to lead to cell death. Further, in certain cases, the radical anions of the acceptors were observed optically and their yields measured.

In Chapter 4 are presented studies of the triplet states of two radiosensitizing drugs, metronidazole and misonidazole (principally by laser flash photolysis), including measurements of their triplet energies. The reduction potentials of these drugs (in acetonitrile) were determined by three methods, which gave comparable results. Attempts were made to develop a fluorescent probe which could be used to measure intracellular concentrations of radiosensitizing drugs.

In Chapter 5, the efficient quenching of both excited uranyl ion and triplet benzophenone by nucleic acid bases is detailed. From the results it is concluded that for uranyl ion, the mode of quenching is by an exciplex or reversible charge transfer mechanism, while for triplet benzophenone, chemical quenching occurs. The appendices are mainly concerned with various computer-based techniques developed for this study. An original method is described for analysing oscilloscope transient decays by photographing the oscilloscope screen using a video camera and transferring and digitising the resulting image into a microcomputer screen ram area, where it is manipulated to yield the transient decay constant. Also given is a

computer program developed to enable optimum fitting of quenching data to the Weller equation, when the donor oxidation potential is unknown. Finally, evidence for the triplet state of 5-nitroindole is reported.

A part of this work has been published, *viz.* "Electron-transfer Quenching of Triplet State Thymine and Uracil", T.J. Kemp, A.W. Parker, and P. Wardman, *J. Chem. Soc., Chem. Commun.*, 1985, 1377.

ABBREVIATIONS

A	adenosine
AMP	adenine monophosphate
AMT	4-aminomethyl-4-5',8-trimethylpsoralen
BrU	5-bromouracil
C	cytosine
CMP	cytosine monophosphate
$^1\Delta E_{o,o}$	singlet excited state energy
$^3\Delta E_{o,o}$	triplet excited state energy
$\Delta G^{\ddagger}(O)$	intrinsic free energy barrier for self exchange reaction
$\Delta G^{\ddagger}$	intrinsic free energy barrier
ΔG^{0}	free energy change for a reaction
DNA	deoxyribonucleic acid
DPBO	diphenylbenzopyrylium oxide
DPIO	diphenylindenone oxide
e^-_{aq}	solvated electron
e.s.r.	electron spin resonance
ε	molar extinction coefficient
E.R.	enhancement ratio
G	guanosine
GMP	guanosine monophosphate
ic	internal conversion
isc	intersystem crossing
K_{SV}	Stern-Volmer constant
MeCN	acetonitrile (methyl cyanide)
MET	metronidazole

ABBREVIATIONS (Continued)

MIS	misonidazole
MQ	2-methylnaphthoquinone
MV^{2+}	methyl viologen (paraquat)
NHE	normal hydrogen electrode
PBA	1-pyrenebutanoic acid
ø	quantum yield
PNAP	*p*-nitroacetophenone
poly U	polyuridylic acid
Pyr	pyrimidine
q	quenching
r	radiative
s	sensitizer
SCE	saturated calomel electrode
T	thymine
τ	lifetime
TMP	thymine monophosphate
T-T	triplet-triplet
U	uracil
UMP	uracil monophosphate
u.v.	ultraviolet
vr	vibrational relaxation

CONTENTS

/Cont... ...

CONTENTS (Continued)

/cont... ...

CONTENTS (Continued)

List of Figures

List of Figures (Continued)

List of Figures (Continued)

List of Figures (Continued)

List of Tables

List of Tables (Continued)

CHAPTER 1

INTRODUCTION

1. Introduction

In cancer radiotherapy, electronically excited states of both nucleic acid bases and radiosensitizing drugs have been implicated as reactive intermediates capable of bringing about cancer cell death *via* damage to DNA. The main aim of the project summarised in this thesis is to investigate these claims by directly exciting each component using pulsed lasers.

Ionising radiation interacts with DNA to produce thymine^{-} and guanine^{+} radical ions. In the so-called "charge sequestration model" electroaffinic radiosensitizers are believed to prevent recombination of the charges, thus allowing the fixation of damage by further reactions of the radical cation. Triplet excited bases are also formed from ionising radiation, and it has been postulated that these may form additional base cations by acting as electron donors to the electron-affinic radiosensitizers. The theory of electron transfer reactions of excited states, due to Weller, and the closely related theory of electronic energy transfer are discussed in terms of excited state quenching rates. The radiation and photo-chemistry of nucleic acid bases are reviewed.

1.1 Radiotherapy

The fact that tissue originating from both normal cells and malignant tumours may be effectively killed by the action of ionising radiation forms the basis of the radiotherapeutic treatment of cancer. Its importance is illustrated by the statistic that as many as seventy per cent of all patients suffering from cancer will, at some stage of their treatment, receive radiotherapy. The technique of radiotherapy is mainly used for localised tumour deposits, the problem of metastasis being dealt with principally by systematic chemotherapy. It is not often realised that in

many types of cancer, particularly tumours of the brain, neck and cervix, inability to control the growth of the localised primary tumour is, in fact, a major cause of treatment failure. This local control of tumours can lead to curing of the patient, and this approach is referred to as radical radiotherapy.

1.2 The Effect of Ionising Radiation on Mammalian Cells

Radiation is said to be ionising if it has sufficient energy to remove electrons from atoms or molecules. In therapy, *X*- and γ-rays are the most commonly used forms, but charged particles (*e.g.*, electrons, neutrons, and α-particles) are also used. Unlike the absorption mechanism in photochemistry, where quanta of electromagnetic radiation are absorbed selectively by molecules, or even parts of molecules, this mechanism in ionising radiation chemistry arises principally from Coulombic interactions of fast charged particles with the medium. These fast particles can be electrons (by direct bombardment), secondary electrons (produced by the interaction of high energy photons with the medium), neutrons or α-particles which deposit their energy non-selectively, absorption depending, to a first approximation, only on the electron densities of the components of the medium. Thus solution radiation chemistry is governed by the chemistry of species produced from ionisation or excitation of the solvent, and the role of any solute is restricted to its chemical interaction with solvent-derived species such as ions, radicals and excited states.

Harmful biological effects, brought about by absorption of radiant energy by cellular tissue arise from early physico-chemical processes producing chemical damage to target sites, the most important acute effect being the destruction of the individual cancer cells. This cell killing is the end result of a series of fast processes (10^{-6} - 10^{-9} s) between radiation-induced, unstable, reactive free radicals and radiosensitive cellular targets.

The main component of biological cells is water, and hence the radiation chemistry of water[1,2] is of primary importance in explaining the biological effects of ionising radiation. The decomposition of water caused by ionising radiation takes place according to the overall process given in equation (1.1)

$$H_2O \xrightarrow{h\nu} {\cdot}OH,\quad H{\cdot},\quad e^-_{aq},\quad H_2,\quad H_2O_2 \qquad (1.1)$$

G-values 2.75, 0.65, 2.65, 0.45, 0.70

The reactive species responsible for initiating chemical effects consists of one oxidising entity, the ·OH radical, and two reducing entities, the hydrogen atom and the solvated electron. Hydrogen and hydrogen peroxide, the "molecular products" arise from fast primary recombination processes. The radical species ·OH and H· have a strong affinity for electrons or weakly-bonded hydrogen atoms. They are able to remove hydrogen atoms from organic molecules within the cell by breaking C-H, N-H or S-H bonds, equation (1.2)

$$e.g.,\qquad {\cdot}OH + RH \longrightarrow HOH + R{\cdot} \qquad (1.2)$$

The G-values quoted below equation (1.1) are the molecular yields for the species formed per 100 eV (1.6×10^{-11} J) of radiation absorbed.

1.3 The Oxygen Effect

Gray[3] in the 1950's found that irradiated tumour cells containing little oxygen (the so-called hypoxic cells) are particularly resistant to the effects of ionising irradiation. This decrease in response is illustrated in Figure (1.1). The relative radiosensitivity of cells increases rapidly between 0 and 0.3% oxygen, and further increases occur up to 30 mm of oxygen, after which additional increases in concentration have little effect. The sensitization of cells to ionising radiation is termed the oxygen enhancement ratio (ER) and defined as the ratio of doses of radiation to produce 50% target destruction in the absence and presence of sensitizer; normally ER has values between 2 and 3.5[4,5]

for the majority of cells.

Hypoxic cells are caused by disorganised cell proliferation within the tumour which rapidly outgrows the normal vascular oxygen supply. Normal intracellular oxygen concentration is greater than 3×10^{-3} mol dm^{-3}, whilst hypoxic cells have less than 10^{-6} mol dm^{-3}. The importance of these hypoxic cells is that when a patient is given radiotherapy treatment the hypoxic cells are not killed off completely and post-treatment[6,7] reactivation of the tumour growth leads to recurrence of the malignant disease.[8,9]

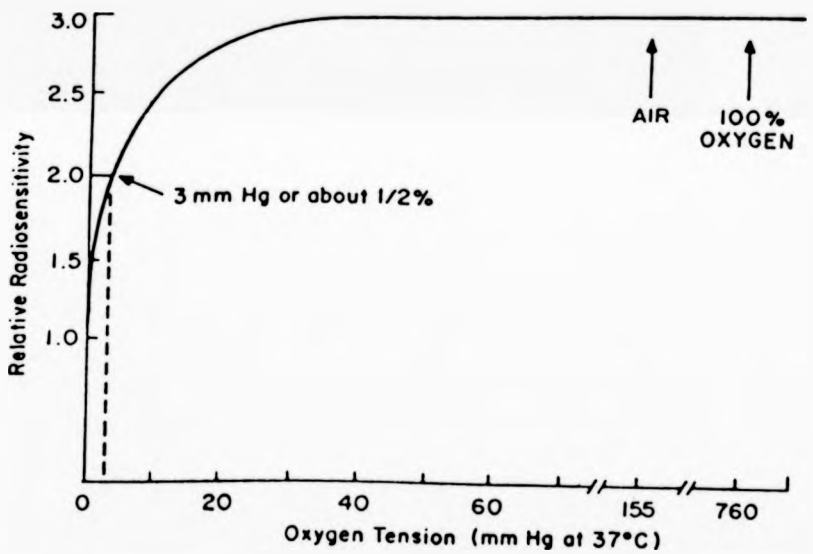

Figure 1.1 Illustration of the dependence of radiosensitivity on oxygen concentration. If the radiosensitivity under anoxic conditions is arbitrarily assigned a value of unity, the radiosensitivity is about 3 under well-oxygenated conditions. Most of this change of sensitivity occurs as the oxygen concentration increases from zero to 30 mm of mercury, further increases having little effect. This diagram is idealised and does not represent any specific experimental data. Experiments performed with yeast, bacteria and mammalian cells in culture: results conform to the general trends summarised. Taken from ref. .

Gray's[3] observations started a search for a drug which would "mimic" the effect of oxygen in tumour cells and hence enhance cell killing by irradiation; these drugs are known as radiosensitizers and are discussed later [see section (1.11.1)].

1.4 Target for Damage

The primary target for radiation-induced cell killing is believed to be the DNA molecule. A brief summary of the evidence for this, based on reference 10, is:-

i) Various elegant techniques have been used to irradiate either the nucleus or the cytoplasm preferentially. These have shown that the nucleus is 100 times more sensitive than the cytoplasm.

ii) The incorporation of certain species into DNA results in efficient cell killing, *e.g.*, [^{3}H]-thymidine or the pyrimidine analogue, 5-bromo-deoxyuridine (a radiosensitizing drug).

iii) Functional damage to DNA is detectable in the required dose range, whereas protein damage is not.

iv) Chromosome damage parallels lethality, and cell killing has been shown to be associated with structural damage to DNA (*e.g.*, by double strand breaks).

v) Increased radiation sensitivity is seen in cells from patients with DNA repair deficiencies.

1.5 The Structure of DNA

The most well-known feature of DNA is that it consists of two polynucleotide chains twisted in an antiparallel manner about a common axis, forming a double helix, see Figure (1.2). The backbone chain of DNA consists of a deoxyribose moiety linked *via* phosphodiester bonds; Figure (1.3) depicts the bonding pattern involved in the repeating deoxyphosphate structure. Attached to the 1'- position of each deoxyribose is a heterocyclic base; the four bases involved in DNA are shown in Figure (1.4) with a fifth base, uracil, found in RNA. The glycosylic bond is formed *via* the 1- position of the pyrimidines and the 9- position of the purines. The helical structure is formed *via* hydrogen bonding between base pairs. Each base specifically pairs with only one other base, thus guanine is paired to cytosine and thymine pairs with adenine, while in RNA, uracil replaces thymine and the ribose sugar is replaced by deoxyribose. The hydrogen bonding is illustrated in Figure (1.2). The terms nucleoside and nucleotide represent bases joined to a sugar group and a sugar phosphate group respectively.

1.6 Mechanism of Damage to DNA

Two mechanisms at the molecular level have been proposed to account for damage to DNA caused by ionising radiation.

1.6.1 The "Indirect" Mechanism

The three radicals produced from the radiolysis of water are all able to attack DNA components.[7,11,12] A summary of these processes is given below:-

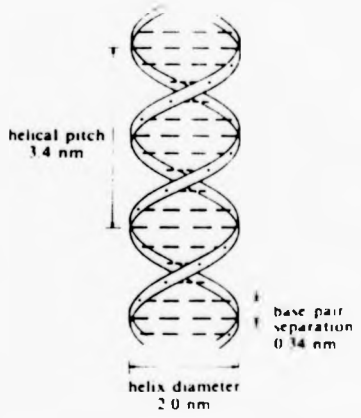

Figure 1.2 A section of the DNA double helix, illustrating the gross structure.

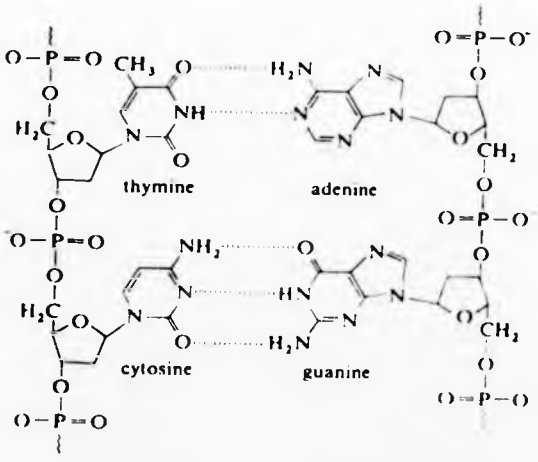

Figure 1.3 A segment of the DNA double helix, showing the hydrogen bonding between base pairs across the axis of the helix.

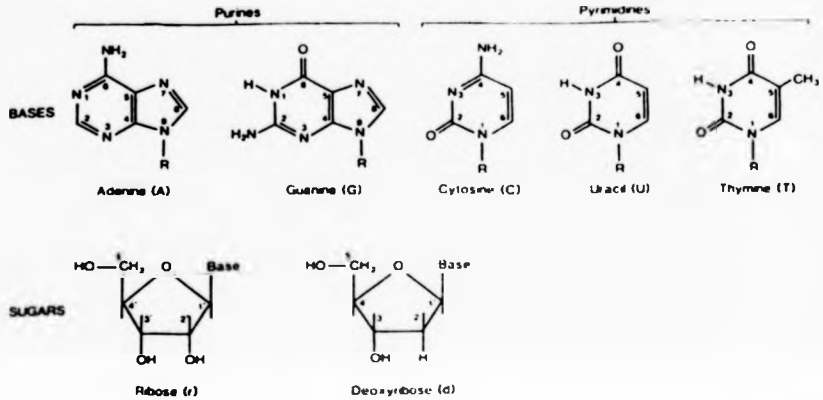

Figure 1.4 The structures of the normal base and sugar constituents of nucleic acids.

i) Abstraction from a C-H bond:

$$RH + \cdot OH(H) \longrightarrow R\cdot + H_2O(H_2)$$

ii) Electron transfer from guanine (G) derivatives:[13]

$$G + \cdot OH \longrightarrow G\cdot^{+} + OH^{-}$$

iii) Addition across a double bond, *e.g.*, to the 5,6-double bond of thymine[14]

$$R + (\cdot OH)(\cdot H) \longrightarrow ROH\cdot(RH\cdot)$$

iv) The solvated electron reacts by nucleophilic addition, *e.g.*, to carbonyl groups:

$$R + e^{-}_{aq} \longrightarrow R^{\cdot -} \xrightarrow{H^{+}} RH\cdot$$

The fate of these short-lived organic free radicals is crucial to the ultimate fate of the biomolecule, the main reactions being dimerisation, dismutation, oxidation and reduction.

The effect of oxygen is to increase cell damage by producing peroxy radicals:

$$R\cdot + O_2 \longrightarrow RO_2\cdot$$

These prevent restitution which may occur from reduction of a labile hydrogen-containing species, *i.e.*, thiols (such as tryptophan, cysteamine) and glutathione:[15]

$$R\cdot + R'SH \longrightarrow RH + R'S\cdot$$

Also, oxygen can combine with radicals produced by water radiolysis, forming a more stable hydroperoxyl radical or its basic form:

$$\cdot H + O_2 \longrightarrow HO_2\cdot$$

$$e^- + O_2 \longrightarrow O_2^{-\cdot}$$

This hydroperoxyl radical is more stable than the radical from which it was produced, yet is still capable of abstracting hydrogen atoms from organic molecules.

1.6.2 Structure of Radicals Formed from the Components of DNA

The free radicals produced from the reaction of the three primary radicals from water radiolysis with pyrimidines, purines, nucleosides, nucleotides and DNA itself have been studied by radiolysis, in particular pulse radiolysis and the following account of these reactions is based on references 11, 16-18.

i) Hydrogen atom addition

Single crystal e.s.r. investigations of guanine have shown hydrogen addition takes place at N-7 and C-8. This is also the major site of attack for adenine, although under certain conditions the N-1 and C-2 positions are attacked.

In the case of pyrimidines the 5-yl (1.I) or the 6-yl (1.II) radicals are formed, the former giving the well known octet e.s.r. spectrum. The 6-yl radical is preferred only if both C-5 and C-6 are bonded to hydrogen or if a non-hydrogen substituent (X) is present at C-6, this tending to

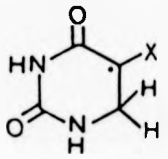

(1.I)

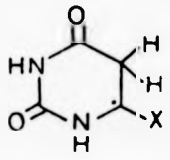

(1.II)

stabilise the radical by delocalisation of the spin. Addition of H-atoms to the exocyclic keto-oxygens has been observed for the pyrimidines but not for the carbonyl-containing purines, *e.g.*, guanosine.

ii) Hydrogen atom abstraction

The bases themselves may act as H-atom donors, as evinced by hydrogen addition products formed from γ-irradiating single anhydrous crystals of the bases.[19,20] For pyrimidines the N-1 position is the site of abstraction, whilst for purines no abstraction products have been observed.

Hydrogen atom abstraction also occurs from substituent groups of pyrimidines and purines, *e.g.*, from the methyl group of thymine and from N-methylated pyrimidines and purines, the spin density in both cases mostly residing at the site of H-loss.

The radical centre generated by H-atom abstraction may induce damage in the neighbourhood by abstracting hydrogen atoms from the aliphatic portions of the system, or it may add to the unsaturated parts of the neighbouring pyrimidine or purine bases.

iii) Reaction of hydroxyl radicals and solvated electrons

(a) Pyrimidines

The 5,6-alkene bond is the most important site of attack by free radicals. Irradiation of aqueous solutions of thymine gives:[21]

and, in the case of thymine, oxidation of the methyl group can also take place,[22] leading to the formation of 5-hydroxymethyluracil (1.III):

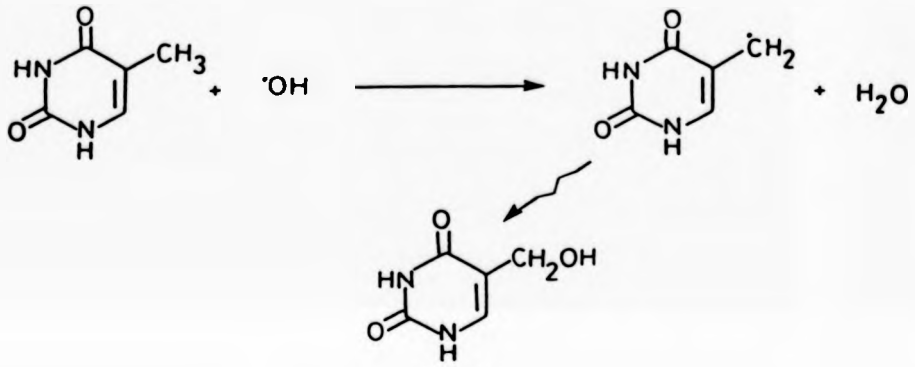

(1.III)

The latter reaction has been shown to be affected by pH.[17]

Damage of the pyrimidine bases by the solvated electron is not as significant because of competition with O_2 leading to the formation of the superoxide anion, equation (1.3)

$$T + e^-_{aq} \longrightarrow T^{-\cdot}$$

$$O_2 + e^-_{aq} \longrightarrow O_2^{-\cdot}$$

$$T^{-\cdot} + O_2 \longrightarrow O_2^{-\cdot} \qquad (1.3)$$

Evidence indicates that in equation (1.3) an intermediate is formed, equation (1.4):[23]

$$T^{-\cdot} + O_2 \longrightarrow TO_2^{-\cdot} \qquad (1.4)$$

the structure of which is based on the free electron being localised on the peroxyl substituent at C-6,[24] *i.e.*,

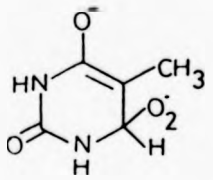

(b) Purines

Addition of ·OH to adenine is believed to take place at the central 4,5- bond.[21,25] In the case of guanosine monophosphate (GMP) reaction with ·OH produces a long lived species which, rather than an ·OH adduct, may be GMP^{+}· radical cation, formed from electron transfer to ·OH.[26]

There is no experimental evidence indicating the site of attack by solvated electrons in purines. Possibilities include N=C double bonds, carbonyl groups, and the central 4,5- linkage. Transient absorption spectra of the e^{-}_{aq} adducts of adenine and guanine have been observed.[27]

iii) Reactions with sugar moieties

Although attack of the three primary species is directed mostly towards the base moieties, a small amount is directed to attack of the sugar part of DNA. About 10-20% of the ·OH radicals are expected to react with the sugar entities, and although this seems a small amount, such damage results in DNA strand breakage causing local unzipping of the DNA chain and loss of hydrogen bonding and also leading to release of the base. Hydrogen atom abstraction from any position in the sugar moiety can lead to DNA strand breakage,[28,29] Scheme (1.1).

Of the three primary radicals produced from the radiolysis of water, the reaction of ·OH with DNA is up to four times faster than the other two.[30] Both base and sugar moieties are affected, the former being three times more susceptible to damage than the latter.[12] In the presence of oxygen the pyrimidines are more susceptible to damage by ·OH than the purines, because in the latter there are repairing back reactions.[31]

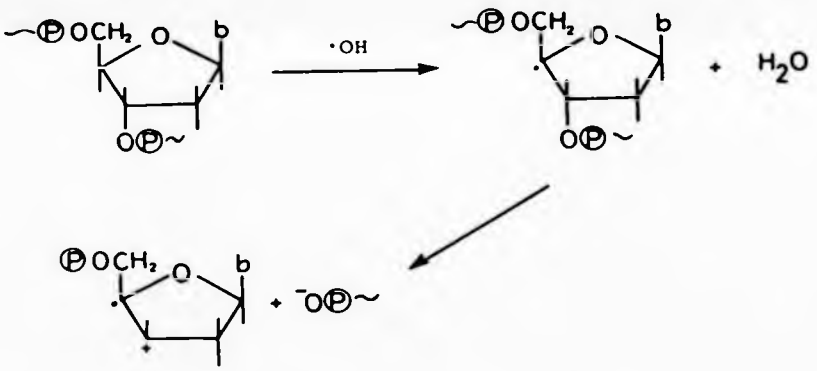

~Ⓟ = phosphate group; b = base

Scheme (1.1)

1.6.3 The "Direct" Mechanism

Direct production of DNA radicals can arise from the deposition of radiant energy in, or very close to, the target molecule. Adams and Cooke[32] propose a model whereby the DNA, by means of its electrical conducting properties, will allow electrons which are ejected by the ionisation process to be rapidly thermalised, migrating along the DNA chain to electron deficient centres. In competition with migration are charge recombination processes leading to harmless neutralisation of the excited species. Molecules with a high electron affinity, either bound to or associated with the DNA, *e.g.*, oxygen or some other radiosensitizer, may capture this thermal electron from DNA. If this process is followed by the loss of a proton from the site of ionisation then the DNA radical is formed, see Scheme (1.2).

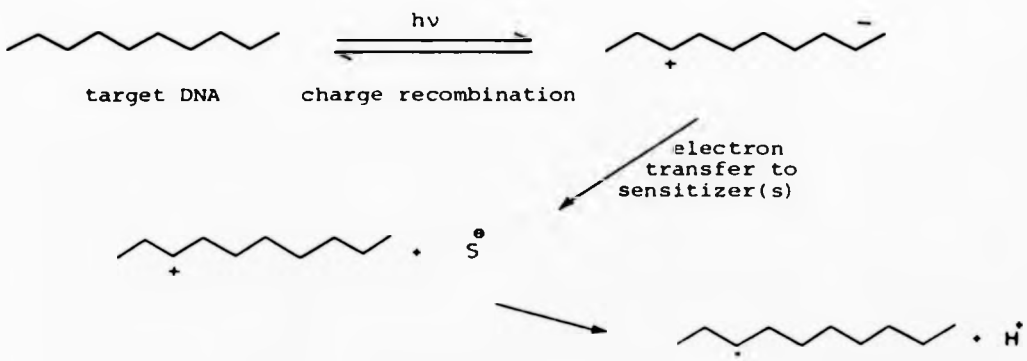

Scheme (1.2)

Evidence for this charge separation model has been obtained from many e.s.r. studies on γ- and 254 nm irradiated DNA, usually frozen as a solid at 77 K.[33,34]

Assignment of the e.s.r. spectra produced is made possible by computer summation of various individual DNA component spectra.

The literature contains conflicting results relating to damage centres in irradiated DNA, but the following radicals are now accepted as having been observed.

i) Formation of $T^{\bullet-}$ (T = thymine) and $G^{\bullet+}$ due to electron and positive hole migration respectively, *via* stacking of the DNA helix.[35-38]

ii) 5-thymyl radical, $TH^{\bullet}$[39,40] formed from protonation of $T^{\bullet-}$ at the C-6 position,[41] with 70 per cent of the unpaired spin density localised on the C-5 atom.[42]

iii) Thymyl peroxyl radicals, formed when oxygen is present, and $T^{\bullet-}$ is warmed above 77 K.[36,37]

An apparent discrepancy as to the eventual sink for electron migration has been reported by Gregoli *et al.*[43] who observed the cytosine radical anion ($C^{\bullet-}$) in preference to the $T^{\bullet-}$ radical anion and from this study of electron migration between two-component nucleotide systems the order of increasing electron affinity was given as C > T > A > G. Although cytosine was found to be the most electronegative base in this study, nonetheless $T^{\bullet-}$ is the observed anion in all other reports concerning DNA polymers. This has been accounted for[16] in terms of the difference between the character of frozen solutions of normal DNA and the stacking complexes of the dinucleotide systems used. When nucleotide mixtures and DNA are frozen, ice rejects the solute molecules which consequently

form aggregates of very high local concentration within the interstices of the ice crystal. These aggregates have a well ordered structure due to contributions from vertical stacking of planar aromatic molecules, as in the DNA bases, and horizontal hydrogen-bonding. The configuration of these aggregates provides good overlap of π-orbitals permitting intermolecular energy and charge migration phenomena to occur. The radiation chemistry of these phase-separated solute molecules in the frozen state is essentially that of the direct effects of radiation and does not involve indirect effects. There is a difference between the structures of frozen DNA and the stacking complexes of the complementary bases studied by Gregoli *et al.* In the latter, the stacking may result in the conjugation of π-orbitals in complementary bases, thus modifying the relative energy of the lowest-energy molecular orbital or LEMO of thymine and cytosine and ultimately altering their electron affinities.

Calculations[44] by frontier orbital theory (FOT) using both INDO and CNDO/2 approximations give the order of electron affinity for the bases as T > C > A > G.

Further evidence in support of preferential $T^{\bullet}$ anion formation in DNA was provided by Hütterman *et al.*[45] using single crystals of DNA irradiated at 4.2 K; the guanine cation was also observed in this study.

How the chemical processes of such radicals formed from this direct mechanism can affect living cells is still a major question. The fate of the thymine anion and guanine cation is the principal subject of investigation. Radical ions $T^{\bullet}$ and $G^{+\bullet}$ are stable at 77 K, but with warming of the sample, their respective yields decrease,[37] indicating both ions enter into conversion reactions. $T^{\bullet}$ undergoes protonation

at C-6[41] in anoxic conditions and peroxylation when O_2 is present, the $T^{\cdot}$ yield decreasing at the expense of $O_2^{\cdot-}$. Evidence concerning the $G^{+\cdot}$ cation by Symons *et al.*[37] indicates that $G^{+\cdot}$ may also undergo peroxidation, although O_2 may not add directly to $G^{+\cdot}$, since this is a highly delocalised radical and would not be expected to add O_2 directly. Possibly $G^{+\cdot}$ undergoes an acid-base reaction prior to reaction with O_2. This study also indicates an increase in strand breakage of DNA when O_2 is present. E.s.r. experiments involving irradiating DNA in the presence and absence of radiosensitizers[35] indicate spectral differences which have been accounted for by an increase in the formation of $G^{+\cdot}$ with some evidence for the formation of the anion radicals of the sensitizer. This reported increase in yield of $G^{+\cdot}$ is not supported by the recent work of Symons *et al.*[46] - see Section (3.7). Symons comments that the spectral integration procedures of Gräslund *et al.*[35] are inappropriate.[47]

A recent room temperature study[48] has new, and as yet uninterpreted, e.s.r. spectra for γ-irradiated DNA. Tentative assignments associate the anions and cations respectively as arising from pyrimidine and purine bases. The spectrum is dominated by a large singlet which may be due to hydrogen adducts at O-2 and O-4 for thymine and cytosine and O-6 for adenine. Again, the $TH^{\cdot}$ radical was observed.

1.6.4 "Indirect" *versus* "Direct" Mechanism

As cells consist of 80% water, one would expect at first sight that DNA damage mainly comes about from the indirect mechanism *via* diffusion of the water derived radicals (*i.e.*, H·, ·OH, and e_{aq}^{-}). This viewpoint is open to criticism as effects within cytoplasmic water can have little

effect on nuclear DNA. The sheer concentration of DNA present (15-50 mg/cm^3,[49] totalling 6×10^{-12} g, about 2 m in length per cell) in the nucleus means that the genetic material is present as a glue-like paste, rather than an ideal, dilute aqueous solution. Further a thin, very ordered film of water, known as the "hydration water" surrounds the polar DNA molecules, making diffusion to the target difficult. Most nuclear water consists of this hydration water, and its chemistry is modified in the structured layers surrounding the DNA helix, and allows charges (H_2O^+ + e^- formed from radiolysis) to be transferred to DNA before solvation can occur.

1.6.5 Electron Transfer from Triplet DNA to Radiosensitizers

A further direct mechanism for radical formation in DNA has been proposed by Smith[50] involving electron transfer from the triplet excited state of the base to the sensitizer molecule. Earlier studies[51] showed that *X*-irradiating frozen solutions (80 K) of calf thymus DNA produced optical emissions. By comparison of both the emission spectra and their kinetics with those produced from u.v. excited nucleotides, the emissions were assigned to phosphorescence from triplet guanine and thymine.

The formation of solute excited states by ionising radiation may occur by four different mechanisms, namely (i) direct excitation, (ii) ion-recombination, (iii) energy transfer from excited solvent, and (iv) sub-excitation electrons.[52]

Flash photolysis[50] of mixtures in aqueous solution of *p*-nitroacetophenone (PNAP) and guanosine monophosphate (GMP) give the transient spectrum of $PNAP^{\cdot-}$, the formation of which was attributed to electron transfer from ground state GMP to ^{3}PNAP, *viz.*:

$$PNAP \xrightarrow{h\nu} {}^1PNAP$$

$$^1PNAP \xrightarrow{isc} {}^3PNAP$$

$$^3PNAP + GMP \longrightarrow PNAP^{\cdot-} + GMP^{\cdot+} \qquad (1.5)$$

The GMP cation radical could not be observed optically. Although reaction (1.5) represents the reverse of the sensitization process, namely:

$$^3GMP + PNAP \longrightarrow GMP^{\cdot+} + PNAP^{\cdot-} \qquad (1.6)$$

by use of the Rehm-Weller equation[53] (a variant of Marcus theory for excited state electron transfer, discussed fully in section 1.8), Smith predicts the sensitization reaction, equation (1.6), to be highly favoured, the triplet excited base acting as an electron donor.

The white light photolysis flash used could create singlet GMP, but because of a very low intersystem crossing, to form the triplet, and suitable adjustment of concentrations, the excitation flash would produce much larger amounts of ^{3}PNAP than ^{1}GMP or ^{3}GMP.

Similar studies of triplet sensitizer molecules acting as electron acceptors have been made by Fisher *et al.*[54,55] using 2-methyl-1,4-naphthoquinone, see section (1.11.1).

1.7 Electronically Excited States of Nucleic Acids

Upon absorbing a photon, a ground state molecule, M, is promoted to a higher energy state, M^*, this being associated with a redistribution of electronic charge in the molecule. Spectroscopically this molecular excitation process is named using the orbitals with which the electron is associated before and after absorption of the photon. Thus, the

electronic transitions in order of increasing energy are $n \rightarrow \pi^*$, $\pi \rightarrow \pi^*$, $\sigma \rightarrow \pi^*$ and $\sigma \rightarrow \sigma^*$. Since σ- bonds absorb energy in the vacuum ultraviolet region (135 - 200 nm), $\sigma \rightarrow \sigma^*$ excitation is of limited importance in the photochemistry and photobiology of nucleic acids. By contrast $\pi \rightarrow \pi^*$ and $n \rightarrow \pi^*$ transitons are prominent in the photochemical study of nucleic acids by virtue of the presence of such π- bonds as C=C, C=N, C=O. The u.v.-visible absorption spectra of purines and pyrimidines are illustrated in Figures (1.5) and (1.6). The main absorption bands located in the 260 nm region are due to π-π^* transition with weaker, underlying n-π^* transitions which are not well-located. These bands are subjected to a small bathochromic shift when the H-atoms at N-9 for purines and at N-1 for pyrimidines are substituted by a ribose group, although going from ribonucleosides to deoxyribonucleosides or nucleotides does not alter the absorption spectra significantly. There is a second absorption peak at 200 nm, due to further $\pi \rightarrow \pi^*$ transitions.

The absorption band at 260 nm for DNA is the sum of its individual constituents, the sugar phosphate backbone making no significant contribution. The electronic transitions of the bases and various components of DNA and RNA are reviewed by Daniels[56] and Hauswirth and Daniels.[57]

1.7.1 Jablonski Diagram for the DNA Bases

The various excited states obtained by absorption of a photon are best described with the aid of a Jablonski diagram, illustrated in Figure (1.7). Organic molecules in their ground state normally have an even number of electrons, which are spin paired, occupying the lowest energy molecular orbitals.

Absorption of u.v. light by the ground state base, $^1B_0$, produces excited singlet states $^1B_1$, $^1B_2$, *etc.* Rapid internal conversion (ic) converts most of these to the lowest vibrational level of the $^1B_1$ state. This excited state has various pathways open to it, allowing its return to the ground state, for example, radiationless decay *via* vibrational relaxation, $^1k_{vr}$, or radiative fluorescence, $^1k_{r2}$, *i.e.*, emission of a photon hν', which has less energy than the photon initially absorbed, hν. Alternatively, some of the excited singlets undergo intersystem crossing, k_{isc}, the excited electron changing its spin and creating a triplet state. This triplet state may return to the ground state by a non-radiative process, $^3k_{vr}$, or by radiative phosphorescence, ^3k_r, emitting a photon of energy, hν". The spin multiplicity is given by (2S + 1) where S is the number of unpaired electrons.

Each of these terms introduced above will be discussed briefly. The process of intersystem crossing is illustrated in Figure (1.8). At point A the molecule has the same potential energy, the same internuclear distances and zero kinetic energy in both states. Singlet → triplet transitions are strongly forbidden (the spin selection rules) and the fact that they occur at all is because of spin orbit coupling. The change of electron spin is brought about by interaction between the magnetic moment of the spinning electron and the orbital magnetic field. The magnitude of this coupling increases with nuclear charge. The type of molecular orbitals involved are also important, thus El-Sayed's rules[58] suggest that $S_{\pi,\pi^*} \rightarrow T_{n,\pi^*}$ and $S_{n,\pi^*} \rightarrow T_{\pi,\pi^*}$ are at least an order of magnitude more probable than $S_{\pi,\pi^*} \rightarrow T_{\pi,\pi^*}$ or $S_{n,\pi^*} \rightarrow T_{n,\pi^*}$.

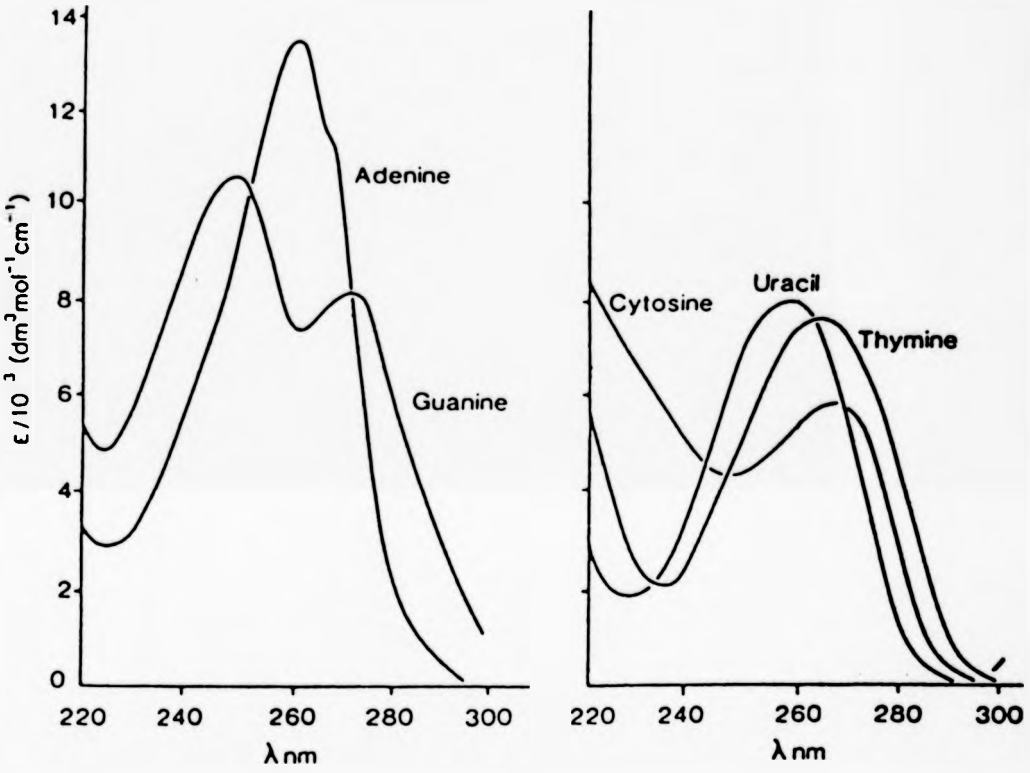

Figure 1.5 and 1.6 Absorption spectra of purine and pyrimidine nucleic acid bases, taken from ref.74.

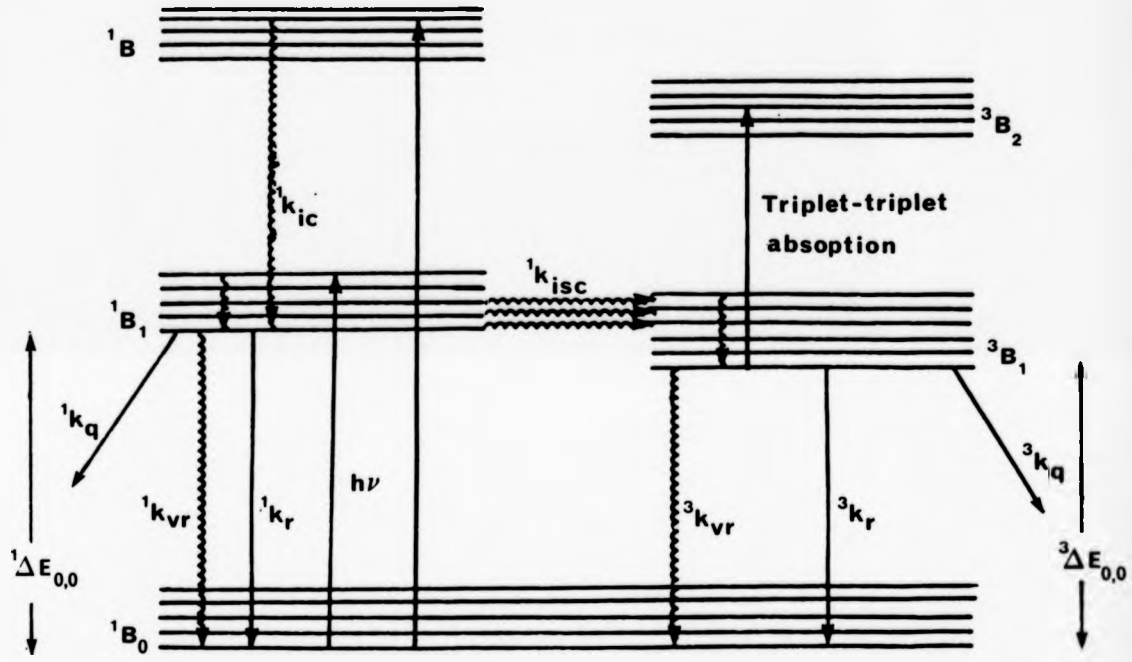

Figure 1.7 Jablonski diagram illustrating the various processes available to DNA bases following absorption of a photon hν; ic = internal conversion, isc = intersystem crossing, q = quenching (*e.g.*, energy transfer, hydrate and dimer formation, *etc.*), r = radiative decay by photon emission, vr = vibrational relaxation.

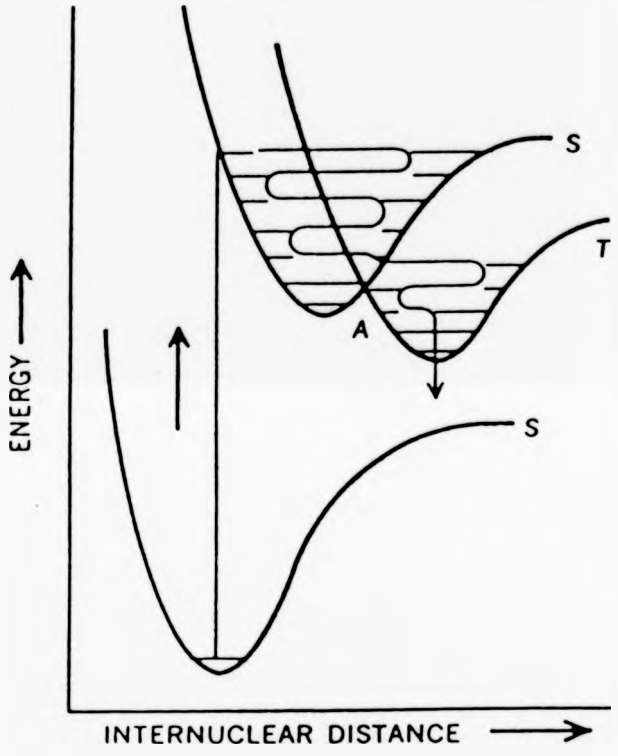

Figure 1.8 The formation of an excited triplet state by inter-system conversion from an excited singlet state. At point A the molecule has the same potential energy, the same internuclear distances in both singlet (S) or triplet (T) electronic configuration. Crossing of one state to the other is therefore made possible.

Triplet states tend to be longer-lived than the corresponding singlets, again due to the $^3T_1 \rightarrow {}^1S_0$ transition being spin-forbidden. Lifetimes of singlets are of the order of 1-1000 x 10^{-12} s, whilst triplets may have lifetimes of the order of seconds.

The quantum yields (ϕ) for the formation of excited species, or products is given by:

$$\phi = \frac{\text{number of moles (molecules) of product formed}}{\text{number of einsteins (photons) of radiation absorbed}}$$

$$= \frac{\text{rate of formation of product}}{\text{intensity of absorbed radiation}}$$

while the quantum yield of triplet state formation (which is the efficiency of intersystem crossing), is given by:

$$\phi_T = \phi_{isc} = \frac{k_{isc}}{{}^1k_q + {}^1k_{vr} + k_{isc} + {}^1k_r} = k_{isc}.{}^1\tau$$

where ${}^1\tau$ is the lifetime of the singlet excited state.

At low temperatures, ${}^3k_{nr}$ for nucleic acids is small, and it is possible to observe phosphorescence, but at room temperature ${}^3k_{nr}$ is much larger and as yet phosphorescence has not been observed at this temperature. Fluorescence emissions at 80 K may also be observed. Such low temperature emission studies have been reviewed by Whillans and Johns[59] and in articles in Wang's book.[60] A further pathway of excited state decay is *via* photochemical reactions discussed next.

1.7.2 Photochemical Reactions of Excited State Bases

The photochemical reactions of nucleic acids and their constituents have been the subject of many investigations, and for recent reviews see Wang[60] and Saito *et al.*[61] The photochemical reactions of pyrimidines have been studied in more detail than those of the purines. The greater interest in pyrimidine photochemistry is due to the fact that whilst purines form part of the light absorbing system in nucleic acids, they do not apparently effect significant photochemical change, the absorbed energy being transferred to other moieties, namely the pyrimidines, which subsequently undergo reaction.

(a) Purine photoproducts

The photochemistry of purines is affected by the nature of the ring substituents, for example ultraviolet irradiation of adenine in the presence of oxygen results in deamination to yield hypoxanthine (1.IV). This indicates that the amino group is the initial point of attack, Scheme (1.3).

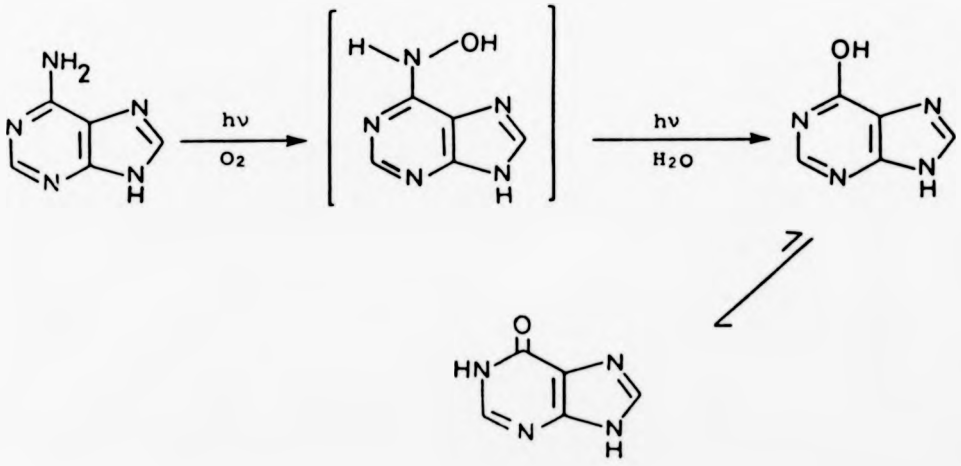

(1.IV)

Scheme (1.3)

In the absence of O_2, adenine is only partially destroyed, whilst the breakdown of guanine is actually inhibited by the presence of oxygen.

Photosensitized oxidations, the so-called "photodynamic effect", have been studied widely since it was shown that guanine residues are preferentially destroyed during the methylene blue-sensitized photo-oxidation of DNA.[62] The photodynamic effect and its implications in photomedicine have been reviewed recently by Spikes.[63]

Alkylation by alcohols of guanine and adenine and their derivatives may take place at C-8, *e.g.*, for guanine:

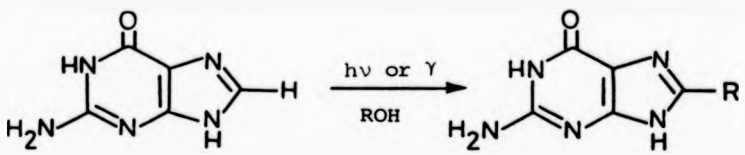

This photochemical reaction has been induced both directly with light of $\lambda > 260$ nm and indirectly using acetone as sensitizers with light $\lambda > 290$ nm.

(b) Pyrimidine photoproducts

The major photoproducts of pyrimidine bases in aqueous solution are cyclobutane-type dimers and photohydrates. As early as 1931 it was noticed that u.v.-irradiation of uracil derivatives in aqueous solution resulted in the loss of the characteristic absorption peak near 260 nm. This change results from the addition of water across the alkene double bond, the addition taking place in the case of pyrimidines to give the 6-hydroxy-5,6-dihydropyrimidines.[64] Hydrate formation is accepted as occurring *via* the excited singlet state, the evidence being that the presence of O_2 does not affect the quantum yield[65,66] and the process is not

instigated by triplet sensitizers.[67]

The mechanism of this seemingly simple addition has yet to be completely elucidated, and any theory must account for both the substituent effects and the pH dependence of the quantum yield for photohydrate formation. A recent study[68] indicates proton transfer takes place from water to the C-5 position of the excited singlet state. The resulting carbo-cation (1.V) is thought either to undergo solvolysis forming the photohydrate (1.VI) or to eliminate a proton at N-1, depending upon pH, the latter producing an intermediate isomeric form of the pyrimidine ,isopyrimidine, (1.VII), see Scheme (1.4), which rearranges to the parent pyrimidine.

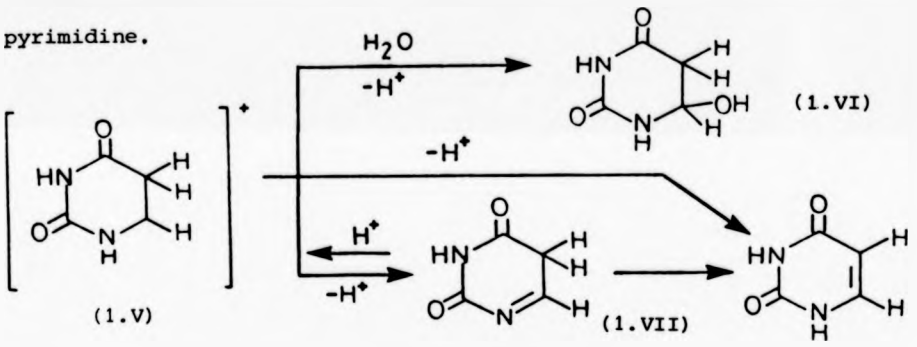

Scheme (1.4)

The second major photo-product is the cyclobutane dimer, in which two bases are linked *via* a four-membered ring between the C-5 and C-6 positions of each base. All four isomeric forms of the dimer uracil and thymine have been found, and are illustrated in Figure (1.9). In fluid solution this dimerisation probably takes place through interaction of a triplet base with a molecule in the ground state.

The particular isomers and quantum yields for the formation of dimers are strongly dependent upon irradiation conditions. For example, thymine in ice or in crystals is orientated in such a way as to allow only formation of the *cis-syn* isomer,[69] which is also the principal dimer formed in native DNA, although the *trans-syn* form is also produced.[70]

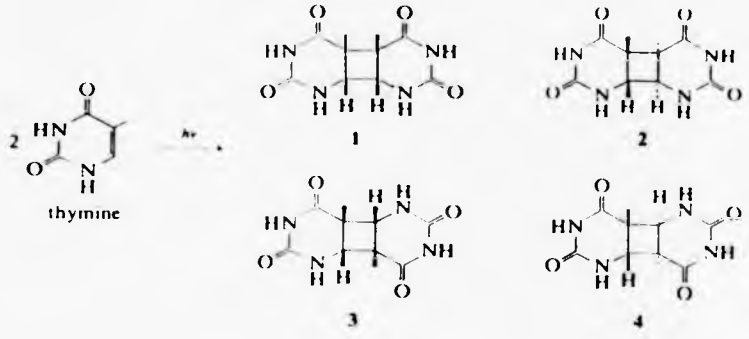

Figure 1.9 The four cyclobutane dimer isomers formed from irradiation of thymine:

(1) *cis-syn*, (2) *trans-syn*, (3)*cis-anti*

(4) *trans-anti*.

In solution, however, all the isomers are produced, but the ratios are dependent upon pH, temperature and concentration and these latter effects are reviewed by Fisher and Johns.[64]

As stated above, the mechanism for dimer formation is believed to be *via* the reaction between an excited triplet and a ground state base. However, in frozen solutions or when pyrimidines are bonded together by a sugar phosphate linkage, as in DNA, dimer formation may occur *via* the singlet.[64,71]

The formation of pyrimidine dimers has been induced in aqueous solutions of DNA or of single bases through triplet-triplet energy transfer from sensitizer to base. The sensitizers which have been used are acetone, benzophenone and acetophenone.[72] In this study the ketones were also shown to react chemically with pyrimidines, forming an oxetane derivative (1.VIII):

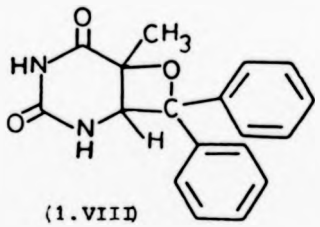

(1.VIII)

An oxetane is formed from thymine and benzophenone whilst for purines, ketyl radicals are formed *via* H-atom abstraction from the purine ring.

Other photochemical processes of pyrimidines include reactions between alkylamines and thymidine.[73] This results in ring-opening of thymine at the N-1 position giving, after heating, ring closure yielding 1-methylthymine. This reaction is very specific towards thymine and has been used to release selectively thymine from DNA.

1.7.3 Triplet State Properties of Pyrimidine Bases

Various values for the intersystem crossing yields have been reported.[74] These have been determined by many methods including energy transfer to both europium ion and retinol, *cis-trans* isomerisation of 1,3-pentadiene and kinetics of dimerisation.

The most direct method for determining the isc yields for the pyrimidine bases has been performed by Salet and Bensasson[75] and Salet *et al.*[76] using laser flash photolysis by energy transfer from triplet base to retinol. These results obtained are the most likely to be correct and agree well with those of Fisher *et al.*,[77] and are given in Table (1.1). Also, the kinetic parameters for the triplet bases and their nucleosides obtained from the studies are presented in Table (1.2).

The triplet states of the bases and their derivatives are quenched by ground state molecules (self quenching) according to equation (1.7) where k_{obs} is the observed rate of triplet decay, k_o is the unimolecular rate constant in the absence of self quenching, k_s is the bimolecular, second order, rate constant for quenching by ground state molecules, M.

$$k_{obs} = k_o + k_s [M] \qquad (1.7)$$

The higher triplet yields in acetonitrile compared with water may be due to the absence of the chemical pathway for the deactivation of the singlet by forming a hydrate which is impossible in the aprotic solvent. A further possibility may be a different ordering of the n,π^* and π,π^* excited states. Attempts to assign the orbital parentage of the lowest energy transitions have been made by Salet *et al.*,[76] but positive identification has yet to be achieved. Figure (1.10) illustrates

Table (1.1)

Intersystem crossing yields (ϕ_T) for thymine and uracil and the corresponding nucleosides and nucleotides†

Base	Solvent	ϕ_T	Ref.
Thymine	Acetonitrile	0.06	75
	Water	0.006	75
Thymidine	Acetonitrile	0.069	76
	Water	0.014	76
TMP	Ethanol	0.055	76
	Water	0.015	76
Uracil	Acetonitrile	0.2	75
	Water	0.023	75
Uridine	Acetonitrile	0.078	76
	Water	0.015	76
UMP	Ethanol	0.044	76
	Water	0.011	76

†Excitation 265 nm (50 mJ, 35 ns) laser pulse.

Table (1.2)

Kinetic parameters of the triplet states of thymine and uracil and their corresponding nucleosides

Base	Solvent	k_{obs} (s^{-1})	Base con. (mol dm^{-3})	k_o (s^{-1})	k_s (dm^3 mol^{-1} s^{-1})	Ref.
Thymine	Acetonitrile			1.0×10^5	0.6×10^9	75
	Water	1.7×10^6	10^{-3}			75
Thymidine	Water			4.0×10^5	1.0×10^8	76
Uracil	Acetonitrile			5.0×10^5	2.0×10^9	75
	Water	2.9×10^6	10^{-3}			75
Uridine	Water			5.0×10^5	8.0×10^8	76

the possible orderings of the energy levels for excited state pyrimidines in aprotic and protic solvents. Both proposals would predict a higher yield of isc in aprotic solvents. In the first case the lowest excited singlet state is principally of $^1(n,\pi^*)$ origin in non-hydrogen bonding solvents while the lowest triplet state is $^3(\pi,\pi^*)$. Under these conditions a moderate degree of spin-orbit coupling exists which would promote intersystem crossing (El-Sayed's rules). In protic solvents the $^1(n,\pi^*)$ and $^3(n,\pi^*)$ states would be shifted to higher energies, whilst the $^3(\pi,\pi^*)$ would move to a lower energy. In hydrogen-bonding solvents it is likely that a $^1(\pi,\pi^*)$ state will be the lowest, rendering spin-orbit coupling very small. In the second case a relatively forbidden state of principally $^1(\pi,\pi^*)$ character could be of lowest energy in aprotic and protic solvents. An increase in value of ϕ_T would occur in an aprotic solvent because of a $^3(n,\pi^*)$ state between the $^1(\pi,\pi^*)$ and $^3(\pi,\pi^*)$ states. However, in protic solvents, the $^3(n,\pi^*)$ state will be above the lowest $^1(\pi,\pi^*)$ state, thus reducing ϕ_T. Thymine fluorescence data[78] would favour the first possibility.

1.7.4 Triplet Energies

The triplet energies for the four mononucleotides have been determined from phosphorescence spectra in low temperature glasses. The values summarised in Table (1.3) are given with various known sensitizers for dimerisation for comparison. Room temperature values have not yet been obtained, although they would not be expected to be very different from those prevailing at 77 K. Even so, triplet energies obtained by an independent method for fluid solution would be of general interest and value.

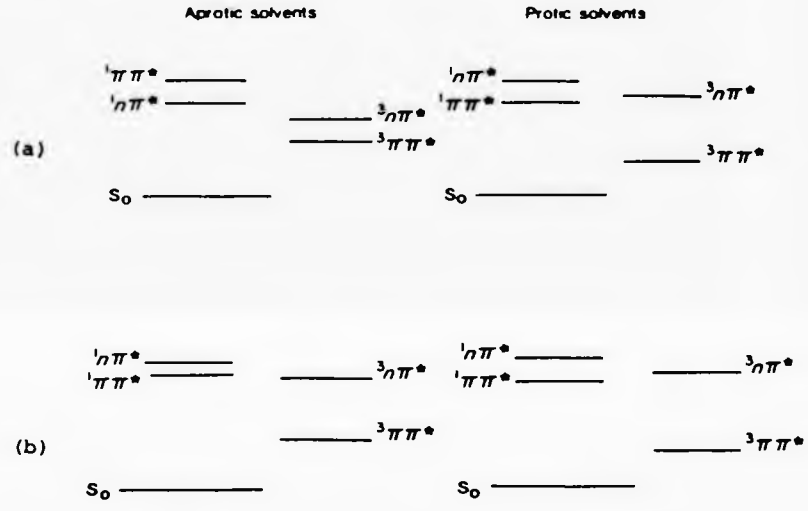

Figure 1.10 Possible orderings of excited states of pyrimidines in aprotic and protic solvents:
(a) assuming $^1(n,\pi^*)$ to be the lowest excited singlet and (b) assuming a forbidden $^1(\pi,\pi^*)$ to be the lowest excited singlet, taken from ref.76.

Thymidine has the lowest triplet energy of all the nucleotides and because of ready intramolecular energy transfer in DNA, the triplet energy of DNA rapidly locates on thymine. This localisation of energy on thymine makes it particularly important as the potential site of photo-damage in DNA.

Table (1.3)

Triplet energies of nucleotides and sensitizers of dimerisation adapted from reference 60

Compound	Triplet energy /10^3 kJ mol^{-1}
Acetone	337
CMP	334
UMP	329
GMP	325
AMP	319
Acetophenone	317
TMP	315
Benzophenone	297
Orotic acid	255

1.7.5 Triplet-triplet Absorption Studies by Flash Photolysis

The fluorescence and phosphorescence of the DNA bases in frozen solutions have been studied extensively;[60] however these results give little indication of how excited state bases will behave in solution as regards decay times, *etc.*

Observations of the triplets, as already mentioned, of thymine and uracil and their nucleosides and nucleotides have been made using the technique of flash photolysis. The triplet-triplet absorption spectra of these compounds have been observed in various

solvents;[75-77] the spectra for uracil and thymine in acetonitrile and water are illustrated in Figure (1.11). From this figure, it can be seen that the extinction coefficients for these triplet species are rather low and for this reason, as well as the low triplet yields, triplet quenching studies for the bases are particularly difficult to perform and hitherto very few direct kinetic data have been obtained.

The extinction coefficients (ε_T) for the triplet pyrimidines in acetonitrile were obtained by the energy transfer technique using retinol triplet as standard. The value for ε_T in water was estimated assuming that the oscillator strength of the triplet transition is independent of solvent.[75,76]

The triplet state of uracil is reported to have been produced by the pulse radiolysis of its solutions in acetonitrile, dimethylformamide and isopropanol.[79] However, the spectra produced differ considerably from that obtained in the flash photolysis studies.[75-79]

The triplet state of purine in ethanol, acetonitrile and water has been observed[80,81] in absorption as well as triplet 2-aminopurine in water.[82]

Room temperature u.v. laser flash photolysis of aqueous adenine and its derivatives at various pH[83] produced many transients. These were assigned to hydrated electrons, radical cations, radical anions and/or neutral radicals formed *via* neutralisation reactions of the charged radicals. The triplet state was not detected, although results using known triplet quenchers indicate that the bases may photoionise *via* their triplet state.

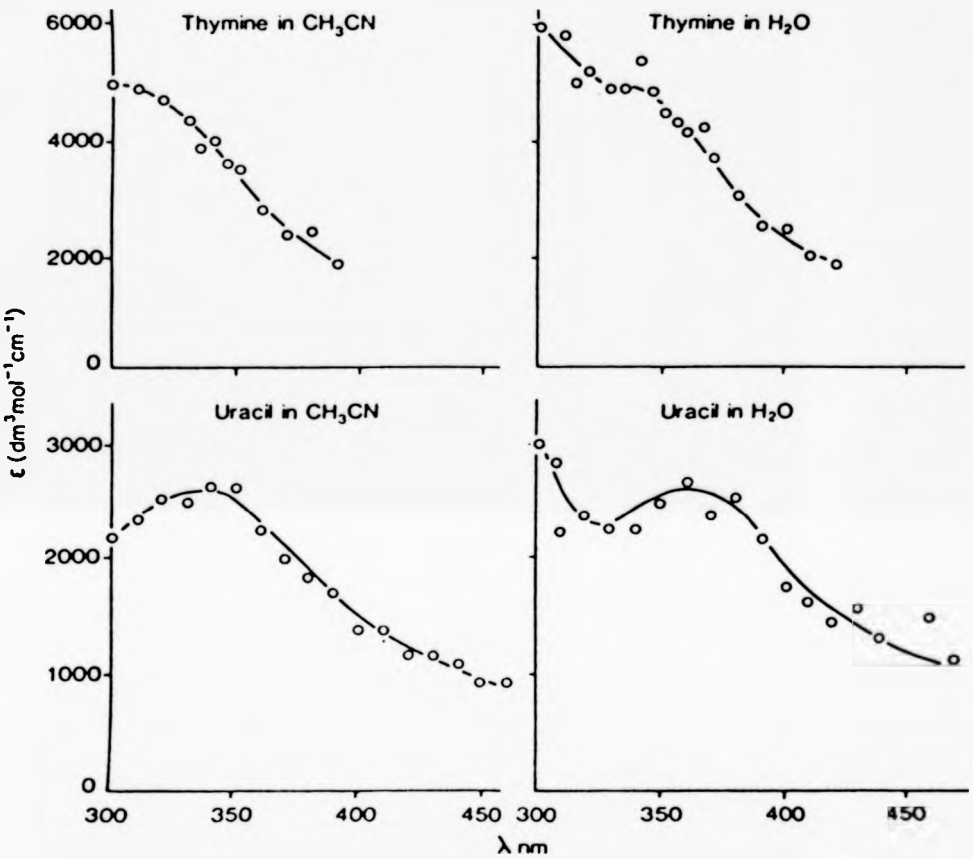

Figure 1.11 Triple-triplet absorption spectra of thymine and uracil, taken from ref.75.

1.8 Electron-transfer Reactions of Excited States

A molecule in an electronically excited state normally has completely differing chemical properties from its corresponding ground state, extending even to its gross geometry. The properties of the excited states may, however, often be predicted from information regarding the ground state. In particular, the rates of outer-sphere electron transfer reactions, *i.e.*, oxidation reduction reactions in which no bonds are made or broken, is an area of photochemistry capable of a good level of prediction.[84-86]

The theory of excited state electron-transfer has, as its roots, the Marcus theory,[87-90] for ground state electron-transfer, which is discussed later in section (1.8.3).

1.8.1 Redox Properties of Excited States

An excited state species, because of its higher energy content, equation (1.8), is both a stronger reductant, equation (1.9), and a stronger oxidant, equation (1.10), than the corresponding ground state.

$$M^{n+} + h\nu \longrightarrow {}^*M^{n+} \qquad E^*(M/{}^*M) \qquad (1.8)$$

$$M^{(n+1)+} + e^- \longrightarrow {}^*M^{n+} \qquad E^o(M^+/{}^*M) \qquad (1.9)$$

$${}^*M^{n+} + e^- \longrightarrow M^{(n-1)+} \qquad E^o({}^*M/M^-) \qquad (1.10)$$

${}^*M$ represents the excited state and E^* its excitation energy. Redox potentials for the excited state couples may be calculated from those of the corresponding ground state:

$$M^{(n+1)} + e^- \longrightarrow M^{n+} \qquad E^o(M^+/M)$$

$$M^{n+} + e^- \longrightarrow M^{(n-1)+} \qquad E^o(M/M^-)$$

and the excitation energy, *i.e.*,

$$E^{o}(M^{+}/{}^{*}M) = E^{o}(M^{+}/M) - E^{*} \quad (1.11)$$

and

$$E^{o}({}^{*}M/M^{-}) = E^{o}(M/M^{-}) + E^{*} \quad (1.12)$$

The redox potentials *versus* a reference electrode are related to the free energy change:

$$\Delta G = \Delta H - T\Delta S = nfE$$

The entropy change, however, between the ground and excited states may generally be neglected (*i.e.*, $\Delta S \approx 0$) and hence

$$\Delta G \approx \Delta H$$

The effects of absorption of a photon on the redox potential of the ground state, M, as given by equations (1.11) and (1.12) are illustrated in Figure (1.12). Organic molecules usually have a large separation between oxidation states and hence a given molecule can normally serve either as an electron-donor or electron-acceptor but rarely as both. Moreover, a singlet excited state has enhanced redox properties compared with the corresponding triplet state, due to its higher excitation energy. Transition metal complexes are different because redox sites exist on both the metal and the ligand. The oxidation states are often closely spaced, allowing the excited state to function as both a donor and acceptor of electrons. Figure (1.12) illustrates that when the oxidation and reduction states of a molecule are close enough, light-driven crossing of the excited state potentials may take place.

The applications of excited state redox properties are many, the principal areas being:[31]

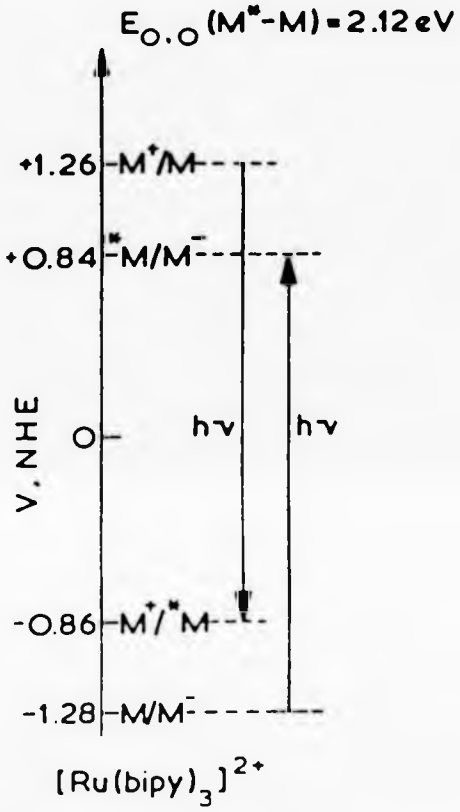

Figure 1.12 Oxidation-reduction potentials in aqueous solution of $*[Ru(bipy)_3]^{2+}$, according to equations (1.11) and (1.12), taken from ref.84.

i) Catalytic processes; here a reduction in the activation energy for the process concerned is provided by the photon energy. The reaction between an excited state species (A^*) and some ground state species (B) may be orders of magnitude faster than that between A and B.

ii) The photochemical transformation of low energy reactants into high energy products, *i.e.*, the conversion of light energy into chemical energy, as in the quest for the photochemical conversion of solar energy.

iii) Chemical generation of excited states from highly exoergonic reactions, *i.e.*, the conversion of chemical energy into light as in "cold light" devices.

1.8.2 Classification of Redox Processes

There have been two main mechanisms proposed for electron transfer, *i.e.*, the inner-sphere mechanism and the outer-sphere mechanism, and these are defined differently for inorganic and organic systems.

Inorganic reactions

The inner-sphere mechanism requires the two reactants to share one, or more, ligands in their first co-ordination sphere, in the activated complex, and the electron transfer is considered to occur *via* the bridging ligand. For the outer-sphere mechanism the inner co-ordination spheres of both metal ions remain intact in the activated complex, *i.e.*, no ligand-to-metal bond is broken or formed.

Organic Reactions

In electron transfer reactions when one or both reactants are organic, Littler[92] has proposed the terms "non bonded" and "bonded" instead of outer-sphere and inner-sphere, respectively, since there is no general way of systematising organic compounds.

1.8.3 The Marcus Theory of Electron-transfer

This is the theory most widely applied, because it utilises simple arithmetical calculations and has a reasonably good record for predicting rate constants. The following brief qualitative account is based on reference 93. Marcus firstly considered the problem of estimating the rate constant for electron-transfer between two metal complexes, approximated as structureless spheres:

$$M_1^{Z_1} + M_2^{Z_2} \rightleftharpoons M_1^{Z_1-1} + M_2^{Z_2+1}$$

The primary step is the diffusion together of the two reactants, which may be aided or hindered by electrostatic forces amenable to calculation. The second stage is the actual electron-transfer step, which is assumed to occur at a contact distance (0.5-1.0 nm) between the two complexes. There is, however, a barrier to this electron-transfer which stems from the Franck-Condon principle, which states that the transfer of an electron takes place in such a short time (10^{-15}-10^{-16} s) that nuclear motions do not occur (the time of a nuclear vibration is $\sim 10^{-13}$ s).

This barrier may best be explained by assuming the electron-transfer takes place between two complexes differing only by oxidation state, as in equation (1.13):

$$[Fe'(H_2O)_6]^{+} + [Fe''(H_2O)]^{3+} \longrightarrow [Fe'(H_2O)_6]^{3+} + [Fe''(H_2O)_6]^{2+} \qquad (1.13)$$

Application of the Franck-Condon principle indicates that since immediately after electron-transfer, when no nuclear movements will have occurred, the Fe-O bond distances in $[Fe'(H_2O)_6]^{2+}$ will be the same as those in the $[Fe'(H_2O)_6]^{3+}$; likewise $[Fe''(H_2O)_6]^{2+}$ will have retained the configuration of $[Fe''(H_2O)_6]^{3+}$. This self exchange reaction has apparently violated the first law of thermodynamics, $\S\Delta H^0 = 0$, having created two vibrationally excited states from two ground states. The conundrum may be explained, however, if the Franck-Condon principle is applied in reverse, *i.e.*, by assuming the co-ordination spheres of M' and M" (including their surrounding solvent spheres) are distorted (expanded, compressed or asymmetrically rearranged) so as to make the geometries of the two species identical. This corresponds to movement along the potential energy surfaces, see Figure (1.13), until they cross, making their energies identical, when the electron may be transferred without offence to the first law.

Marcus developed this model further, formulating expressions for the inner-sphere and solvent reorganisation energies, denoted λ_i and λ_o respectively. Organic molecules are generally far from spherical and one is faced with problems in the calculation of λ_o, using more realistic geometries. On the other hand, λ_i is often assumed to be equal to zero, and in most organic systems one of the reactants is uncharged, making electrostatic effects negligible. The free energy change, $\Delta G^{\ddagger}$, for such an electron transfer may thus be written in terms of three components:

$$\Delta G^{\ddagger} = \Delta G_c^{\ddagger} + \Delta G_i^{\ddagger} + \Delta G_o^{\ddagger}$$

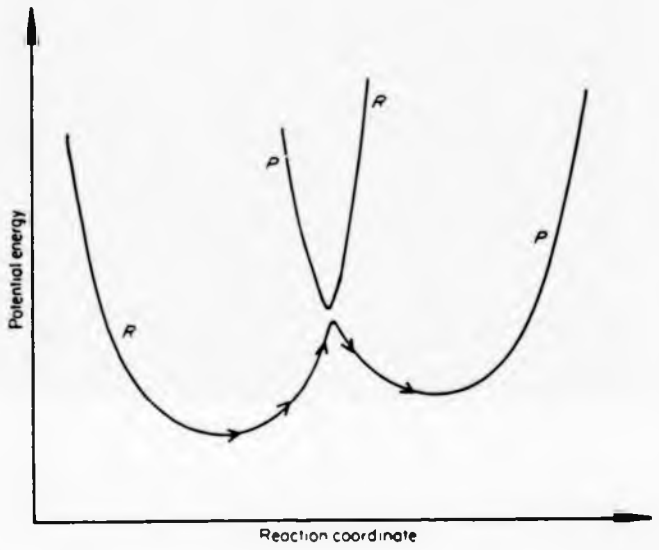

Figure 1.13 Potential energy surface for a system going from reactants (curve R) to products (curve P).

If dipole-dipole interactions are excluded for reactions with one species uncharged, then $\Delta G_c^{\ddagger}$ is taken as equal to zero. With this assumption, the expression for $\Delta G_i^{\ddagger}$, from a treatment by Marcus[87] involving statistical mechanics and treating $\Delta G_o^{\ddagger}$ from a classical dielectric continuum model of the solvent[94] gives:

$$\Delta G^{\ddagger} = \frac{\lambda}{4}\left(1 + \frac{\Delta G^{0'}}{\lambda}\right)^2 \qquad (1.14)$$

where $\lambda = \lambda_i + \lambda_o$.

λ is the total reorganisational energy obtained by summing the reorganisational energies due to inner-sphere (λ_i) and the solvent ionic atmospheres (λ_o), while $\Delta G^{0'}$ corresponds to the free energy change for the reaction in the medium used (not necessarily equal to the standard free energy change, but nevertheless often put equal to it), plus the electrostatic term originating from the change in the charge of the transition state upon electron-transfer.

An alternative form of equation (1.14) is equation (1.15),[89] where $\Delta G^{\ddagger}(O)$ replaces $\lambda/4$, and is the change in the free energy of activation for a process with $\Delta G^{0'} = 0$.

$$\Delta G^{\ddagger} = \Delta G^{\ddagger}(O)\left[1 + \frac{\Delta G^{0'}}{4\Delta G^{\ddagger}(O)}\right] \qquad (1.15)$$

These free energy surfaces are depicted in Figure (1.14). Other expressions for $\Delta G^{\ddagger}$ have been proposed and are discussed in section (1.8.5).

1.8.4 The Kinetics of Electron-transfer involving Excited States

For the kinetic study of excited state electron-transfer the reaction scheme (1.5) first proposed by Rehm and Weller, has now been universally adopted.[94,95]

$$D + h\nu \longrightarrow D^*$$

$$^*D + A \underset{k_{21}}{\overset{k_{12}}{\rightleftharpoons}} {}^*D\text{---}A \underset{k_{32}}{\overset{k_{23}}{\rightleftharpoons}} D^{+}\text{---}A^{-} \xrightarrow{k_{30}} \text{Products or separated ions}$$

encounter complex

solvated ion pair

$^1/_{\tau_0}$

D

Scheme (1.5)

where k_{30} comprises all possible processes whereby $D^{+}\text{---}A^{-}$ can disappear, with the exception of the back electron transfer process, k_{32}.

Using steady state approximations, the following equation can be derived for the quenching rate constant:

$$k_q = \frac{k_{12}}{1 + \frac{k_{21}}{k_{23}} + \frac{k_{21}}{k_{30}} \cdot \frac{k_{32}}{k_{23}}} \qquad (1.16)$$

According to classical rate theory, the rate constant for the unimolecular reaction may be written as:

$$k_{23} = k_{23}^0 \exp(-\Delta G_{23}^{\ddagger}/RT) \qquad (1.17)$$

$$k_{32}/k_{23} = \exp(\Delta G_{23}^0/RT) \qquad (1.18)$$

where k_{23}^0 is the pre-exponential factor, $\Delta G_{23}^{\ddagger}$, is the standard free activation energy, and ΔG_{23}^0 is the standard free energy change for the forward electron-transfer step.

$$k_{23}^0 = \kappa_{23} (kT/h) \qquad (1.19)$$

κ_{23} is the so-called transmission coefficient[96] and (kT/h) is a universal frequency factor (6 x 10^{12} s^{-1} at 25 °C).

Figure (1.15) shows the zero order potential energy surfaces crossing; this would be the case if there is no electronic interaction, between the zero order initial and final states. If there is an electronic interaction, the degeneracy will be removed and two new surfaces will be formed,[84,97] as illustrated in the insert to Figure (1.15). This separation is equivalent to $2H_{if}$, where H_{if} is the interaction energy[97] (the electronic coupling matrix element). This interaction energy was assumed by Marcus[87-90] to be so small that it could be neglected, but large enough to allow the conversion of reactants to products, with unit probability. This is called the adiabatic assumption, which makes the transmission coefficient, κ, of equation (1.19) equal to unity. However, more generally, in the weak interaction limit this assumption is invalid and the possibility exists of a system arriving from the initial state, continuing along the original zero order curve and then returning without undergoing reaction. This is termed 'non-adibatic' behaviour and is accounted for by adopting a transmission coefficient of less than unity.

The work terms for bringing the reactants and products together from an infinite distance apart to their separation distances in the activated complex, assuming only an outer-sphere mechanism, are practically zero when one of the reactants is uncharged. Utilising equations (1.17) and (1.18), equation (1.16) becomes

$$k_q = \frac{k_{12}}{1 + \frac{k_{21}}{k_{30}} \exp(\Delta G^0_{23}/RT) + \frac{k_{21}}{k_{23}} \cdot \exp(\Delta G^{\ddagger}_{23}/RT)} \qquad (1.20)$$

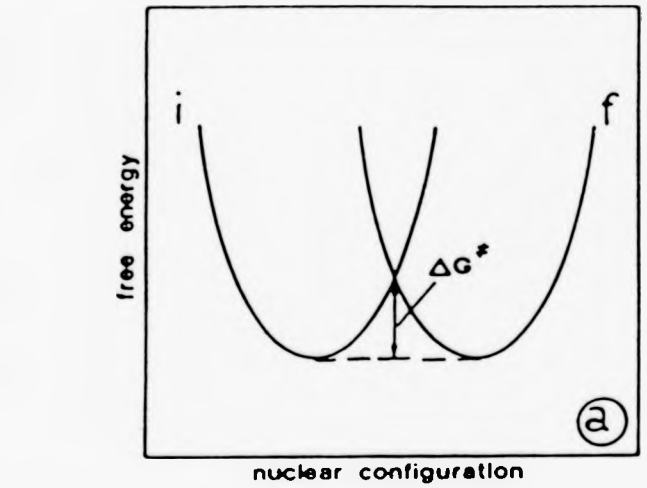

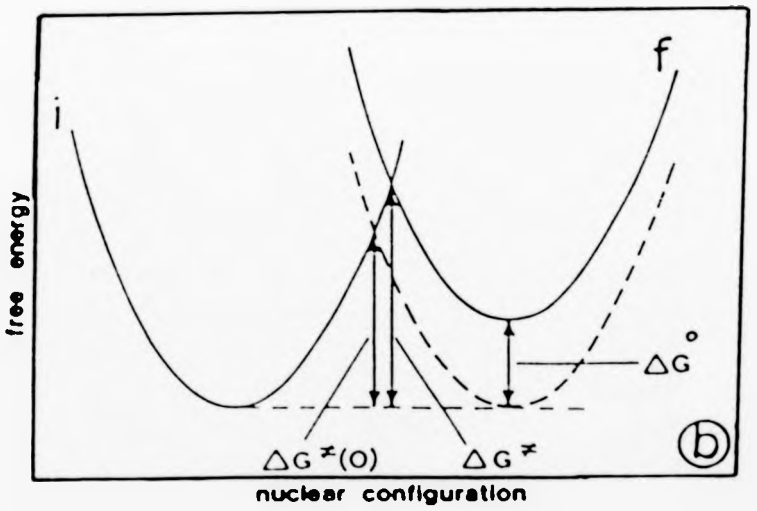

Figure 1.14 Schematic representations of the energy surfaces of the initial (i) and final (f) states for self exchange (a) and cross-electron transfer (b) reactions.

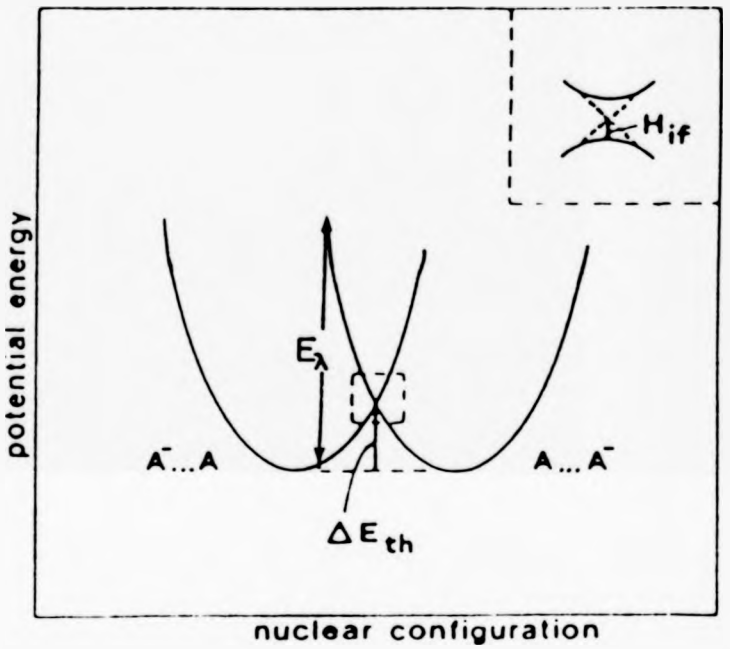

Figure 1.15 Profile of the potential energy surfaces as a function of the nuclear configuration for a self exchange electron transfer reaction. The insert shows in greater detail the "intersection" region. ΔE_{th} is the barrier for the thermal electron transfer, E_λ is the energy for the light-induced electron transfer, and the splitting at the intersection of the surfaces is equal to $2H_{if}$, where H_{if} is the electronic coupling matrix element. Note that $E_\lambda = 4(\Delta E_{th} + H_{if})$ and that $H_{if} << \Delta E_{th}$ in the weak interaction model.

The free energy change, ΔG^0_{23} for the electron transfer process from the encounter complex to the ion pair may be calculated according to equation (1.21).[53]

$$\Delta G^0_{23} = E(D/D^+) - E(A^-/A) - e_o^2/\varepsilon_a - \Delta E_{o,o} \qquad (1.21)$$

The respective terms refer to the oxidation potential of the electron donor (D), the reduction potential of the acceptor (A); e_o^2/ε_a is the free energy gained by bringing the two radical ions to an encounter distance, a, in a solvent of dielectric constant, ε. The electronic energy of the excited state is denoted by $\Delta E_{o,o}$.

Although Scheme (1.5) represents the excited state acting as the donor, it can equally well be formulated with the excited state functioning as the electron acceptor. The role which will be played by each molecule is given by the sum $E(M/M^+) + E(M^-/M)$,[53] which gives the "electronegativity" of the molecule M; for any two components, the one with the greater sum always acts as the acceptor.

1.8.5 Relationships between the Free Energy of Activation, $\Delta G^{\ddagger}_{23}$, and the Standard Free Energy Change, ΔG^0_{23}

There have been four principal relationships proposed between these parameters;[98]

i) As already mentioned, the Marcus quadratic equation (1.15), which is again given here for completeness:

$$\Delta G^{\ddagger}_{23} = \Delta G^{\ddagger}_{23}(O)\left[1 + \frac{\Delta G^0_{23}}{4\Delta G^{\ddagger}_{23}(O)}\right] \qquad (1.15)$$

ii) Various linear free energy relationships of the type proposed by Brønsted and Pedersen[99] and by Polanyi *et al.*[100]

$$\Delta G^{\ddagger}_{23} = \alpha \Delta G^{0}_{23} + \beta \qquad (1.22)$$

where α and β are two empirical parameters, being conceptually similar to $\Delta G^{\ddagger}_{23}(O)$, but not always equal to it.

iii) Rehm and Weller[53] proposed the empirical relationship, equation (1.23):

$$\Delta G^{\ddagger}_{23} = \Delta G^{0}_{23}\{(\frac{\Delta G^{0}_{23}}{2})^2 + [\Delta G^{\ddagger}_{23}(O)]^2\}^{\frac{1}{2}} \qquad (1.23)$$

iv) Agmon and Levine[101] derived a relationship from a thermodynamic-like treatment of concerted reaction kinetics:

$$\Delta G^{\ddagger}_{23} = \Delta G^{0}_{23} + \frac{\Delta G^{\ddagger}_{23}(O)}{\ln 2} \ln\{1 + \exp[-\frac{\Delta G^{0}_{23} \ln 2}{\Delta G^{\ddagger}_{23}(O)}]\} \qquad (1.24)$$

Graphical representations of these equations (1.15), (1.23) and (1.24) are given in Figure (1.16) which depicts the variation of $\Delta G^{\ddagger}_{23}$ with ΔG^{0}_{23}

The Marcus equation (1.15) behaves very similar to equations (1.23) and (1.24) when $\Delta G^{0}_{23} \leqslant \Delta G^{\ddagger}_{23}(O)$. A peculiarity occurs when $\Delta G^{0}_{23} < -4\Delta G^{\ddagger}_{23}(O)$, *i.e.*, the highly exoergonic region known colloquially as the Marcus inverted region, in which the equation (1,15) predicts an increase of $\Delta G^{\ddagger}_{23}$ with decrease in ΔG^{0}_{23}. The variation of $\Delta G^{\ddagger}_{23}$ with ΔG^{0}_{23} is depicted in Figure (1.17). The equations (1.23) and (1.24) predict very similar curves for the variation of $\Delta G^{\ddagger}_{23}$ with ΔG^{0}_{23}, as illustrated in Figure (1.16). Equation (1.24) proposed by Agmon and Levine is preferred because it is based upon a theoretical treatment.[103]

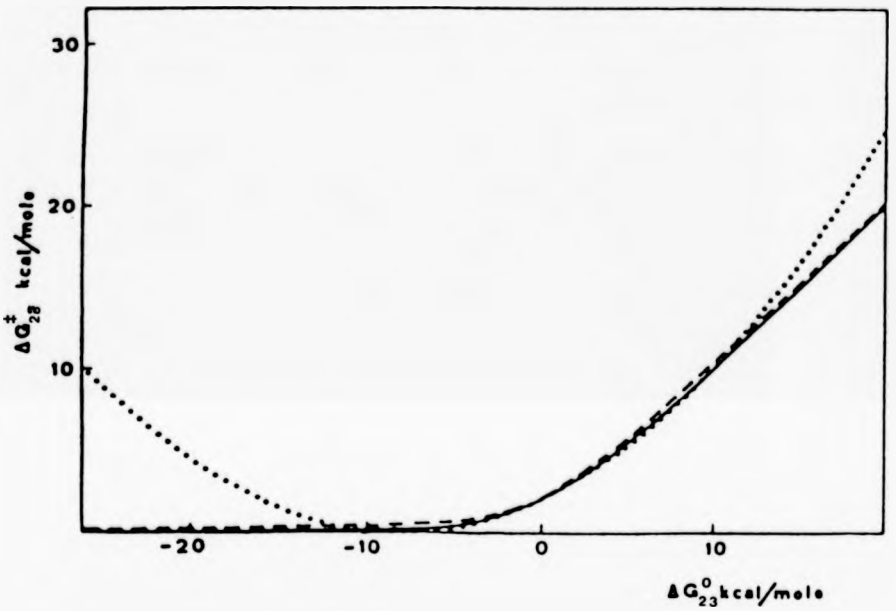

Figure 1.16 Graphical representation of the free energy relationships for electron-transfer processes:
full line, equation (1.24); broken line, equation (1.23); dotted line, equation (1.15). Calculation performed with $\Delta G^{\ddagger}_{23}(0)$ = 2 kcal mol^{-1}, taken from ref.101.

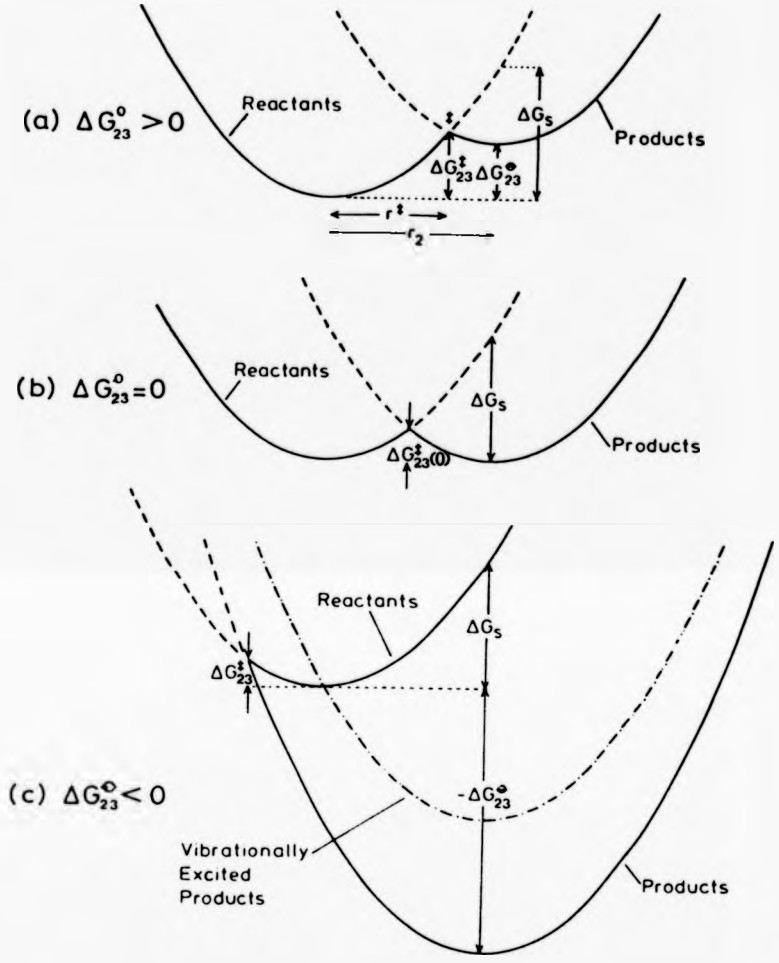

Figure 1.17 Schematic diagram illustrating the increase in the value of $\Delta G^{\ddagger}_{23}$ for outer-sphere electron-transfer reactions, in which the activated complex occurs at the intersection of similar, solvent or ligand re-organisation free energy paraboles (ΔG_s), as the value of ΔG^{*}_{23} increases from (c) the exoergonic region to (b) the isoergonic region, then to (a) the endoergonic region, taken from ref.102.

The results of substituting these equations (1,23) and also (1.24) into equation (1.20) in order to predict the rate constants is depicted in Figure (1.18). The curves consist of:

i) A plateau region for sufficiently exoergonic reactions.

ii) An Arrhenius-type linear region of slope 1/2.3RT for sufficiently endoergonic reactions

iii) An intermediate region, centred at $\Delta G^{0}_{23} = 0$, in which log k_q increases in a complex, but monotonic, way as ΔG^{0}_{23} decreases.

The variation of $\Delta G^{\ddagger}_{23}$ (O) is depicted in Figure (1.19). As its value increases, the intermediate region becomes more prominent: for values of $\Delta G^{\ddagger}_{23}$ (O) of 20-30 kcal/mol^{-1} the curve may be approximated to a straight line, for about 10 units of log k_q. It is believed that the linear free energy relationships, equation (1.22) are just such special cases. A substantially linear region has been confirmed by Shizuka *et al.* for the fluorescence quenching of aromatic molecules by the electron-transfer to halides and pseudo-halides,[104] and for quenching of triplet aromatic ketones by inorganic anions.[105] In both these studies the experimental data fitted the Polanyi equation best.

1.9 Energy Transfer

An excited state molecule may transfer its electronic energy, equation (1.25), to a ground state molecule in a number of ways. In so doing, an excited state of the energy acceptor is produced, which will be of lesser energy than that of the donor.[106-109]

$$D^{*} + A \longrightarrow D + A^{*} \qquad (1,25)$$

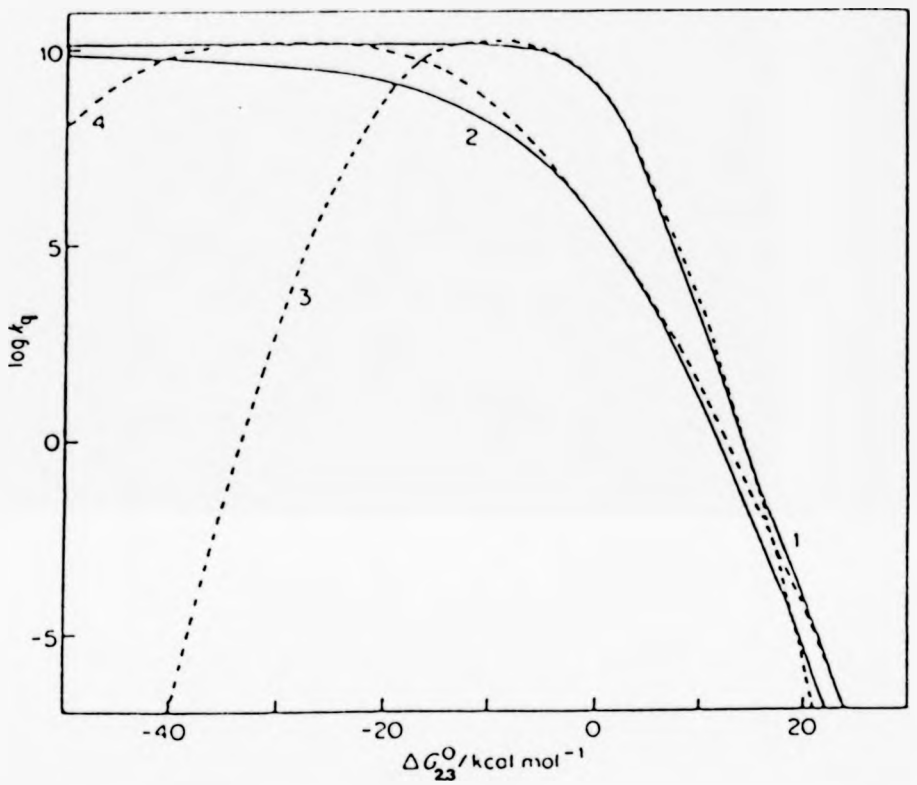

Figure 1.18 Variation of log k_q against ΔG^0_{23} by Rehm and Weller (——), equation (1.23), Marcus (- - -), equation (1.15), for $\Delta G^{\ddagger}_{23}(0)$ = 2.4 (1 and 3) and 7.2 (2 and 4) kcal mol^{-1}, taken from ref.93.

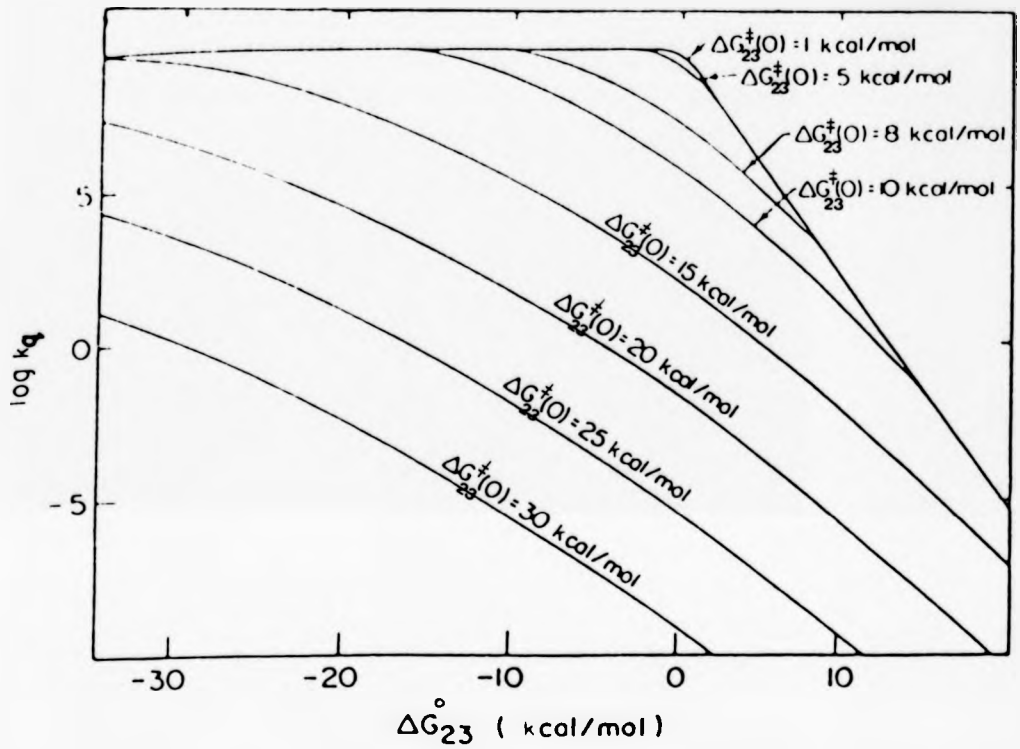

Figure 1.19 For log k_q *versus* ΔG_{23}° plots as $\Delta G_{23}^{\ddagger}(0)$ is increased from 1 to 30 kcal mol^{-1}, the intermediate region of the curve becomes more prominent. Curves calculated using equations (1.20) and (1.24), taken from ref.98.

1.9.1 Radiative Energy Transfer

This process occurs when the emitted photon from D^* is absorbed by A, the probability for absorption by the acceptor is given by the Beer-Lambert law,[110] *i.e.*, the light absorbed is proportional to the number of absorbing molecules, A.

$$\text{Absorbance} = \log \left(\frac{I_0}{I}\right) = \varepsilon.l.c. \qquad (1.26)$$

where I_0 and I are the intensities of the incident and transmitted light respectively, l is the path length (cm), c is the concentration of the acceptor (mol dm^{-3}) and ε is its molar extinction coefficient. Radiative transfer does not affect the lifetime of the excited state of the donor, but does affect its emission spectrum. In luminescence measurements these inner filter effects must be corrected.[110] The extent of the overlap between the donor emission and acceptor absorbance spectra may be expressed mathematically as a spectral overlap integral,[106,108] J, equation (1.27):

$$J = \int_0^\infty F_D(\bar{\nu})\, \varepsilon_A(\bar{\nu})\, d\bar{\nu} \qquad (1.27)$$

where $F_D(\bar{\nu})$ is the emission spectrum of the donor and $\varepsilon_A(\bar{\nu})$ is the decadic molar extinction coefficient of A at wavelengths $\bar{\nu}$. This overlap is illustrated in Figure (1.20). Radiative energy transfer to a ground state species is only allowed where there is no change in the multiplicity of the acceptor, the excitation coefficient for the singlet-triplet absorption being so low as to make the integral of equation (1.27) very small.[110]

1.9.2 Non-radiative Energy Transfer

There have been several theories put forward to explain how the energy of an excited state molecule may be transferred to an acceptor without the passage of a photon. The transfer of energy requires a close interaction between D^* and A which may be described by a perturbation Hamiltonian operator, H_{DA}.[109] The system (D^* + A) is not a stationary state of the total Hamiltonian ($H_{D^*} + A_H + H_{DA}$). If an isoenergetic system (D + A^*) exists where the excitation energy can reside on the acceptor, then time-dependent perturbation theory shows the interaction of H_{DA} will cause the system to change from (D^* + A) to (D + A^*) and *vice versa*. This degeneracy is readily achieved for organic molecules because of the many vibrational and rotational levels available. If H_{DA} is sufficiently small, as in the general case, the rate of vibrational relaxation will be much greater than the rate of energy transfer, this being especially so for energy transfer between molecules in solution. Hence, the energy of the donor will be transferred to the acceptor from the $\Delta E_{o,o}$ level after vibrational relaxation has occurred. Further, A will vibrationally relax removing the degeneracy of (D^* + A) and (D + A^*) making the energy transfer unidirectional when A^* and/or D are formed, as is usually the case, in an excited vibrational level; this process is depicted in Figure (1.21). The perturbation H_{DA} contains many components, but the major two are the electrostatic (Coulombic) and electron exchange interactions which will be discussed briefly in turn.

1.9.3 The Electrostatic (Coulombic) Term in Non-radiative Energy Transfer

This may be visualised as a transmitter-antenna mechanism,[109,110] and is illustrated in Figure (1.22a). The motions of electron 1 in D^* cause perturbation of the electron 2 in A. Energy transfer may take place if

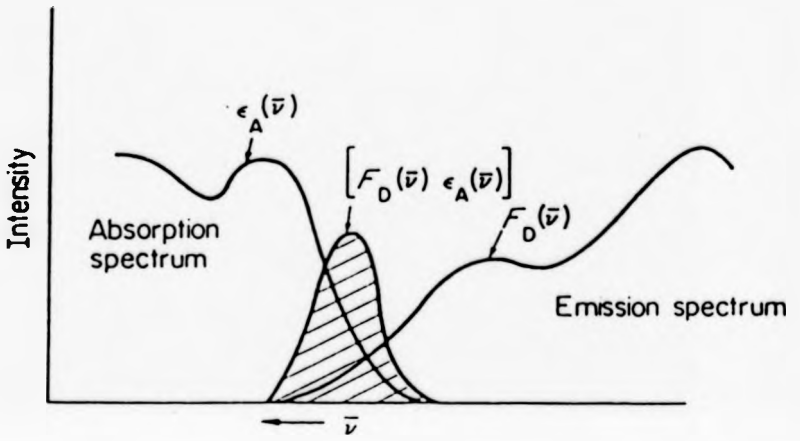

Figure 1.20 The shaded area is the integral $\int_0^\infty F_D(\bar{\nu})\,\epsilon_A(\bar{\nu})\,d\bar{\nu}$.

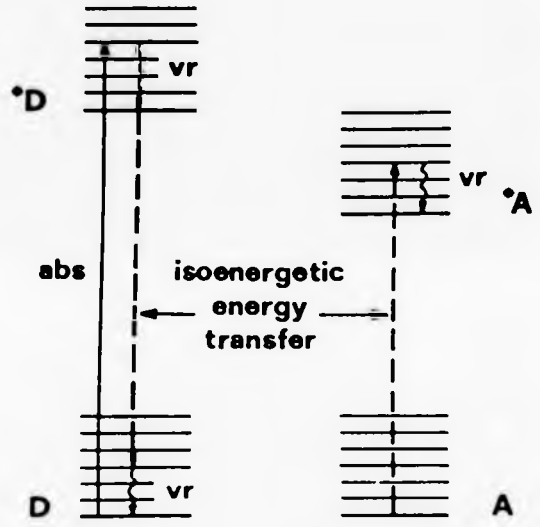

Figure 1.21 Schematic representation of non-radiative energy transfer from an excited donor, *D, to a ground state acceptor, A; "vr" indicates vibrational relaxation.

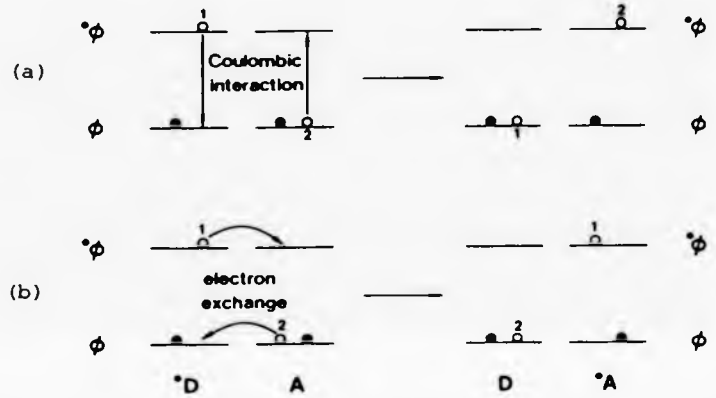

Figure 1.22 Simplified orbital representation of non-radiative energy transfer by (a) Coulombic and (b) electron exchange interactions.

resonance occurs, allowing excitation of electron 2 and relaxation of electron 1. This interaction takes place *via* the electromagnetic field, and no physical contact between D^* and A is necessary. The most important term of the Coulombic interaction is the dipole-dipole interaction[108] given by:

$$\beta_{d-d} \approx \frac{M_D \cdot M_A}{r^3} \qquad (1.28)$$

where M_D and M_A are the transition dipole moments of the $D^* \rightarrow D$ and $A \rightarrow A^*$ transitions respectively. The dipole-dipole interactions obey the same selection rules[110] as the corresponding electric dipole transitions, *i.e.*, for light emission and light absorption in the separated partners.

1.9.4 The Exchange Interaction Term in Non-radiative Energy Transfer

This requires collision between the two partners, because it involves orbital overlap, and is a quantum mechanical effect arising from the symmetry properties of the wavefunctions with respect to exchange of spin and space co-ordinates of two electrons separated by a distance r_{12} within the D-A system. The space part of the interaction is given by:[108]

$$\beta_{ex} = \int \phi_{D^*}^{(1)} \phi_A^{(2)} \frac{r^2}{r_{12}} \phi_D^{(2)} \phi_{A^*}^{(1)} \delta\tau \qquad (1.29)$$

where ϕ_A and ϕ_D are the contributions of the spatial wavefunctions to the total wavefunctions ψ_A and ψ_D. Integration over the spin co-ordinates yields the Wigner spin selection rules[108,109] (the only selection rules for this type of interaction), *e.g.*,

$$^1D^* + {}^1A \longrightarrow {}^1D + {}^1A^*$$

$$^3D^* + {}^1A \longrightarrow {}^1D + {}^3A^*$$

$$^3D^* + {}^1A \longrightarrow {}^1D + {}^3A^*$$

The transfer rate, k_{en}, is given by the Fermi golden rule[58,108]

$$k_{en} = \frac{2\pi}{h} \beta^2 \rho \qquad (1.30)$$

where ρ is a measure of the density of the initial and final states which can interact, as determined by the Franck-Condon factors, and is related to the overlap integral, J, given in equation (1.27).

The Förster[111,112] relation, equation (1.31), for the long range dipole-dipole energy transfer is obtained by substitution of equations (1.28) and (1.29) into equation (1.30):

$$k_{en}^{d-d} = 1.25 \times 10^{17} \left(\frac{\phi_E}{n^4 \tau_D r^6}\right) \int_0^\infty F_D(\bar{\nu}) \epsilon_A(\bar{\nu}) \frac{d\bar{\nu}}{\bar{\nu}^4} \qquad (1.31)$$

where ϕ_E is the quantum yield for donor emission, τ_D is the lifetime of the emission, n is the refractive index of the solvent and r is the distance in nm between D^* and A. The latter term is the overlap integral normalised to unity, *i.e.*,

$$\int_0^\infty F_D(\bar{\nu}) d\bar{\nu} = 1$$

If R_0 is taken as the distance at which energy transfer and spontaneous decay of the excited donor are equally probable, then at distance R_0 (the critical transfer radius), and making

$$k_{en} = {}^{1}/\tau_{D}$$

its substitution into equation (1.31) gives:

$$R_0^6 = 1.25 \times 10^{17} \frac{\phi_E}{n^4} \int_0^\infty F_D(\bar{\nu})\, \varepsilon_A(\bar{\nu}) \frac{d\bar{\nu}}{\bar{\nu}^4} \qquad (1.32)$$

When reasonable values are substituted into this equation, k_{en} can be expected to be larger than k_{diff} and energy transfer by dipole-dipole interaction can take place over distances of the order of 10 nm.

The short-range electron exchange interaction has been formulated by Dexter:[113]

$$k_{en}^{ex} = \frac{2}{h} KJ \exp\left(\frac{-2R}{L}\right) \qquad (1.33)$$

where R is the distance between D and A, L is the average orbital radius involved in ψ_i and ψ_B and K is a constant which is not related to any spectroscopic experimental parameter and thus, unlike R_0, has only a qualitative value. Providing R is greater than 2 nm, energy will be transferred mainly by the Förster mechanism. In solution molecular diffusion plays an important role and energy transfer becomes diffusion controlled, in the limiting case where $R_0 < 2$ nm exchange interaction becomes noticeable.

1.9.4 Singlet-singlet Collisional Energy Transfer

Absorption by the acceptor may be so sufficiently weak as to make the Förster critical distance approach the collisional diameter for the donor-acceptor pair. In such a case the rate of singlet-singlet energy transfer in fluid solution cannot be faster than the diffusion controlled rate. When the spectral overlap integral is larger, the dipole-dipole energy transfer mechanism is greatly favoured because of the large rate

constants, this process being characterised by faster than diffusion controlled rates.[106]

Many examples of this form of quenching have been provided by Dubois *et al.*[114,115] proving that the energy transfer from many donors to biacetyl takes place at diffusion controlled rates, as expected for exothermic energy transfer.

1.9.5 Triplet-triplet Energy Transfer

This phenomenon was first demonstrated by Terenin and Ermolaev,[116,117] who discovered that the phosphorescence emission of benzophenone in a ridged glass was progressively quenched with the addition of napthalene, the emission of benzophenone being replaced by the phosphorescence of naphthalene. The wavelength of excitation used could only excite benzophenone, and since the singlet energy level of naphthalene is greater than that of benzophenone, energy transfer *via* the singlet level could not have occurred, and must therefore be *via* the triplet states of the two molecules, equation (1.34):

$$^1(Ph_2C{=}O) \xrightarrow{isc} {}^3(Ph_2C{=}O) + C_{10}H_8 \longrightarrow Ph_2C{=}O + {}^3(C_{10}H_8) \qquad (1.34)$$

Triplet-triplet energy transfer in solution has also been studied. Bäckstrom and Sandros[118,119] found that the phosphorescence of biacetyl in benzene solution at room temperature was quenched at a diffusion controlled rate when the acceptor triplet level of the hydrocarbon was sufficiently below that of the biacetyl. The rate of energy transfer was found to decrease as the acceptors triplet energy was increased. Porter and Wilkinson[120] made a similar study on a variety of aromatic ketones.

1.9.6 Kinetics of Energy Transfer in Solution

In general, the transfer kinetics in solution do not follow simple Förster formulae.[108] The maximum rate of energy transfer in solution is dependent upon the rate of encounters between the excited donor and acceptor molecules.[106] If the energy of the donor excited state is insufficient to promote excitation of the acceptor (endothermic energy transfer), then the energy deficiency has to be made up by vibrational excitation.[106,121] Sandros[121] obtained equation (1.35) from simple Boltzmann distribution arguments:

$$k_q^{en} = \frac{k_d}{1 + \exp\{-[E(^*D/D) - E(^*A/A)]\}/RT} \qquad (1.35)$$

However, for a number of systems[122] the rate constants for endothermic energy transfer were found to be much higher than those obtained by the use of equation (1.35) on substituting available spectroscopic data. When systems obey equation (1.35) they are said to behave classically. The non-classical systems have donor and/or acceptor equilibrium geometries which are different for their ground and excited states. To describe these geometries Hammond *et al.*[123,124] introduced the ill-defined terms "non-vertical excitation" and "phantom triplet" for the behaviour shown by *cis*-stilbene when acting as a triplet energy acceptor. The former terms for this non-classical behaviour have been discussed by various workers[127] and yet another term called the "hot band" mechanism has been introduced, which allows a favourable distortion co-ordinate according to the Boltzmann distribution law.[122] The validity of these concepts has been, however, questioned by Bylina[125] with regard to their satisfying various Franck-Condon factors.

Another aspect of energy transfer for spin-allowed exothermic reactions is that in solvents of low viscosity diffusion controlled rates are not observed.[126] Evidence exists that intrinsic molecular factors can limit the energy transfer rates to a lower than diffusion controlled rate for some sterically hindered molecules and also for transition metal complexes,[110,127] where stepwise plots of log k_{en} *versus* $E(^*D/D)$ are obtained.[128]

1.9.7 A Classical Treatment of Energy Transfer

A classical treatment of the energy transfer process has been provided by Balzani *et al.*[129] which parallels the electron transfer process described in section (1.8.4).

Outer-sphere electron transfer and exchange energy transfer are conceptually related processes, both requiring spatial overlap of donor and acceptor orbitals. No bond breaking need take place and Franck-Condon restrictions must be obeyed, because the electronic rearrangement (with/without the electron transfer process) taking place in such a small time that the nuclear motions have insufficient time to occur. Electronically excited states involved in the bimolecular quenching process may be regarded as thermally equilibrated species, that may be considered as new chemical entities with respect to the ground state molecule.

The kinetic scheme for the energy transfer is identical to that for electron transfer, *viz.*:

$$D + h\nu \longrightarrow {}^*D$$

$$^*D + A \underset{k_{21}}{\overset{k_{12}}{\rightleftharpoons}} {}^*D\text{---}A \underset{k_{s2}}{\overset{k_{1s}}{\rightleftharpoons}} D\text{---}A^* \underset{k_{21}}{\overset{k_{12}}{\rightleftharpoons}} D + A^*$$

$$1/\tau^0 {}^*D \qquad\qquad 1/\tau^0 {}^*A$$

Scheme (1.x)

Here k_{12} and k_{21} are the rate constants for the formation and dissociation of the encounter complex, which may be taken as the same for both reactants and products in considering only physical encounters.

Using steady state approximations, assuming $1/\tau^0{}_A^* >> k_{12}[D]$, and adapting the analogies of equations (1.16) and (1.19), the full expression for the bimolecular quenching rate constant becomes:

$$k_q^{en} = \frac{k_{12}}{1 + \exp\left(\frac{\Delta G^0_{23}}{RT}\right) + \frac{k_{21}}{k^0_{en}} \exp\left\{\frac{\Delta G^0_{23} + \frac{\Delta G^{\ddagger}_{23}(O)}{\ln 2} \cdot \ln\left[1 + \exp\left(\frac{-\Delta G^0_{23} \ln 2}{\Delta G^{\ddagger}_{23}(O)}\right)\right]}{RT}\right\}} \qquad (1.36)$$

The free energy change, ΔG^0_{23} is given by:[129]

$$\Delta G^0_{23} = -E_{o,o}(^*D/D) + E_{o,o}(^*A/A) \qquad (1.37)$$

and is obtained by assuming the entropy difference between the ground and excited state is zero. The dependence of the intrinsic energy barrier, $\Delta G^{\ddagger}_{23}$, on ΔG^0_{23} is expressed by equation (1.24), assuming, as in electron transfer theory, it is the preferred form.[103] The pre-exponential factor is given by k^0_{en}. As in electron transfer processes, the intrinsic energy barrier is made up of contributions from inner-sphere, ΔG_i and outer-sphere, ΔG_0 re-organisational energies. However, contrary to electron transfer processes, ΔG_0 is usually very small because for energy transfer the electronic charges on the reactants do not change.

Comparing equation (1.35) with (1.36), it follows that when energy transfer processes have high pre-exponential factors, the ratio of k_{32}/k^0_{en} will be much less than unity, and when $\Delta G^{\ddagger}_{23}(O)$ is very small (*i.e.*, the excited states are only slightly distorted), the third term

in the denominator of equation (1,36) can be neglected. Equation (1.36) is then reduced to the Sandros equation (1.35), ΔG^{0}_{23} being given by equation (1.37). The introduction of the intrinsic energy barrier thus causes a corresponding decrease in the calculated rate constant, and the fact that an increase in observed rates has been found,[122] based on equation (1.35) is due to the rates being calculated using the vertical absorption energies of the distorted excited states of the acceptors. (These are higher than the zero-zero spectroscopic energies which would have been more appropriate.)

Equation (1.36) may be used when the quenching rate constants have been measured for the transfer between a single donor (or acceptor) by a homogeneous series of acceptors (or donors): it may be applied to evaluate unknown parameters from "best of fit" computer iteration techniques as follows:

i) The "best fit" value of $\Delta G^{\ddagger}_{23}(0)$ may be taken as a measure of the "overall" distortion of the excited states involved.

ii) The value of ΔG^{0}_{23} obtained may be used to determine the zero-zero spectroscopic energy of the acceptor (or donor).

iii) The value of k^{0}_{en} obtained allows an evaluation of the orbital spin, and (to a minor extent) Franck-Condon restrictions.

This equation has, indeed, been successfully applied to various donor and acceptor systems including stilbenes, α-diketones and metal β-diketonate complexes.[1]

1.10 Competitive Electron and Energy Transfer

When both electron transfer and energy transfer processes are favourable for the quenching of an excited state by a particular species, the two processes have been shown to occur competitively.

Whitten *et al.*[130] studied the quenching of various sensitizers by a series of dimethyltetrafluoroborate salts of various 1,2-bis(pyridyl)ethylenes These stilbene-like quenchers undergo *trans* → *cis* isomerisation relatively inefficiently upon direct irradiation, but efficiently when sensitized by high-energy triplet sensitizers (> 200 kJ mol^{-1}). The results obtained, given in Table (1.4), suggest that for benzophenone and $[Ru(bipy)_3]^{2+}$ competitive energy transfer and electron transfer quenching are occurring; in the latter case almost exclusive electron transfer is occurring for $[Ru(bipy)_3]^{2+}$ and compounds 2 and 3. The reduction products have also been detected by flash photolysis. In contrast, the not so easily oxidised 1,8-dinitronaphthalene, ($^3\Delta E_{o,o} \approx 249$ kJ mol^{-}) resulted in higher isomerisation efficiencies.

Table (1.4)

Quenching constants and isomerisation efficiencies for 1,2-bis(pyridyl)ethylene salts with different sensitizers in deoxygenated acetonitrile solutions (Reproduced from reference 130)

	Sensitizer				
	Benzophenone		$[Ru(bipy)_3]^{2+}$		1,8-Dinitro-naphthalene
BPE salt[a]	k_q /mol^{-1} dm^3 s^{-1})[b]	($\phi_{t \rightarrow c}$)[c]	k_q /mol^{-1} dm^3 s^{-1}[b]	($\phi_{t \rightarrow c}$)[d]	($\phi_{t \rightarrow c}$)[c]
1	1.8×10^9	0.40±0.05	6.1×10^6	0.45±0.05	0.41±0.04
2	n.d.	0.33±0.08	9.1×10^8	0.02±0.01	0.40±0.08
3	1.1×10^{10}	0.16±0.02	2.4×10^9	0.007	0.30±0.40

[a] 1,1,2-bis(3-pyridyl)ethylene; 2,1-(3-pyridyl)-2-(4-pyridyl)ethylene; 3,1,2-bis(4-pyridyl)ethylene.

[b] Measured by luminescence quenching at constant ionic strength.

[c] Limiting quantum yield at high (0.01 M) acceptor concentration.

[d] Extrapolated yields at infinite acceptor concentration.

Wilkinson and Tsimas[131] studied the quenching of triplet organic molecules by tris(hexafluoroacetylacetonato)chromium(III), $Cr(hfac)_3$, and tris(acetylacetonato)chromium(III), $Cr(acac)_3$. The latter compound quenched the organic triplets by an energy transfer mechanism, but for $Cr(hfac)_3$ an electron transfer process is favoured. This was explained by the substitution of the CH_3 groups in $Cr(acac)_3$ in the ligand by CF_3 groups, making $Cr(hfac)_3$ a much better electron acceptor than $Cr(acac)_3$.

1.11 Mechanisms of Radiosensitization

1.11.1 Radiosensitizers

There is now general agreement that the molecular mechanism for the action of radiosensitizers on DNA mimics the action of oxygen.[132,133] Structures of some of these are illustrated in Figure (1.23), most having the strongly electron-affinic nitro group. The drugs used must have a low toxicity and high metabolic stability, and the most important nitro-compounds so far studied are the nitroimidazoles, metronidazole (flagyl) and misonidazole, which are now undergoing clinical trials. These molecules, because of their high electron affinity, act as electron carriers and electron transfer agents enhancing radiobiological damage by increasing the effective diffusion of hydrated electrons produced by irradiation.[134]

Adams and Dewey[135] suggested that the efficiency of radiosensitization was related to the electron affinity of the sensitizer. Figure (1.23a) shows a plot of sensitization efficiencies for a range of hypoxic cell radiosensitizers as a function of their one-electron redox potential.[136,137] The one-electron reduction potentials, which are quantitative measures of electron affinities have been determined by pulse radiolysis as follows.

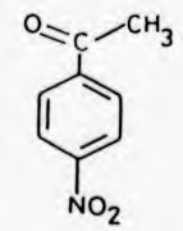

4-Nitroacetophenone
(PNAP)

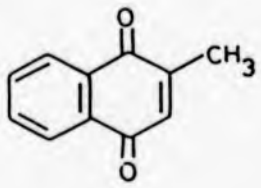

2-Methylnaphthaquinone
(Menadiene)

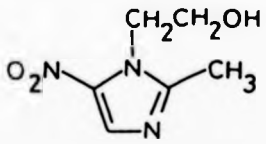

Metronidazole

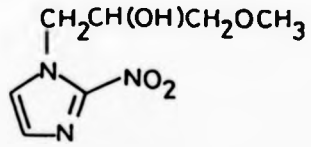

Misonidazole

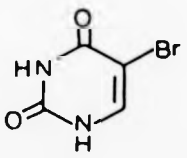

5-Bromouracil

Figure 1.23 Structures of some radiosensitizers

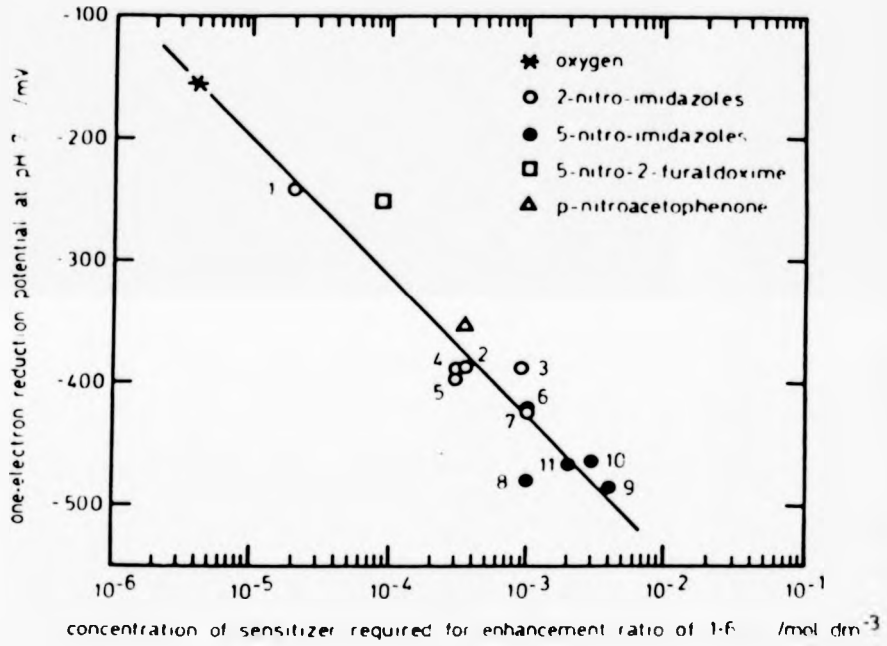

Figure 1.23a Dependence of radiosensitization efficiency of nitrocompounds with hypoxic Chinese hamster V79-379A cells in vitro with one-electron reduction potential, taken from ref. 13c

Firstly, the electron adduct of the sensitizer is formed by reaction with, for example, hydrated electrons, $CO_2^{\cdot-}$ or $(CH_3)_2COH^{\cdot}$ radicals. Single electron transfer from the adduct is allowed to take place to a standard electron acceptor such as duroquinone, [see equation (1.38)],[138] or antraquinone-2-sulphonate of known E_7^1 value which are close to that of the sensitizer. From the position of equilibrium, the difference in

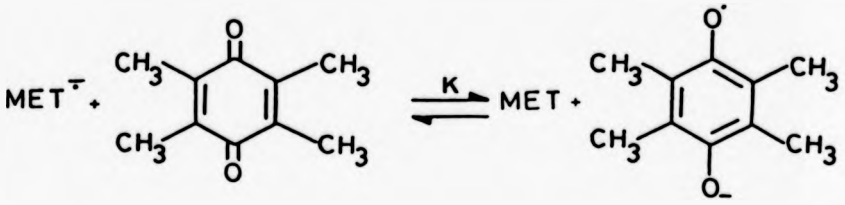

(1.38)

E_7^1 between the sensitizer and the calibrant molecule may be obtained, the equilibrium constant, K, gives the difference between the redox potentials, E_7^1, between the sensitizer and standard systems [equation (1.39)].

$$\Delta E_7^1 = \frac{RT}{nf} \ln K \qquad (1.39)$$

The concentrations of the various radical ions are determined from the transient absorption traces produced upon pulse radiolysis of the solutions.

While the electron affinity is obviously a very important property, other parameters have been investigated by use of the Hansch equation and related variants.[133,139,140] for the development and design of drugs. This equation relates the biological activity of a drug to its chemical properties or the concentration of a drug required to give some constant biological effect, equations (1.40). For example, the partition of the sensitizer in hypoxic tumour cells is of fundamental importance for effective-

$$\text{biological activity} = (\text{chemical properties})$$

$$(\text{concentration}) = f(\text{electronic}) + f(\text{partition}) + f(\text{steric}) + \textit{etc.} \quad (1.40)$$

ness *in vivo*, it is reasoned that high solubility of the drug in lipids might be a desirable feature in enhancing diffusion of the drug to the needed site. This has been tested by use of the octanol:water partition method on the sensitizers.[139] Results show that side effects, such as neurotoxicity, may be enhanced if the drug partitions itself in high-lipid-containing tissue such as brain. Once the parameters have been studied then mathematical modelling methods assess the relative importance for each chemical property on the biological activity, allowing (hopefully) improvements to be made.

The rates of electron transfer from the thymine radical anion, formed from pulse radiolysis, to various sensitizers, with their E_7^1 values, are given in Table (1.5). These results are of particular interest, because of the formation of the thymine radical anion *via* thermal electron migration in the radio-ionisation of DNA.

Table (1.5)

Second order rate constants for electron transfer from the thymine radical anion to various radiosensitizers (adapted from ref.74)

Radiosensitizer	Rate constant /10^9 dm^3 mol^{-1} s^{-1}	E_7^1 (V *versus* SCE)
4-nitroacetophenone	4.8	-0.355
2-methyl naphthoquinone	4.0	-0.240
nifuroxime	6.4	-0.253
metronidazole	3.1	-0.486
misonidazole	3.1	-0.389

The sensitizing effect of 2-methylnaphthoquinone (MQ) has been studied.[54,55] Triplet MQ, formed by 353 nm, 20 ns laser pulses, is quenched by various pyrimidines (Pyr) by a charge transfer process, equation (1.41), forming the $MQ^{\cdot-}$ anion radical and presumably the pyrimidine cation radical. The second order rate constants for this

$$^3MQ + Pyr \longrightarrow MQ^{\cdot-} + Pyr^{\cdot-} \qquad (1.41)$$

quenching are all near diffusion controlled.

Nine major photo products for the u.v.-photosensitization of thymine by MQ in oxygenated aqueous solution have been characterised.[55] Six of the photo-products, representing 70% of the thymine lost, are also formed by γ- and X-ray irradiation of oxygenated aqueous solutions of thymine and include the photohydrates. The remaining three products are thymine di-adducts formed by linkage of the N-1 to the C-5 (1.IX) or N-1 to C-6 (1.X) positions. The nine major products, formed from the MQ-sensitized photo-oxidation of thymine in water, result from subsequent reactions of the thymine radical cation *via* spontaneous dissociation along two parallel pathways, giving neutral radicals localised on N-1 and C-6 positions of the ring. These pathways are illustrated in Scheme (1.7).

Halogenated pyrimidines form another class of radiosensitizer, although their mode of action is slightly different. Cells grown in a medium containing 5-bromouracil (5BrU) or 5-bromodeoxyuridine (5-BUdR) incorporate these sensitizers into their DNA in place of thymine. Since the bromine atom has about the same radius at the methyl group in the replaced thymine, there is little distortion in the modified DNA structure. The enhanced sensitivity of these cells to ionising radiation is due to the

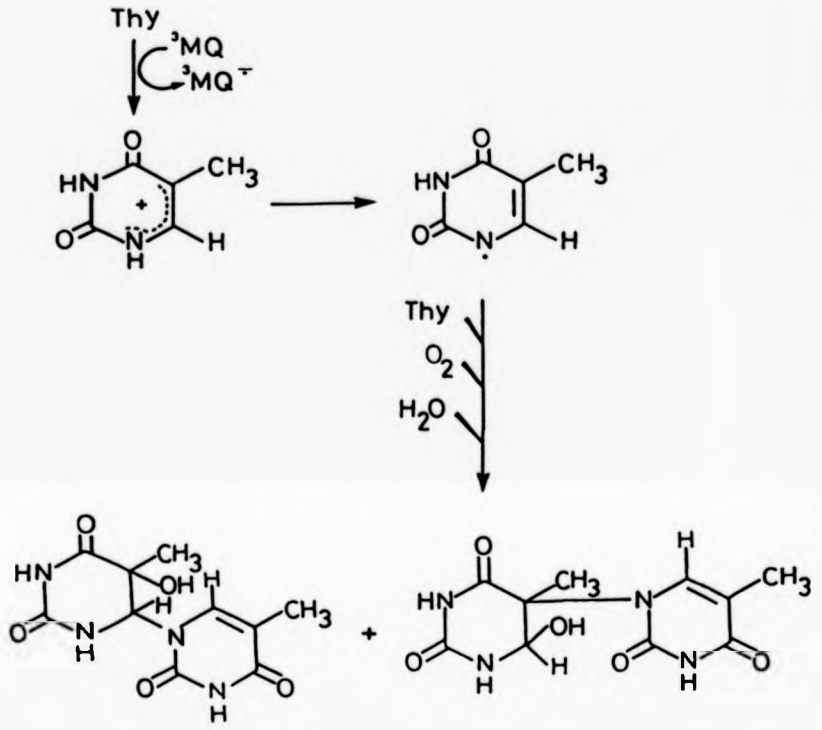

Scheme (1.7)

highly electronegative bromine atom in the incorporated base. The bromine acts as a long range trap for mobile electrons produced from the direct absorption of energy in DNA.[141]

Electron capture by bromouracil would be expected to lead to dissociation of the C-Br bond generating Br^- ions and uracilyl radicals, and has been shown to occur by Zimbrick *et al.*[142] The uracilyl radical is able to abstract H-atoms from a variety of molecules and such attack at the C-2' position of the ribose would lead to transfer of the radical centre to the DNA backbone causing chain breakage.

Energy transfer may also be important for the sensitizing effect of bromouracils; the irradiation of BrU substituted DNA by wavelengths between 254-280 nm causes single strand breakage.[143]

1.11.2 Other Types of Drugs:- the Furocoumarins

Another series of drugs which induce damage in DNA are the psoralen derivatives. The action of these drugs differs from that of the radiosensitizers because the excited state of the drug (rather than the DNA) provides the impetus for reaction. The reaction of importance is formation of the cyclobutane dimer between the nucleic acid base (in particular thymine) and the drug. The psoralen derivatives have been used successfully in the treatment of vitiligo (characterised by a loss of melanin pigmentation), mycosis fungoides (which leads to tumourous lesions) and, in particular, psoriasis.[144] The disease psoriasis is characterised by over reactive DNA synthesis and cell division in the basal cells of the epidermis. The mutation of the basel cells to squamas cells taking, as a result, 3-4 days, instead of the 28 days as in normal skin. The mechanism of these sensitizers involves the reaction of their excited states with DNA bases. Some of these sensitizers are illustrated in Figure (1.24).

Furocoumarin triplet states are quenched by nucleic acids and DNA, and the rate constants[18] vary over three powers of ten in the range $< 2 \times 10^6$ to 7.5×10^8 mol^{-1} dm^3 s^{-1}, depending on the particular quenching base

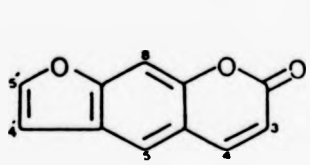

Psoralen

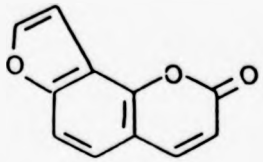

Angelicin

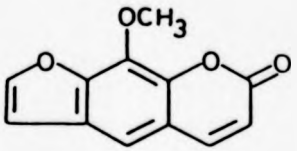

8-Methoxypsoralen

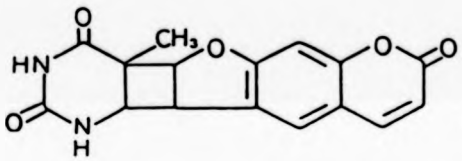

4',5'-Psoralen-thymine

Monoadduct

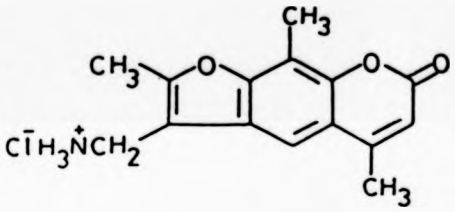

4'-Aminomethyl-4,5',8-trimethyl Psoralen

hydrochloride

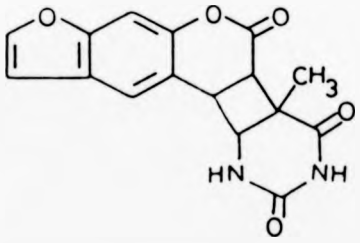

3,4-Psoralen-thymine

Monoadduct

Figure 1.24 Structures of some psoralen derivatives and their thymine adducts.

and furocoumarin. The quenching process cannot be energy transfer from the furocoumarin to the base because the bases all have much higher triplet energies. The photobiological efficiency of psoralen derivatives is probably due to their ability to form intercalation complexes with DNA. The furocoumarin is then able to photoreact successively with two pyrimidine bases forming a cross-linkage between the two separate DNA strands, which inhibits the over reactive DNA synthesis associated with psoriasis. The cross-link comprises two cyclobutane adducts formed from 3,4-pyran and 4',5'-furan double bonds with the 5,6-double bonds of two pyrimidine bases; in Figure (1.24) the bonding with thymine is illustrated. Whether these adducts within DNA are formed *via* the psoralen singlet or triplet state is uncertain. Excitation of psoralens complexed with DNA by laser flash photolysis using 347 nm pulses (a wavelength too high to excite DNA) have shown that as the concentration of DNA is increased, the yield of psoralen triplet decreases.[145] Further, when stronger chelating psoralens are used, *e.g.*, 4-aminomethyl-4-5',8-trimethylpsoralen[146] (AMT) the triplet yield is less than that observed for a weaker complexing psoralen at the same concentration of DNA. For 0.05% w/v of DNA, triplet AMT could not be observed.[147] This effect may be caused by either (i) the singlet → triplet intersystem crossing yield decreasing to practically zero, which would mean the photoreaction occurring *via* the singlet state, or (ii) the quenching of the triplet state being so efficient that it decays too rapidly to be observed by ns flash photolysis. For 8-methoxypsoralen, on the other hand, there is no decrease in yield of triplet, indicating that for different psoralen derivatives, differing quenching mechanisms occur.

The cross-linkage of DNA by AMT has been found to occur *via* a two-photon process,[148] only mono-adducts being produced after the first 15 ns, 347 nm laser pulse. Bensasson *et al.*[149] found the 4',5'-psoralen-thymine mono-adduct triplet did indeed react with another thymine molecule, the second order rate constant being 1.2×10^8 mol^{-1} dm^3 s^{-1}. Later work now indicates that it is plausible for cross-linking of DNA to occur *via* a single photon process;[150,151] and it is postulated that a conformational change in DNA has to occur within 1.3 μs[151] before a newly formed adduct can absorb a photon leading to cross-link formation. Clearly further work has still to be done in order to elucidate these complex mechanisms.

1.12 Experimental Approach

(i) Chapter 3. If triplet pyrimidine bases are able to act as electron donors to electronafficinic molecules, then the second-order quenching rates would be expected to fit the Weller equation for electron transfer. Such an approach requires that the ground state oxidation/reduction potentials of both the donor and acceptor be known. The oxidation potentials of the donor bases are not available in the literature and needed to be determined. Further, to substantiate the process of electron transfer it should be possible to observe spectroscopically the free radical anions of the electron acceptors, and in certain cases these have been observed. The implications of this electron transfer process, with regard to DNA strand breakage, are discussed in terms of the current literature concerning the charge sequestration model.

(ii) Chapter 4. Although triplet excited states of radiosensitizers have been implicated as possible intermediates in radiotherapy, there are few data on the proven nitro imidazole drugs, in particular metronidazole and misonidazole. An investigation of the triplet states of these drugs has been undertaken using laser flash photolysis. The triplet energies may be determined using the model of Balzani *et al.* for the quenching rates of triplet-triplet energy transfer. The ability of excited states to act as electron acceptors was tested using inorganic ions (*i.e.*, Br^-, I^- and SCN^-). The chosen solvent for quenching the pyrimidine bases was acetonitrile. The $E_{\frac{1}{2}}$ reduction potentials of the two drugs were unknown for this solvent and to use the Weller equation it has been necessary to determine these quantities. In all, three different methods have been applied successfully and good agreement between the results has been obtained. Finally, an attempt was made to develop a probe which can be used to determine intracellular concentrations of these drugs.

(iii) Chapter 5. This deals with the photochemical interaction with nucleic acid bases by such systems as benzophenone triplet and excited uranyl ion. An initial possibility was that these would sensitise the production of triplet base: however, it was found that although strong interaction exists, it takes the form of hydrogen-atom abstraction (by triplet benzophenone) and fast, reversible exciplex formation (uranyl ion).

CHAPTER 2

EXPERIMENTAL

2. Laser Flash Photolysis

The technique of flash photolysis is now widely used in the study of light induced fast reactions. Norrish and Porter[152] in 1949 first demonstrated that a very intense flash of light could initiate a very large range of reactions, which could be analysed optically using a second synchronised flash lamp. This allowed reactants, products, and especially intermediates, to be studied both kinetically and spectroscopically. The time resolution for the monitoring of these species, produced from the first (photolysis) flash, is dependent upon the flash duration. Early apparatus produced ms and tens of μs flashes from xenon lamps, restricting anslysis to these time domains. With the advent of pulsed lasers, lifetimes in the nanosecond and even picosecond and femtosecond regions have been measured.

2.1 Laser Flash Photolysis Apparatus

For this work two types of nanosecond pulsed laser have been used. Ultraviolet excitation was performed using a model KX-2 rare gas excimer laser built by Oxford Lasers Ltd., giving 249.1 nm, ∿200 mJ, 15 ns pulses. The second type of laser used was a model K-347 frequency-doubled Q-switched ruby laser with a pulse of 347 nm, ∿70 mJ, 20 ns, as supplied by Applied Photophysics Ltd. (London).

The KX-2 rare gas halide (RGH) laser belongs to a class of lasers known as excimer (excited dimer) lasers able to provide intense (∿15 MW) ultraviolet radiation. Laser oscillation is obtained by rapid electrical discharge excitation in a high pressure gas mixture of He, Kr and F_2. The laser transitions occur in molecules which are characterised by bound electronically excited molecular levels and very weakly bound - or

even repulsive - lower levels. This gives, in essence, complete population inversion, because after a photon has been emitted, dissociation of the molecule occurs in about 100 picoseconds, which prevents any build up of population in the lower laser level.

The excitation mechanisms of RGH lasers are not fully understood, but the following set of reactions is currently believed to include those most important for the krypton fluoride laser using helium as the support gas.

$$Kr + e \longrightarrow Kr^+ + 2e \quad \text{(slow)}$$

$$F_2 + e \text{ (slow)} \longrightarrow F^- + F$$

$$F^- + Kr^+ + He \longrightarrow (KrF)^* + He$$

$$(KrF)^* + h\nu \longrightarrow Kr + F + 2h\nu$$

The resulting high efficiency is attributed to: (a) Kr^+ being formed very efficiently in a high current glow discharge, and (b) the fact that of the energy stored in Kr^+, about 30% reappears in the emitted photon. The excited species $(KrF)^*$ has only a short lifetime ($\sim$10 ns) for spontaneous radiative decay and significant populations of the exicted levels are only achieved because its formation is extremely rapid.

In use, the laser gas builds up impurities which intefere with its lasing action, resulting in a decrease in power of the pulse. A gas purifier pumps the laser gas around a cooled bath of liquid nitrogen, where the impurities are cryogenically removed without loss either of the halogen or the rare gas.

The laser beam, see Figure (2.1), is directed onto the sample cell by means of an optical train of two lenses, a mirror and a prism producing

a high population of sample excited states. Transients are observed by means of right angle analysis incorporating a 250 watt xenon arc lamp beam close to the front face of the sample cells. The change in intensity of the analysing beam, as some of its light is absorbed by newly formed species, is monitored at a preset wavelength (between 200 nm and 800 nm) by the analysing high radiance monochromator and photomultiplier tube (either a Hamamatsu R666S or R.C.A. model I.P.28). The band pass may be selected between 1 nm and 20 nm. The light gathering power of >0.25 allows a satisfactory photomultiplier signal-to-noise ratio to be obtained with a reasonable bandwidth. The transient photomultiplier output is recorded on a Tetronix model 7623 storage oscilloscope, equipped with model 7A15A (Y) and 7B50 (X) amplifiers. The oscilloscope is triggered externally by means of a 10 mV, 5 ms synchronised output pulse with a delay of <100 ms from the laser discharge. The trace is stored on the oscilloscope and photographed using Polaroid type 46L film employing a Telford type A oscilloscope camera. The film transparencies are fixed using a Polaroid Dippit containing a solution of 0.03 mol dm^{-3} of tin(IV) tetrachloride in propan-2-ol. The fixed negatives are then enlarged using a Johnson V/4-S enlarger onto graph paper, and the curves are then digitised manually and rate constants obtained from linear regression analysis.

The ruby laser set up is illustrated in Figure 2.2. The lasing material is a cylindrical ruby rod, which is an alumina crystal in which 0.5% of Al^{III} has been replaced by Cr^{III}. The Cr^{III} ions are excited to the $^4T_{2g}$ state by an intense flash of light from a flash tube sitting parallel to and above the ruby rod; the electrical discharge causing the flash comes from a 680 μF capacitor bank charged to 2 kV, with a 3 kV trigger voltage. Rapid intersystem crossing populates the ^2E_g

state of the Cr^{3+} ions from which the characteristic red 694 nm emission occurs. At both ends of the rod is a pair of parallel mirrors, one of which is partially transparent. These mirrors are separated by an integral number of half-wavelengths and as a result, reflected light from the mirrors will be in phase with the incident wave, causing constructive interference. When a population inversion has been achieved, (*i.e.*, more Cr^{3+} ions are excited than remain in the ground state), spontaneous emission provides a few photons, which on collision with excited Cr^{3+} ions, stimulate the latter to emit in phase with the incident photon. Thus the wave builds up in intensity. One giant pulse is produced by use of a Q-switch. This is a bleachable dye of vanadyl phthalocyanin in nitrobenzene, which acts as a shutter placed in front of the rear, fully-reflecting mirror. This prevents laser action taking place until it is opened, when the beam is intense enough to cause bleaching, allowing population inversion to reach levels very much higher than the lasing threshold. Once the dye is bleached, stimulated emission occurs very quickly and all excess energy is lost in the time taken for light to traverse between the mirrors a few times, the dye reverting back to its normal state within a few nano seconds if the light has fallen sufficiently low. The laser pulse (694 nm, 1 J, 20 ns) is frequency-doubled using a crystal of rubidium dihydrogen arsenate (RDA) thermostatted at 323 K. This process of second harmonic generation of the laser beam is inefficient and reduces the laser power to about 70 mJ. The remaining 694 nm light is removed by passage of the beam through a solution of copper sulphate. The laser beam is reflected and focussed onto the sample cell, and the arrangement for the analysing beam, monochromator and oscilloscope system is the same as that

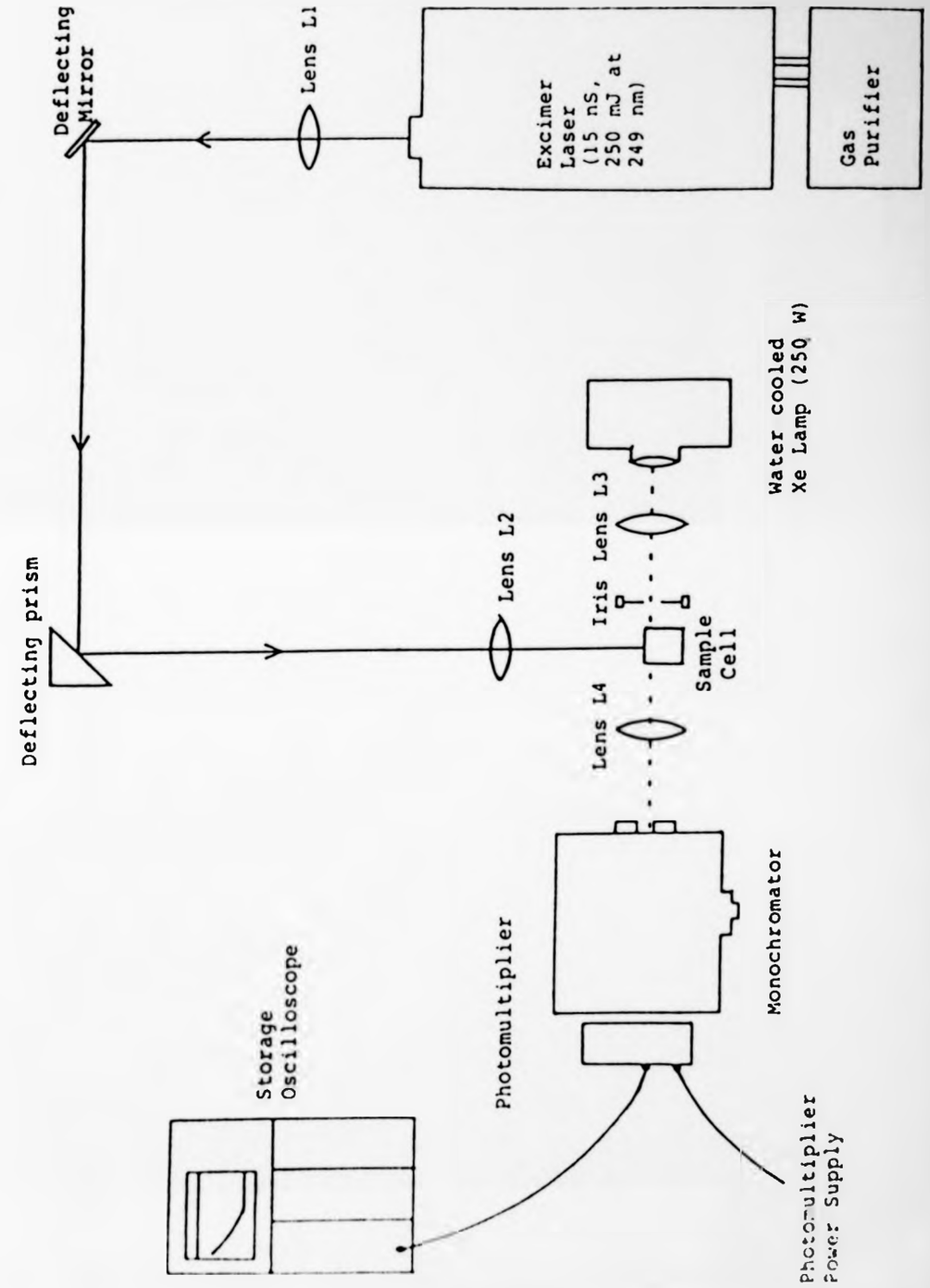

Figure 2.1 Rare gas halide excimer laser flash photolysis assembly.

Figure 2.2 Ruby laser flash photolysis assembly

described for the excimer KX-2 laser above. The triggering and cell alignment is different, however, triggering of the Tektronix model 7623 storage oscilloscope being performed externally by means of a photo-diode picking up back scatter of the laser beam from the RDA crystal and housing. The photo-diode signal is displayed on an Iwatsu model DMS-510 digital storage oscilloscope, allowing variation of laser pulse intensity and multiple pulsing to be monitored. Two types of cell alignment were employed. For emission work, no analysing beam is necessary, while for excited state absorption studies, a co-linear alignment, depicted in Figure (2.2) was used. Traces were analysed using the photographic method described above, with the exception of the study of the fluorescence quenching of pyrene butyric acid and luminescence of ruthenium metal complexes (see Chapter 4), in which an assembly consisting of a video camera and a BBC model B microcomputer was used as described in Appendix A.

2.2 Other Instrumentation

Fluorescence studies were made using a Perkin Elmer MPF-3 double beam spectrofluorimeter. The double beam configuration means that spectra are corrected automatically for variations in excitation lamp intensity. Monitoring of emission is performed at right angles to the excitation beam, which reduces effects from scattered and transmitted light. The source of excitation is a 150 W xenon lamp, the beam from which passes through a monochromator, allowing an excitation wavelength of between 200 nm and 800 nm to be selected with a band pass of 1 nm to 40 nm. Emission is detected *via* a similar monochromator by a photomultiplier having its output fed to a chart recorder. Both emission and excitation wavelengths may be scanned at preset speeds by means of a motor to give

either emission or excitation spectra, depending on whether the emission or excitation wavelength control is engaged.

Visible and ultraviolet absorption measurements were made either with a Shimadzu model 365 or Perkin-Elmer model 552 spectrophotometer. Infra-red spectra were obtained using a Perkin-Elmer model 580B spectrophotometer.

Pulse radiolysis work was carried out at Mount Vernon Hospital (Northwood, Middlesex) using a linear electron accelerator (pulse of 2 μs, 1.8 meV) with the help of Dr. P. Wardman, to whom I express my thanks.

2.3 Syntheses

2,3-Diphenylindenone Oxide.[153] To diphenylindenone (2.82 g, 9.5×10^{-3} mol) in hot ethanol (300 cm^3) was added H_2O_2 (5% vol, 15 cm^3) and sodium hydroxide (5 cm^3, 4 mol dm^{-3}). The red solution was stirred for 15 minutes after which its colour changed to light yellow. The product was precipitated by the addition of distilled water (150 cm^3), and filtered, dried and recrystallised to a constant melting point of 142-3 °C (lit., 142-3 °C)[153] using a mixture of ethanol/water (25:1); yield 2.94 g (68%).

Cis-*Dicyanobis(2,2'-bipyridine)ruthenium(II).*[154] This was a two-stage synthesis with an intermediate of oxalatobis(2,2'-bipyridine)-ruthenium(II)-4-hydrate.[155] A mixture of potassium pentachloroaquo-ruthenate(III) (0.5 g), potassium oxalate (0.75 g) and water (20 cm^3) was heated on a steam bath for 1 hour, after which a solution of bipyridine (0.4 g) in ethanol (5 cm^3) was added, and heating continued for a further 3 hours. Upon cooling this solution, crystals appeared which were filtered, washed with warm water until the washings became pink in colour, and finally rinsed with ether. The crystals were then air dried. The crude yield was 46%.

After drying, the crude oxalatobis(2,2'-bipyridine)ruthenium(II) (0.39 g) was dissolved in methanol (50 cm^3) and a solution of sodium cyanide (0.5 g) in water (12.5 cm^3) added. The reaction mixture was refluxed for 16 hours until no starting material could be detected by t.l.c. on silica gel using methanol as eluent. Apart from products, a spot with an R_f of zero was also observed. After evaporation to dryness at room temperature, the residue was extracted with two 15 cm^3 portions of boiling water. The solid was air dried, dissolved in methanol and treated successively with a 1 g portion of silica gel and a 1 g portion of alumina; after each treatment the sample was filtered hot. T.l.c. showed no starting material remaining, but the unidentified impurity (R_f = 0) still to be present. This impurity was removed by passage through a 10 cm column of alumina, and a 10 cm column of silica gel, the eluent being methanol. T.l.c. showed only the product, which was recrystallised twice from boiling water. The overall yield was 0.17 g, *i.e.*, 24%.

2.4 Purity of Chemicals

Acetonitrile used was manufactured by Fluka (Switzerland). On comparison with other makes, this was found to give both the highest transmission at 249 nm and the longest lived solute triplets by laser flash photolysis. Acetonitrile purified according to various methods[156] was of equal quality.

Diethylacetal was removed from dioxane (1 l) by refluxing this solvent with concentrated HCl (14 cm^3) and water (100 cm^3) for 12 hours with a steady stream of N_2. After cooling the solution, KOH pellets were added slowly with shaking until no more would dissolve and a second layer had separated. The dioxane was decanted and treated with fresh

Table 2.1 Purification of organic compounds according to ref.156. Each compound was recrystallised from given solvent until literature m.p. was obtained, where no m.p. determination was possible, due to decomposition, 2 x recrystallisation was performed.

Compound	Solvent	M.p. (° C)
9,10-Dicyanoanthracene	Benzene	238-239
5-Nitroindole	Water:Ethanol (8:2)	139-141
1-Pyrenebutanoic acid	Water:Ethanol (7:3)	
N,N,N',N'-tetramethyl-*p*-phenylenediamine	Ethanol	49-51
Thymidine	Ethylacetate	185
Thymine	Water	326
Uracil	Water	Decomposition

KOH pellets to remove any aqueous phase. Finally, the dioxane was dried by refluxing over sodium for 9 hours until freshly added sodium stayed bright. The dioxane was then distilled twice under completely anhydrous conditions. Other organic solvents used were of commercially available spectroscopic or analytical grade and were used without purification. Compounds which could be obtained as "Gold Label" purity or analytical grade were used without further purification. Compounds not available in high purity grades were purified according to Table 2.1.

2.5 Sample Preparation

Excimer laser excited state absorption studies were carried out using a 1 cm x 1 cm quartz fluorescence cell fitted with a narrow bore teflon tap. Deoxygenation of samples was carried out by bubbling the samples with high purity argon (B.O.C. 99.999%) for 15 minutes. Acetonitrile solutions of the pyrimidine bases were made up by making a saturated stock solution and aliquots of this were diluted to 10 cm^3, giving an O.D. of 2.1 at 249 nm. This ensured that substantial absorption of the laser pulse took place at the front of the cell. Laser alignment was crucial to obtain usable excited state absorption traces for the pyrimidine bases, which are generally very weak. Initially alignment was achieved using a solution of 1,2,3,4-dibenzanthracene (6.0×10^{-5} mol dm^{-3}); when an absorption trace maximum of >50% had been obtained, fine alignment was made using a solution of the base until an absorption trace of about 10-15% was achieved.

Emission work using the excimer laser was performed using a similar cell as above and with the same sample preparation. For co-linear alignment using the ruby laser excitation source, a quartz 2 cm diameter x 2 cm length cylindrical cell, fitted with a narrow bore teflon tap, was used.

Emission work using the ruby laser was carried out using a round glass tube of 1 cm bore.

Since all excited state lifetime measurements made are extremely sensitive to impurities, all glassware was cleaned by soaking in chromic acid solution, rinsed thoroughly with distilled water and dried before use.

2.6 Analysis of Results

2.6.1 Fluorescence Measurements

The results from fluorescence quenching experiments were analysed by means of the Stern-Volmer equation (2.1):

$$\frac{\Phi_f^\circ}{\Phi_f} = \frac{I_f^\circ}{I_f} = 1 + K_{sv}[Q] \qquad (2.1)$$

where Φ_f° and Φ_f are the quantum yields for fluorescence respectively in the absence and presence of a known concentration of quencher [Q]. I_f° and I_f are the intensities of fluorescence with and without quencher. The Stern-Volmer constant K_{sv} equals $k_q \tau_0$ where k_q is the second order bimolecular quenching rate constant and τ_0 is defined as the fluorescence lifetime in the absence of any quencher; this is the reciprocal of its first order decay constant equation (2.2):

$$\tau_0 = 1/k_0 \qquad (2.2)$$

2.6.2 Excited-state Absorption Measurements

Absorption spectra for transients were obtained by measuring from the oscilloscope the percentage transmission of the displayed transient, a pre-determined time after the laser pulse, with the monochromator set to a particular wavelength. This procedure was repeated at different

monochromator wavelength settings until the complete spectrum in the spectral region of interest had been obtained. The excimer laser gives reproducible (within 2%) pulse intensities and correction of spectra is unnecessary. The ruby laser pulse intensity, however, can vary from point to point, making correction of spectra necessary. This was done using the second digital oscilloscope (see Section 2.1). The displayed peak height was directly proportional to the laser beam's intensity.

For kinetic studies, it is assumed that the Beer-Lambert law is obeyed, and at any given time (t) the absorption of the transient may be calculated:

$$\text{Absorbance} = \log_{10}\left(\frac{I_0}{I_t}\right) = \varepsilon_\lambda C_t l \qquad (2.3)$$

where I_0 and I_t are the values of light transmission at t = 0 and t = t respectively. ε is the extinction coefficient at wavelength λ, C is the concentration of the species at time t, and l is the path length in cm.

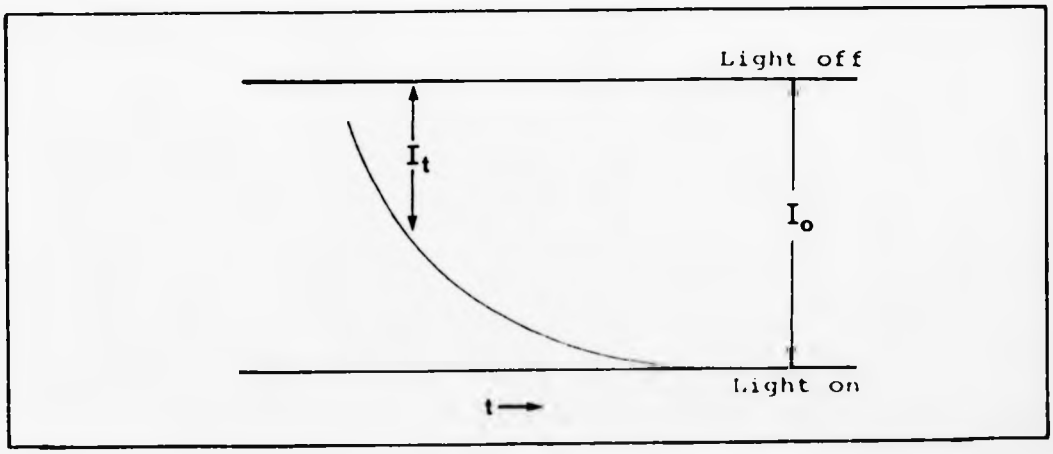

Figure 2.3 Representation of a transient absorption decay curve.

In order to use the trace, see Figure (2.3), to evaluate a rate constant, a value of the light-off position is required. This is obtained by closing down the lamp shutter. Measurements of I_0 and I_t, after graphical enlargement are utilised in the first order rate equation:

$$\ln(\frac{C_0}{C_t}) = kt \qquad (2.4)$$

and substitution of equation (2.3) for C_t gives:

$$\ln(\log_{10}\frac{I_0}{I_t}) = \text{constant} - kt \qquad (2.5)$$

hence the first order or pseudo-first order rate constant (k) may be evaluated.

The bimolecular second order rate constants for the quenching of the excited states by various quenchers was obtained from equation (2.7). The observed increase in the rate of decay (k_{obs}) was plotted against variation of quencher concentration [Q], while k_o is the rate of decay of the excited state in the absence of quencher.

Both first and second order rate constants were determined with the use of linear regression computer fitting procedures.

$$k_{obs} = k_o + k_2[Q] \qquad (2.7)$$

For weak transients (>80% transmission) traces were enlarged on the oscilloscope by use of an "offset box". This replaces the 50 Ω terminator, necessary for elimination of RC time constant effects[157] of the photomultiplier output signal to the λ amplifier of the oscilloscope. When the "offset box" is turned on, the negative voltage output from the photomultiplier is offset by a small positive voltage, the value of which

is dependent upon the increase in sensitivity. This effectively lifts the light-off setting upwards, allowing the negative I_0 value to be displayed on the oscilloscope screen as the sensitivity of the Y amplifier is increased. The value of I_0 is determined by turning the "offset box" off and reading between the values of light-off and light-on signals as normal. The offset box, see Figure 2.4), was built by Mr. A.W. Colburn (Warwick University) to whom I wish to express my thanks.

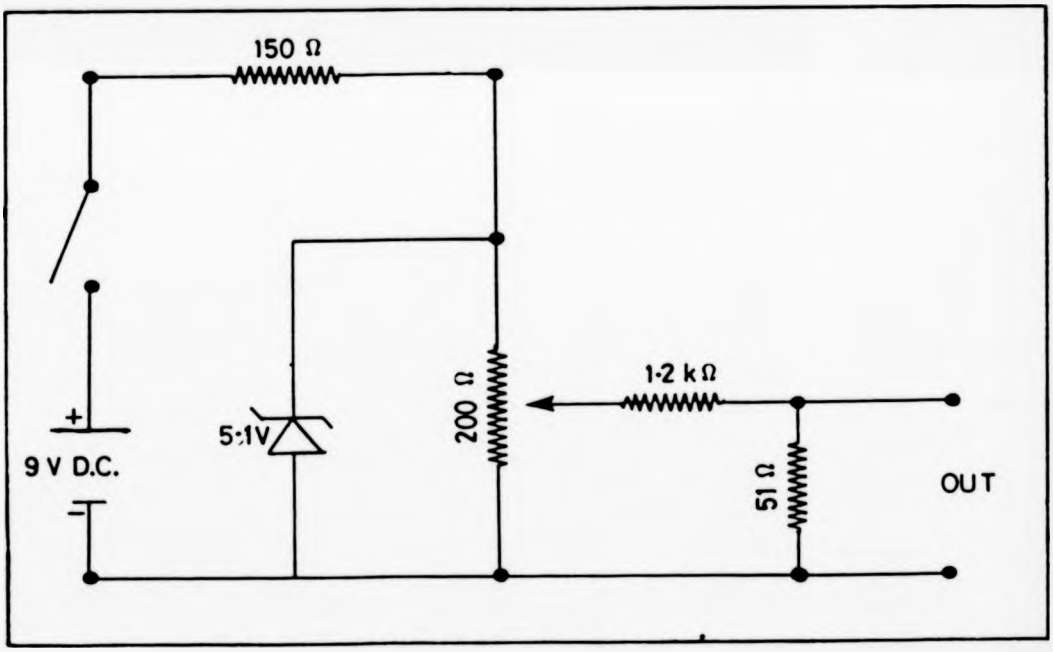

Figure 2.4 Circuit diagram for 'off-set' box used in recording weak transient absorptions

2.6.3 Yields of Anions

When the initial charge up voltage of the KX-2 excimer laser is varied from 41 kV to 21 kV, the laser pulse intensity is altered, see Figure (2.5). Lowering of the pulse energy leads to a lesser yield of excited states produced by the photolysis flash. Provided the extinction coefficient of the transient produced at the monitoring wavelength is known, its concentration may be determined from measurements of the oscilloscope absorbance trace and use of the Beer-Lambert law, equation (2.3). A plot of triplet base yield for solutions of base only against anion yield from a solution of base and acceptor, for the various voltages, gives a slope of fractional yield for the formation of anion from excited base. All yields were corrected for inner filter effects by calculating the percentage of laser light not absorbed by the base.

2.6.4 Data Fitting Procedures

Computer programs were used to calculate energy transfer and electron transfer parameters for quenching systems studied (see Appendix B). Both programs enable calculation of certain parameters by best fitting of experimental data to theoretically derived equations, *e.g.*, the Rehm and Weller equation for electron transfer. Fitting is obtained by varying the necessary values for the parameters to be determined using 'Do and Continue' loops, calculating a theoretical value and comparing it to the value obtained by experiment. Each comparison gives a sum of errors squared value; calculated parameters which have the minimum error value are taken as the value. The programs are written in Fortran and were run on a Burroughs B6800 main frame computer.

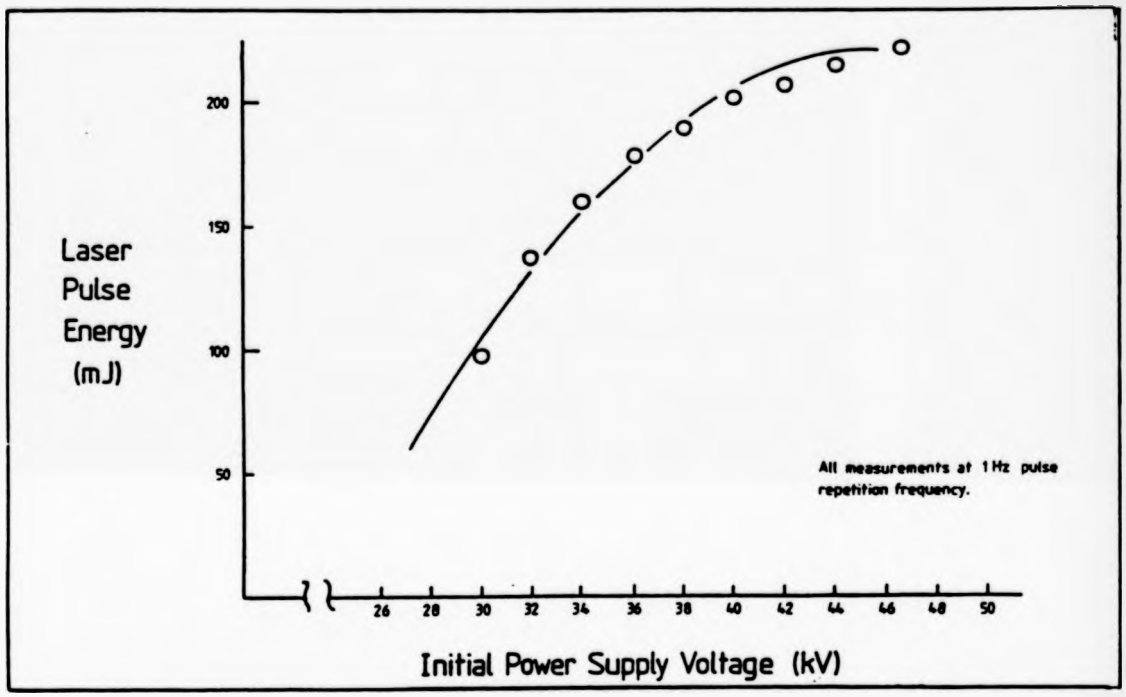

Figure 2.5 ⊙-Variation of KX-2, KrF filled, excimer laser output energy *versus* initial charging voltage; graph supplied by Oxford Lasers Limited, U.K.

CHAPTER 3

Evidence for Electron Transfer from Triplet Excited Pyrimidine Bases to Radiosensitizing Drugs

3. Quenching of Triplet Pyrimidines by Electron Acceptors

3.1 Kinetic Data

The triplet-triplet absorption spectra obtained from the laser pulsing (249 nm, 15 ns, 200 mJ) of deoxygenated acetonitrile solutions of thymine and uracil are given respectively in Figures (3.1) and (3.2). These spectra agree reasonably well with those of Salet and Bensasson,[75] and not with those reported much earlier by Hayon.[79] Attempts to monitor these triplets in water were unsuccessful due to their very small concentrations as a consequence of the very low values for ϕ_{isc} for these molecules. Also attempted generation of these triplet bases by pulse radiolysis of dioxane, acetone, or toluene solutions failed.

The lifetimes of both these triplet states were found to decrease in the presence of various electron-accepting molecules, including the clinical radiosensitizing drugs metronidazole and misonidazole. The resulting second order quenching rate constants are given in Table (3.1); also included are various other parameters of the acceptors.

The quenching mechanism of these systems may be either energy transfer or electron transfer. As can be seen from Table (3.1), the triplet energies of all the quenchers lie below those of thymine (315 kJ mol^{-1})[60] and uracil (329 kJ mol^{-1}).[60] In cases where the difference between the triplet energies of base and acceptor is greater than 12-17 kJ mol^{-1}, the rate of energy transfer would be expected to equal the diffusion-controlled rate.[106]

For an electron-transfer process the quenching rates are expected to fit the equation due to Rehm and Weller[51] (1.20) correlating the rates and the thermodynamics of electron transfer quenching of photo-excited states.

Table 3.1 Correlation of log k_2 with reduction potential in MeCN for the quenching of triplet excited thymine and uracil by electron acceptors

	Quencher	$k_2/10^{10}$ dm^3 mol^{-1} s^{-1}				$-E_{1/2}^{a,b}$	Quencher triplet energy
		Thymine	(±)	Uracil	(±)	V *vs* SCE	/kJ mol^{-1}
1.	1,4-dinitrobenzene	0.482	(0.035)	-		0.71	-
2.	2-methylnaphthoquinone	0.515	(0.036)	-		0.77[c]	244[h]
3.	misonidazole	0.360	(0.031)	0.624	(0.059)	0.97[d]	ca.245[i]
4.	metronidazole	0.426	(0.036)	1.31	(0.11)	1.10[d]	245[i]
5.	4-nitrotoluene	0.138	(0.015)	0.391	(0.045)	1.20	243[j]
6.	nitroethane	0.0148	(0.00078)	0.0749	(0.0042)	1.42	283[k]
7.	1-nitropropane	0.0255	(0.00087)	-		1.458	-
8.	nitromethane	0.0299	(0.0015)	0.0408	(0.0020)	1.46	301[k]
9.	1-nitrobutane	0.0115	(0.00079)	0.036	(0.0023)	1.48	-
10.	1-nitropentane	0.0165	(0.00076)	0.0502	(0.0058)	1.515	-
11.	1,2-dinitrobenzene	-		0.445	(0.033)	0.81	-
12.	1-chloro-4-nitrobenzene	-		0.630	(0.046)	1.06	-
13.	fumaronitrile	-		0.527	(0.042)	1.3[e]	-
14.	2,6-dimethyl-1-nitrobenzene	-		0.285	(0.034)	1.402	-
15.	2-methyl-2-nitropropane	-		0.0456	(0.0036)	1.7	-
	$[Fe(CN)_6]^{3+m}$	0.938	(0.046)	-		-0.44[f]	
	irreversible electron transfer from triplet thymine						
	tetranitromethane	2.3	(0.028)	-		1.4	
	5-bromo-uracil	0.219	(0.021)	-		1.62[g]	307[l]

[a]Measured in MeCN with respect to SCE using 0.1 mol dm^{-3} $NR_4^+ClO_4^-$ (R = Et or n-Pr) as the supporting electrolyte. [b]Except where indicated otherwise, values are taken from ref.158. [c]From ref.159. [d]See section (4.1). [e]From ref.160. [f]From ref.161. [g]From ref.162. [h]From ref.163. [i]See section (4.1). [j]Based upon the figure for 2-nitrotoluene taken from ref.164. [k]From ref.165, a second, lower, value is also given; CH_3NO_2 (156 kJ mol^{-1}) and $C_2H_5NO_2$ (150 kJ mol^{-1}). [l]From ref.166. [m]MeCN solutions with 10% water.

Figure 3.1 O-Triplet-triplet absorption spectrum of thymine (2.6×10^{-4} mol dm^{-3}) in MeCN. Full line-spectrum from Salet and Bensasson.[75]

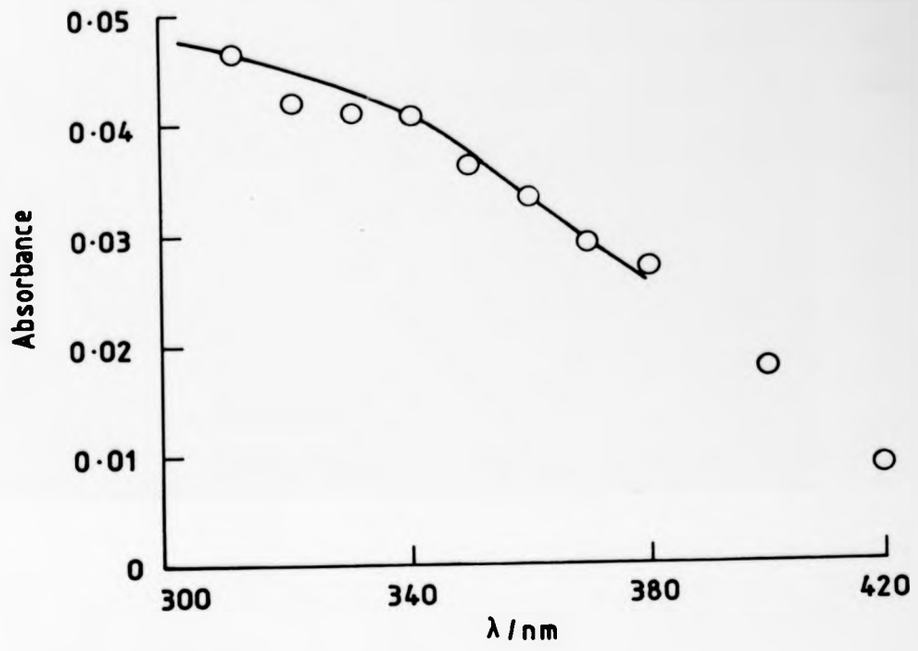

Figure 3.2 O-Triplet-triplet absorption spectrum of uracil (3.4×10^{-4} mol dm^{-3}) in MeCN. Full line-spectrum from Salet and Bensasson.[75]

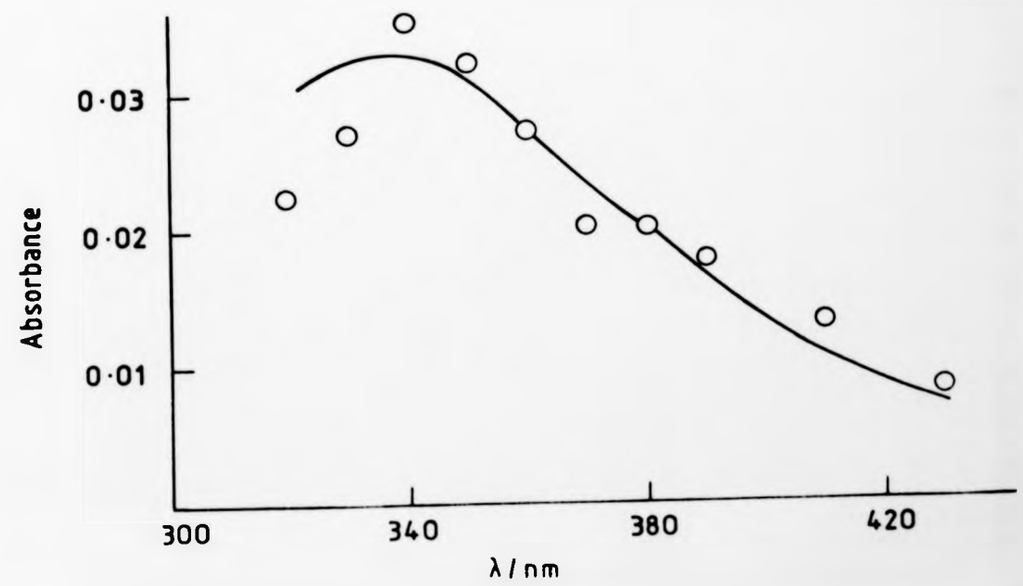

However, in order to apply this equation it is necessary to establish the ground state oxidation/reduction potentials for the donor/acceptor and the relevant excited state energy of the reactants involved, equation (1.21).

3.2 Measurement of Oxidation Potentials of Thymine and Uracil

(i) Electrochemical determination

Attempts to measure the oxidation potentials for thymine and uracil in acetonitrile have proved difficult,[162] the main reasons being interference from impurities present in the acetonitrile, *e.g.*, water, and oxidation of base electrolyte.

At our request, Dr. N. Connelly of Bristol University, examined both thymine and uracil in acetonitrile by cyclic voltammetry with platinum electrodes, finding very weak waves corresponding to the oxidation potentials, respectively, of *ca.* 2.0 V and *ca.*2.3 V *versus* SCE. Dr. Connelly views these figures as tentative, but nonetheless to correspond to real irreversible oxidation of the bases.

(ii) Indirect photochemical method

The fluorescence of 9-cyanoanthracene (CNA) and 9,10-dicyanoanthracene (DCA) has been quenched by a wide variety of reducing substances,[167] the rate constants being related to the half-wave oxidation potentials of the electron donors through the Weller equation.[53] The fluorescence of both CNA and DCA in methanol was quenched by thymine, and the Stern-Volmer plots for thymine are illustrated in Figures (3.3) and (3.4). The Stern-Volmer constants were converted to second-order rate constants using the following lifetimes for CNA (17.2×10^{-9} s)[168] and DCA (15.1×10^{-9} s)[169] in methanol. Due to the very low solubility of thymine in acetonitrile, methanol was the solvent chosen for this approach. By fitting second-order rate constants

for thymine quenching of both $^1CNA^*$ and $^1DCA^*$ between two neighbouring values for each acceptor from the tabulated data given by Erikson and Foote,[167] the values for $E_{1/2}$ (oxidation) fell within narrow ranges of values, see Table (3.2). A similar 'bracketing' method was applied to thymidine. The ranges for the oxidation potential of thymine are 1.52 to 1.62 V (for CNA) and 1.52 to 1.91 V (for DCA), *i.e.*, a figure of 1.7 ± 0.2 V seems acceptable. The analogous figure of thymidine is 1.6 ± 0.1 V. These are roughly compatible with the electrochemical data for thymine, *i.e.*, $E_{ox} \approx 2.0 \pm 0.1$ V.

Table 3.2 Estimation of $E_{1/2}$ (ox) for thymine and thymidine by comparison of k_2 for the fluorescence quenching of CNA and DCA by various electron donors

	Quencher	k_2 /10^{10} dm^3 mol^{-1} s^{-1}	$E_{1/2}$ /V *versus* SCE
CNA	Durene	0.0175	1.62
	Thymine	0.059 (±0.0035)	
	1,1-Diphenylethylene	0.105	1.52
DCA	Biphenyl	0.306	1.91
	Thymine	0.36 (±0.024)	
	1,1-Diphenylethylene	0.849	1.52
	1,1-diphenylethylene	0.849	1.52
	Thymidine	1.08 (±0.071)	
	Anisole	1.22	1.76

(iii) E_{ox} from relation with ionisation energy

Several equations relating gas phase ionisation potentials with solution oxidation potentials have been suggested,[93] and with such a relation,

equation (3.1),[170] literature ionisation potentials[171] (IP) of 9.43 eV (thymine) and 9.82 eV (uracil) led to E_{ox} values of 2.48 V and 2.83 V *versus* SCE respectively.

$$E_{ox} = (0.92\ IP) - 6.2 \qquad (3.1)$$

These figures, while high as expected, seem unrealistically so and may simply reflect the inadequacy of such correlations at their extreme.

(iv) Values from iteration of triplet quenching data

Whilst the above methods (i) and (ii) provide a useful indication of the values of E_{ox} for the pyrimidines, they do not yield very precise estimates. This difficulty was resolved, however, by the use of a computer iteration technique which attempts to fit quenching data to the Weller equation.[53] The program WELLEREKQ, given in Appendix B and devised by ourselves, optimises as adjustable parameters both the oxidation potential and the intrinsic energy barrier, $\Delta G^{\ddagger}_{2\,3}$ (0), improving the fit between k_2 and $\Delta G^{0}_{2\,3}$, see section (1.8.5).

To verify that WELLEREKQ could correctly estimate the oxidative potential of a donor, the literature results for the quenching of tris(2,2'-bipyridine)-ruthenium(II), $[Ru(bipy)_3]^{2+}$, by various organic electron acceptors[172] were used. The program yielded for the ground state potential $E_{1/2}$ for $\{[Ru(bipy)_3]^{3+}/[Ru(bipy)_3]^{2+}\}$ a figure of 1.25 ± 0.05 V *versus* SCE, which is in very good agreement with the electrochemical value of 1.29 V.[173] The second parameter $\Delta G^{\ddagger}_{2\,3}$ (0) was estimated as 13.60 kJ mol^{-1}, which compares with the commonly accepted empirical figure of 10.04 kJ mol^{-1}.[53]

The data for the quenching of thymine and uracil yielded the parameters collated in Table (3.3). The kinetic data are related to the reduction potentials of the quencher in Figures (3.6) and (3.7); using the parameters from Table (3.3), we were able to compile the complete Weller-type curves depicted in Figure (3.8) for thymine and uracil.

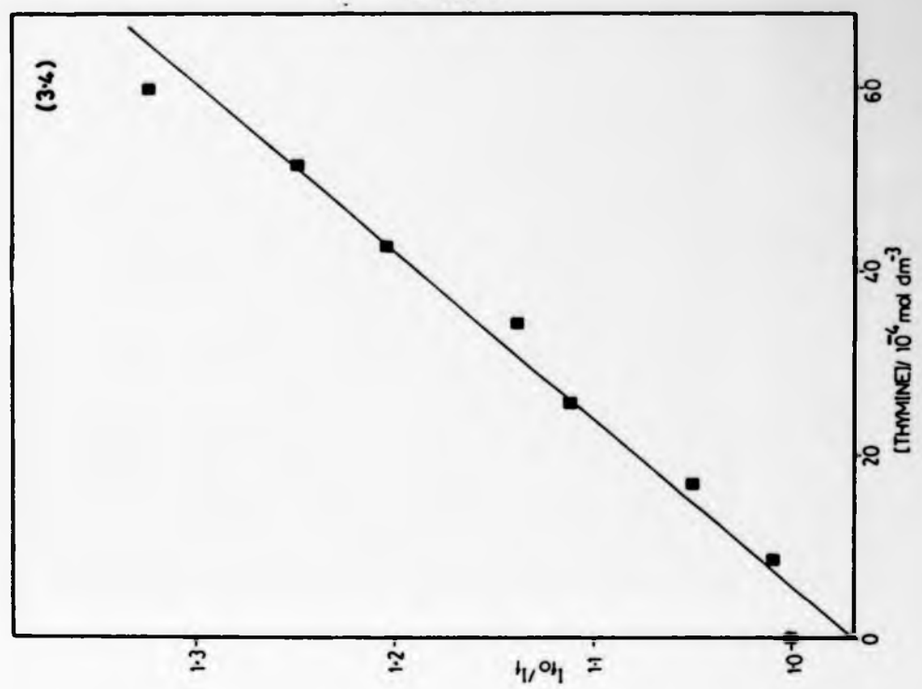

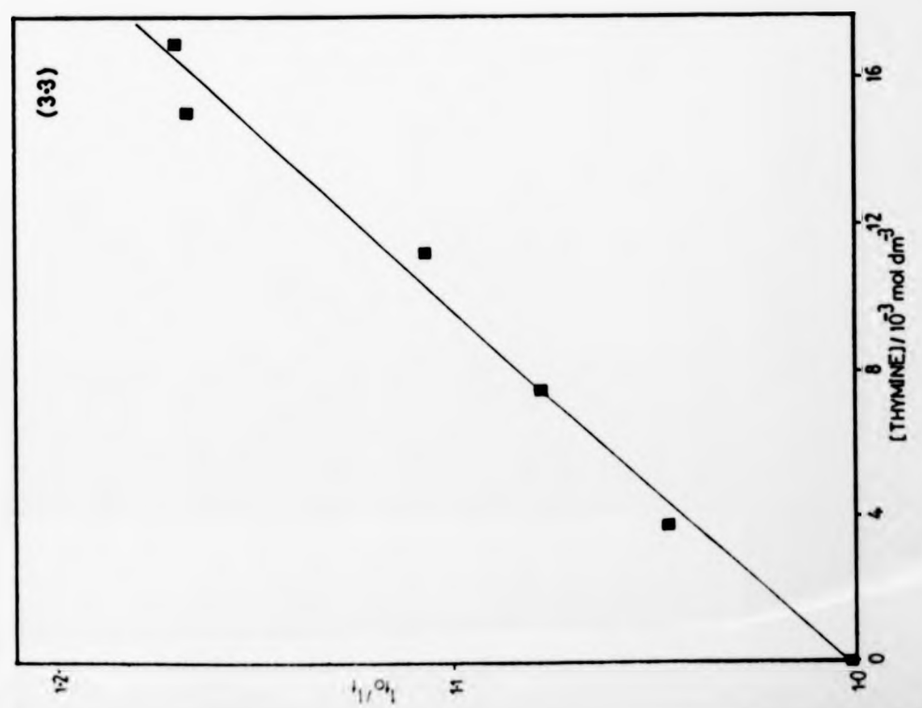

Figures 3.3 and 3.4 Stern-Volmer plots for the quenching of 9-cyanoanthracene (2×10^{-5} mol dm^{-3}), (Figure 3.3), and 9,10-dicyanoanthracene (6.0×10^{-6} mol dm^{-3}), (Figure 3.4), by thymine in methanol.

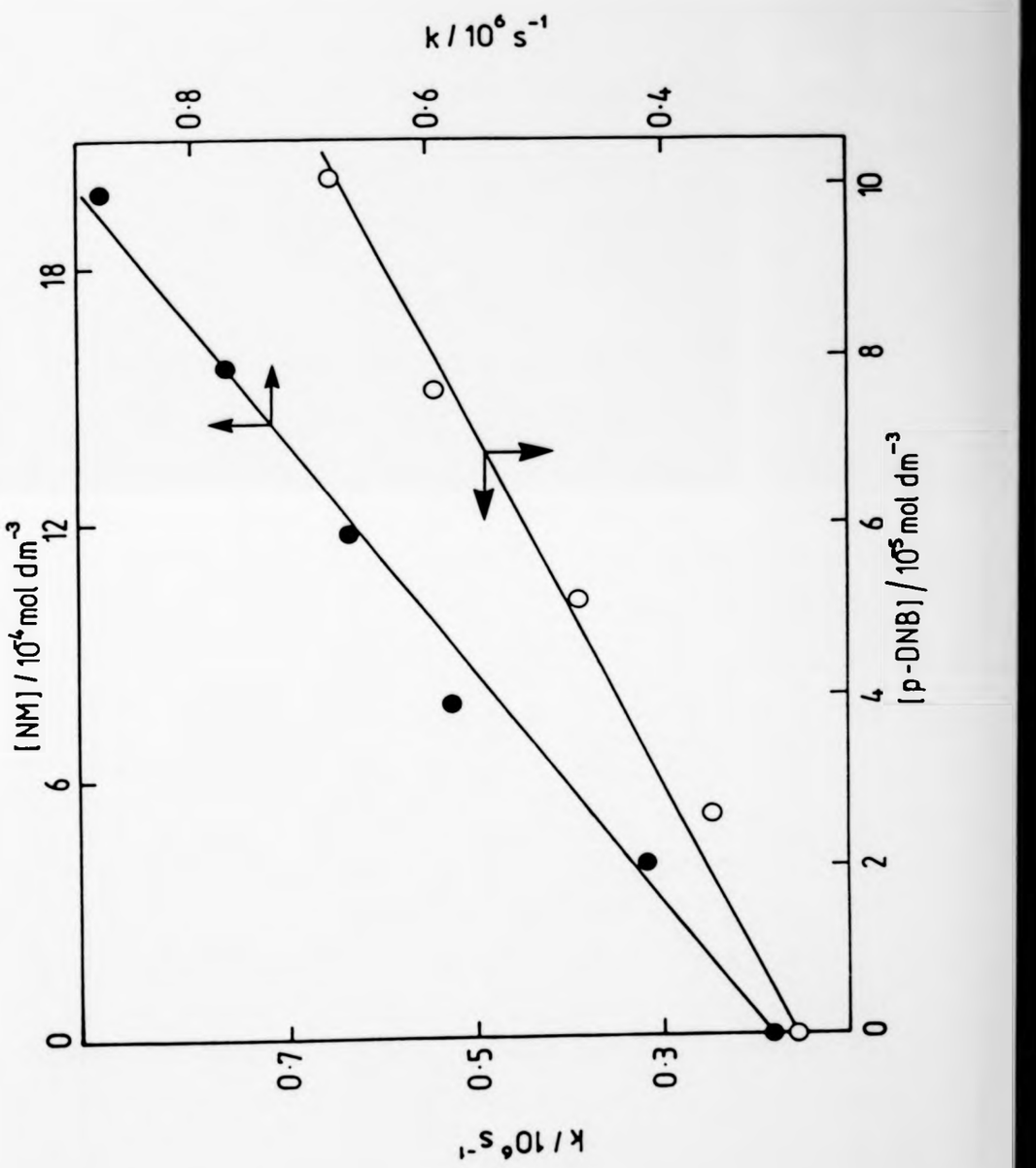

Figure 3.5 Typical plots for the determination of the second-order rate constants for quenching of triplet thymine by various electron acceptors in acetonitrile. The two examples are 1,4-dinitrobenzene (*p*-DNB) and nitromethane (NM).

Table 3.3 The curve fitting parameters obtained from WELLEREKQ for the quenching of triplet thymine and triplet uracil by electron acceptors to the Rehm-Weller equation

	$\Delta G^{\ddagger}_{23}$ (O) kJ mol^{-1}	E^0 ($D/D^{\dagger}$) V *versus* SCE
Thymine	16.5 (±0.05)	1.75 (±0.05)
Uracil	6.7 (±0.05)	2.05 (±0.1)

3.3 Observation of Semi-reduced Acceptor Species

It was possible to observe directly after the laser pulse the presence of the semi-reduced species $A^{\cdot -}$ (A = acceptor) or its breakdown product. This was so when the acceptor was galvinoxyl or $C(NO_2)_4$, when galvinoxyl anion and $C(NO_2)_3^-$ respectively were formed in experiments where >90% of the incident 249 nm pulse was directly absorbed by the base. The transient absorption spectra obtained for both of these anions are given in Figures (3.9) and (3.10).

3.4 Efficiency of the Electron Transfer Process

Variation of the laser pulse intensity resulted, as expected, in concomitant variation in both the triplet base yield and, when the acceptor was present, in the yield of the semi-reduced species. This provided a useful means of examining the degree of electron transfer from triplet base to acceptor and of verifying that $A^{\cdot -}$ was produced solely by a monophotonic process, *i.e.*, absorption of light by pyrimidine base followed by excited state electron transfer. Excitation of solutions of acceptor at the same concentration as in the electron transfer experiments gave only minute quantities of $A^{\cdot -}$ (even when there was no inner-filter effect due to the pyrimidine base). Addition of the pyrimidine gave at least a

Figure 3.6 Correlation of log k_2 with reduction potentials in MeCN for the quenching of triplet excited thymine by electron acceptors. Full line-theoretical curve derived from Rehm-Weller equation using the parameters E^0 $(D/D^{\cdot+}) = 1.75 \pm 0.05$ V *versus* SCE $\Delta G^{\ddagger}_{2,3}$ (O) = 16.5 kJ mol^{-1}. Numbering based on Table (3,3).

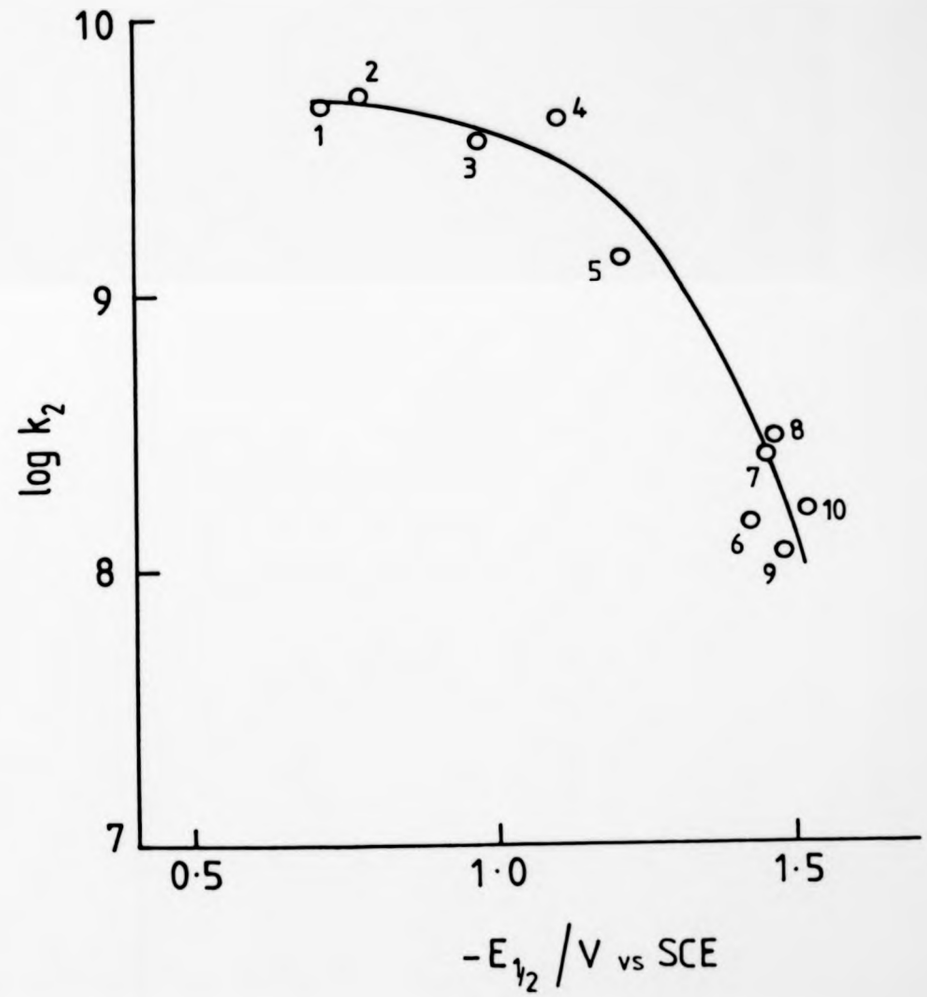

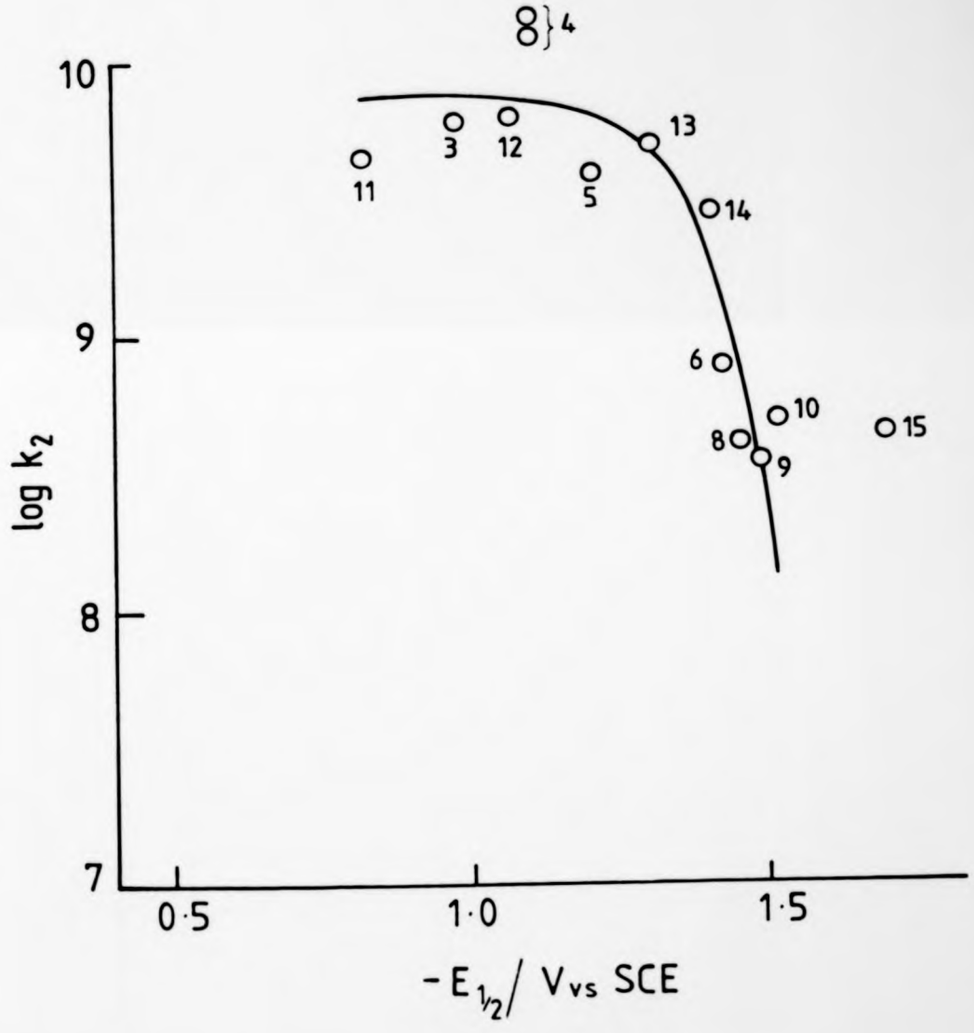

Figure 3.7 Correlation of log k_2 with reduction potential in MeCN for the quenching of triplet excited uracil by electron acceptors. Full line-theoretical curve derived from Rehm-Weller equation using the parameters E^0 ($D/D^{\bullet}$) = 2.05± 0.1 V *versus* SCE, $\Delta G^{\ddagger}_{23}$ (O) = 6.7 kJ mol^{-1}. Numbering based on Table (3.3).

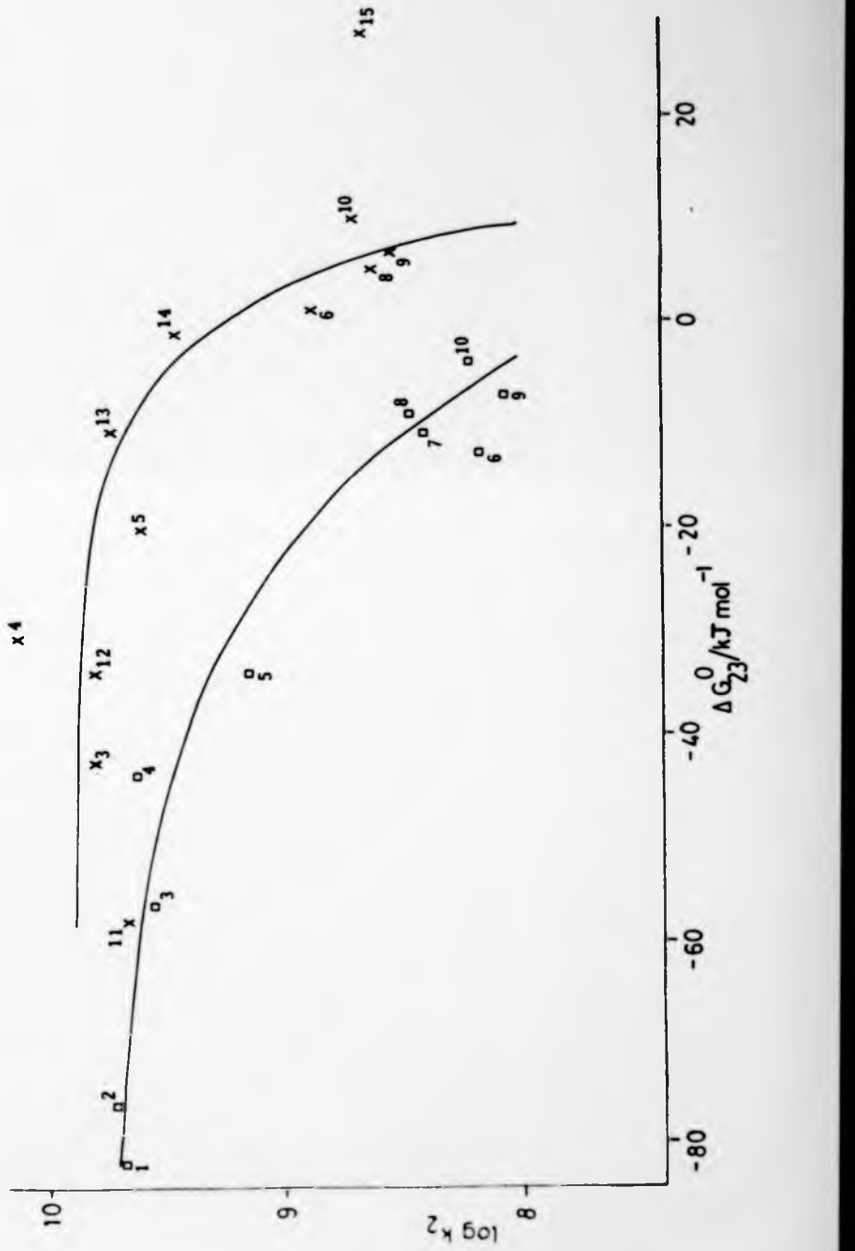

Figure 3.8 Complete Weller type curves for the quenching of triplets thymine (□) and uracil (✕) by various electron acceptors.

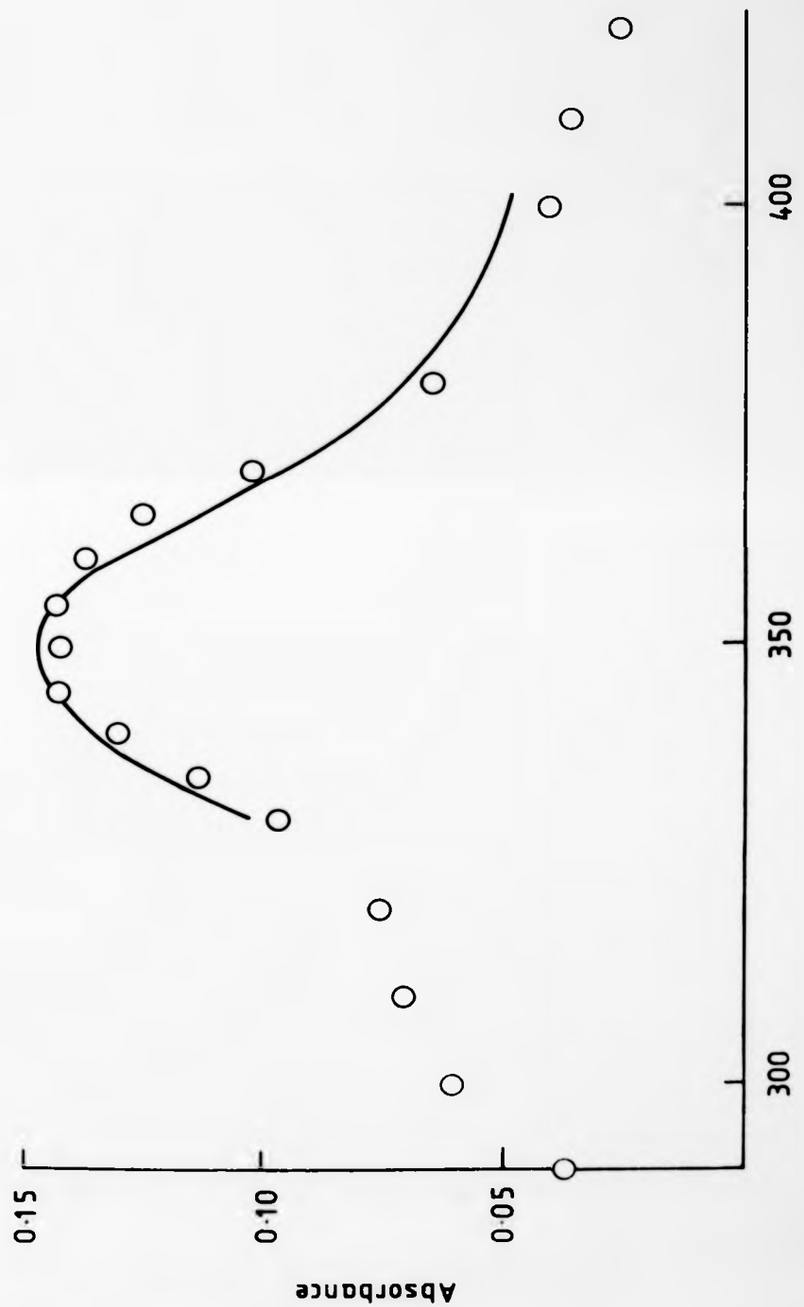

Figure 3.9 Transient spectrum (O) formed on 249 nm laser flash photolysis of thymine (2.6×10^{-4} mol dm^{-3}) and $C(NO_2)_4$ (9.32×10^{-4} mol dm^{-3}) in MeCN. Full line:literature spectrum of $C(NO_2)_3^-$ taken from ref.174.

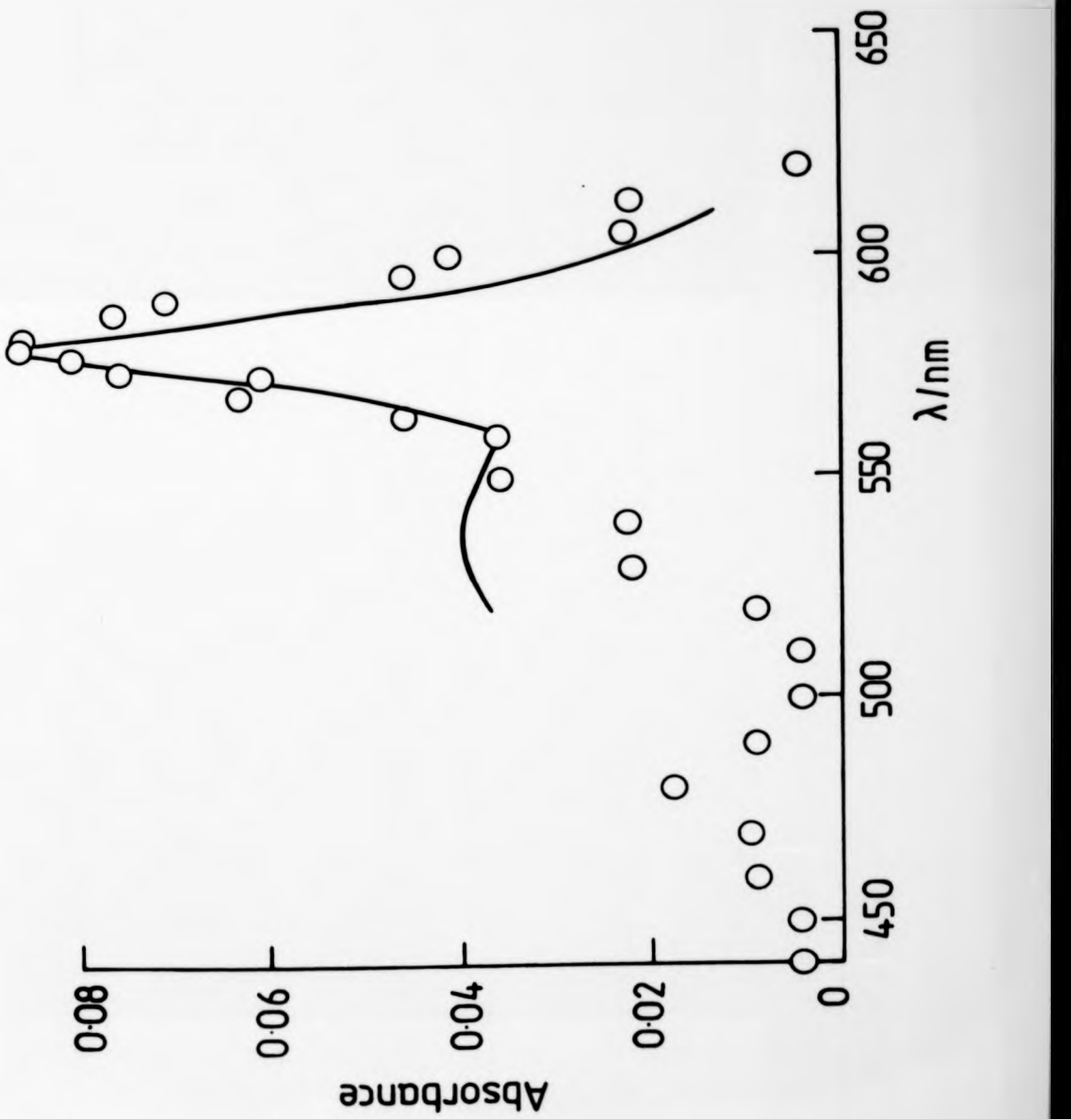

Figure 3.10 Transient spectrum (O) formed on 249 nm laser flash photolysis of thymine (2.6×10^{-4} mol dm^{-3}) and galvinoxyl (9.5×10^{-5} mol dm^{-3}) in MeCN. Full line:literature spectrum of galvinoxyl anion from ref.175, this line shows a small additional absorption in the region 525-540 nm suggestive of an extra species.

five times enhancement of $A^{\cdot-}$ and, after allowing for the inner filter effect of the base, this means a 50-fold enhancement.

Relating the absorbances of triplet base with those of the acceptor anions through the extinction coefficients of both sets of these transients, Table 3.4, enables a quantitative estimate to be made of the degree of conversion. Plots of the concentrations of $A^{\cdot-}$ *versus* those of triplet base, Figures 3.11 and 3.12, are linear and afford the following conversion yields: for $C(NO_2)_3^-$, 0.69 ± 0.03 (for thymine), 0.402 ± 0.03 (for uracil) and for galvinoxyl, 0.023 ± 0.002 (for thymine) and 0.013 ± 0.0005 (for uracil). The ready dissociation of $C(NO_2)_4^{\cdot-}$ according to equation (3.3)[176] presumably accounts for the much higher level of charge separation.

$$C(NO_2)_4^{\cdot-} \rightarrow C(NO_2)_3^- + NO_2 \qquad (3.3)$$

Table 3.4 Absorption data

Species	monitoring wavelength (nm)	ε /dm^3 mol^{-1} cm^{-1}	Reference
Triplet thymine	310	4500	75
Triplet uracil	340	2750	75
Galvinoxyl anion	580	220000	175
$C(NO_2)_3^-$	350	15000	176

Increasing the dielectric constant of the solvent would be expected to enhance charge separation of the ions.[175] The solvent dielectric constant was increased by the additions of small amounts of water (0-10% v/v) to acetonitrile solutions of the base and acceptor. Additions greater than 10% v/v caused the yield of triplet base to fall below accurately measurable levels of detection.

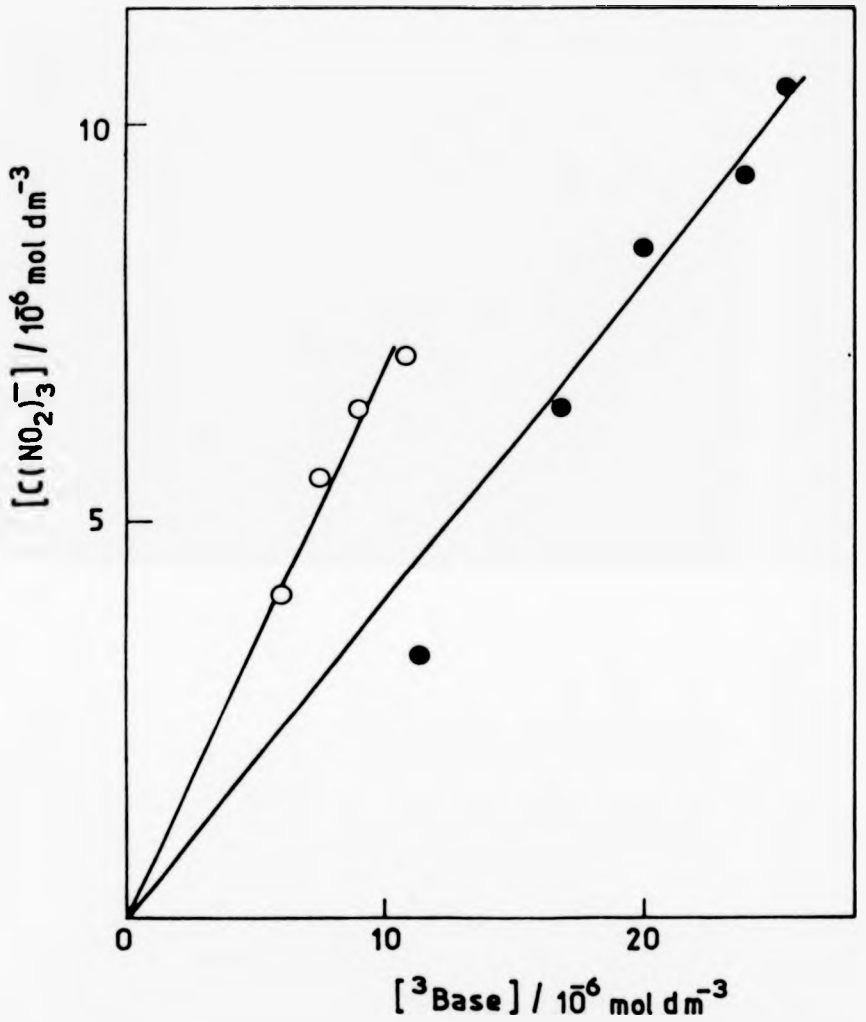

Figure 3.11 Variation of yield of $C(NO_2)_3^-$ with yield of triplet thymine (O) and triplet uracil (●) in MeCN.

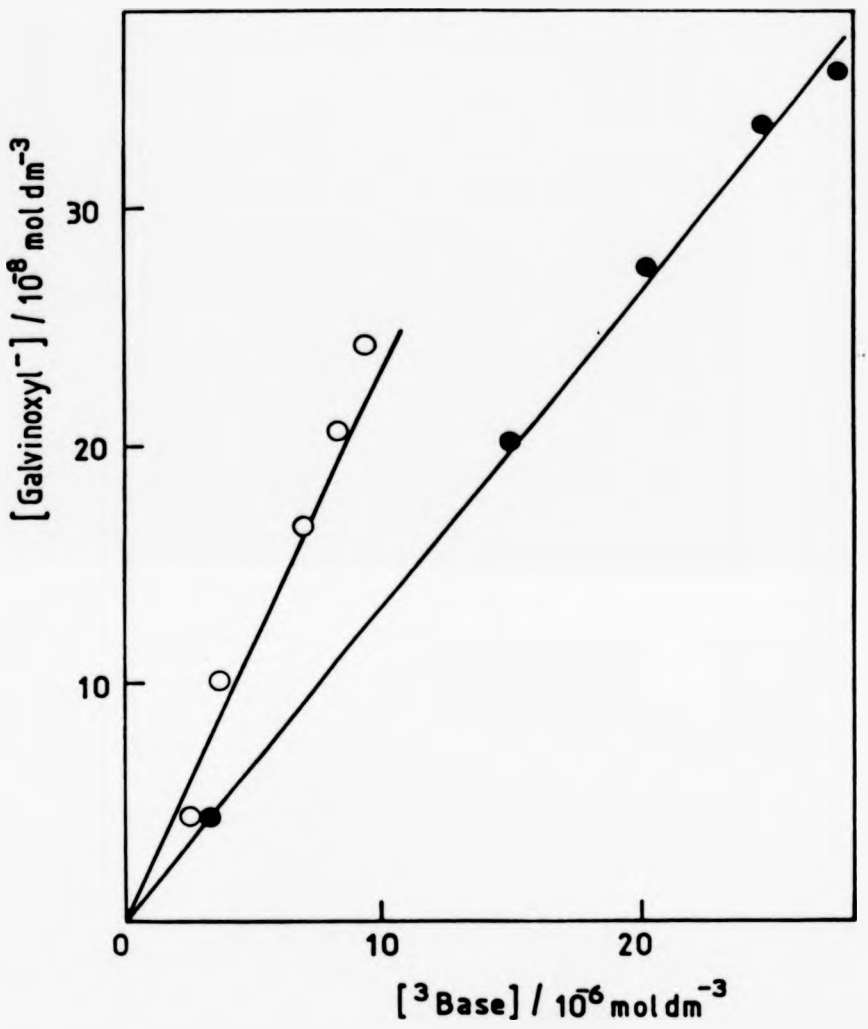

Figure 3.12 Variation of yield of galvinoxyl⁻ with yield of triplet thymine (O) and triplet uracil (●) in MeCN.

For the galvinoxyl$^-$/thymine system there was no noticeable increase in anion yield, whilst for $C(NO_2)_3^-$/thymine, a yield considerably greater than 1.0 was obtained when the addition of water exceeded 6% see Figure (3.13). This indicates the presence of some further reaction leading to the production of the anion which does not occur in the absence of water. The NO_2 formed from equation (3.3) reacts with water according to equation (3.4).[177]

$$2NO_2 + H_2O \longrightarrow HNO_2 + HNO_3 \qquad (3.4)$$

However, nitric acid is oxidising and would not therefore be expected to react with $C(NO_2)_4$.

One possible explanation is that in the presence of water some of the base is photo-ionised according to equation (3.5), producing e^-_{aq} which is known to react with $C(NO_2)_4$ producing $C(NO_2)_3^-$.[176]

$$\text{Base} \xrightarrow{254\ nm} \text{Base}^{+\cdot} + e^-_{aq} \qquad (3.5)$$

Pyrimidine cations have been produced by very intense KrF laser pulsing of finely divided crystalline powders of the bases.[178] The cations were detected using time of flight mass spectrometry after being ejected from the crystal and the source chamber by a field pulse. Further, several DNA base π-cation radicals have been produced by low temperature uv-photolysis of the corresponding base in aqueous glasses (NaOD, K_2CO_3-D_2O, D_3PO_4), the π-cations being characterised by e.s.r. spectroscopy.[179] Against this argument is the fact that the aqueous electron was not detected and the yield of galvinoxyl anion in the presence of water was not similarly

increased. Possibly a base-derived radical acts as an electron donor to the powerfully electroaffinic $C(NO_2)_4$.

3.5 Quenching of the Triplet Bases by 5-Bromouracil

The second order rate constants for the quenching of the triplet bases by 5-BrU are higher than expected in view of the low reduction potential of the 5-BrU, (1.62 V *versus* SCE[162]). The explanation for this may be due to the dissociative mechanism whereby electron transfer to 5-BrU results in cleavage of the C-Br bond.[180] This prevents back electron transfer [*cf.*, $C(NO_2)_4$], the instability resulting in the shortening of the lifetime of the exciplex formed between base and 5-BrU.

Evidence for the highly reactive uracilyl radical transient could not be obtained due to overlap of its weak absorption spectrum (λ_{max} 335 nm) with the triplet-triplet spectrum of the base.

3.6 Quenching of Triplet Thymidine by Electron Acceptors

Although this study has been mainly concerned with pyrimidine bases, we have extended it to the nucleoside thymidine. Table (3.5) gives the quenching results which are illustrated in Figure (3.14). The computed values using WELLEREKQ were E_{ox} = 1.55 ± 0.2 V *versus* SCE and $\Delta G_{23}^{\ddagger}$ (0) = 19.46 kJ mol^{-1}. Whilst a fitting of the thymidine quenching data to the Weller equation[53] has been achieved, the goodness of fit is *ca.*25% less than that obtained for thymine and uracil.

Figure 3.13 Variation in yield of $C(NO_2)_3^-$ from laser pulsing (249 nm) of thymine (2.6×10^{-4} mol dm^{-3}) and $C(NO_2)_4$ (9.32×10^{-4} mol dm^{-3}) in $MeCN/H_2O$ solutions with varying % v/v compositions.

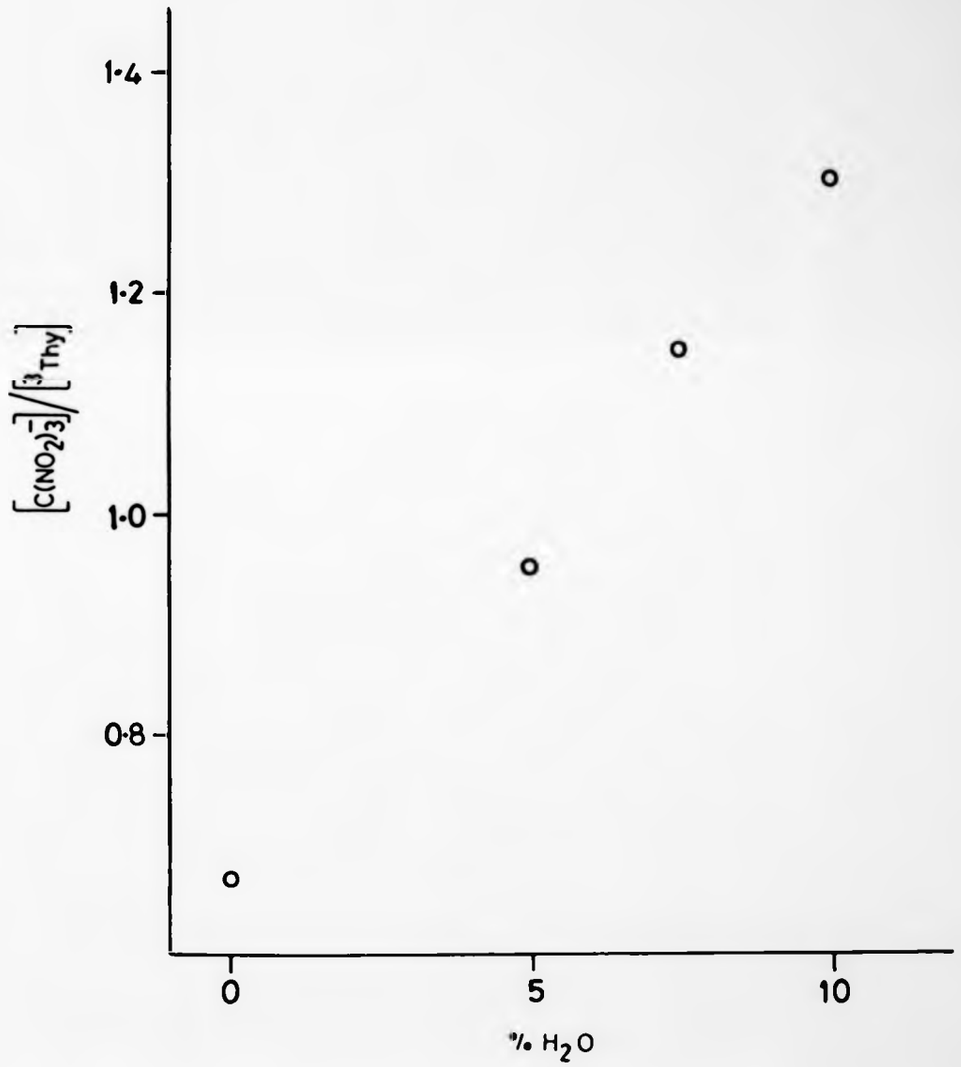

Table 3.5 Quenching of triplet thymidine by electron acceptors in MeCN

	Quencher	$k/10^{10}$ /dm^3 mol^{-1} s^{-1}		$-E_{1/2}$[a] /V *versus* SCE
1.	1,4-dinitrobenzene	0.284	(0.013)	0.71
2.	2-methylnaphthaquinone	0.515	(0.036)	0.77
3.	misonidazole	0.368	(0.028)	0.97
4.	metronidazole	0.729	(0.049)	1.1
5.	nitroethane	0.043	(0.00028)	1.424
6.	1-nitropropane	0.0080	(0.00093)	1.458
7.	nitromethane	0.0127	(0.00038)	1.46
8.	1-nitrobutane	0.0066	(0.00053)	1.48
9.	1-nitropentane	0.0132	(0.0012)	1.514
	$[Fe(CN)_6]^{3+}$[b]	0.62	(0.029)	-0.69
	irreversible electron transfer from triplet thymidine			
	tetranitromethane	2.77	(0.0052)	1.35
	5-bromouracil	0.219	(0.021)	1.62

[a] Details and references as for Table 3.1.

[b] MeCN solutions with 10% water.

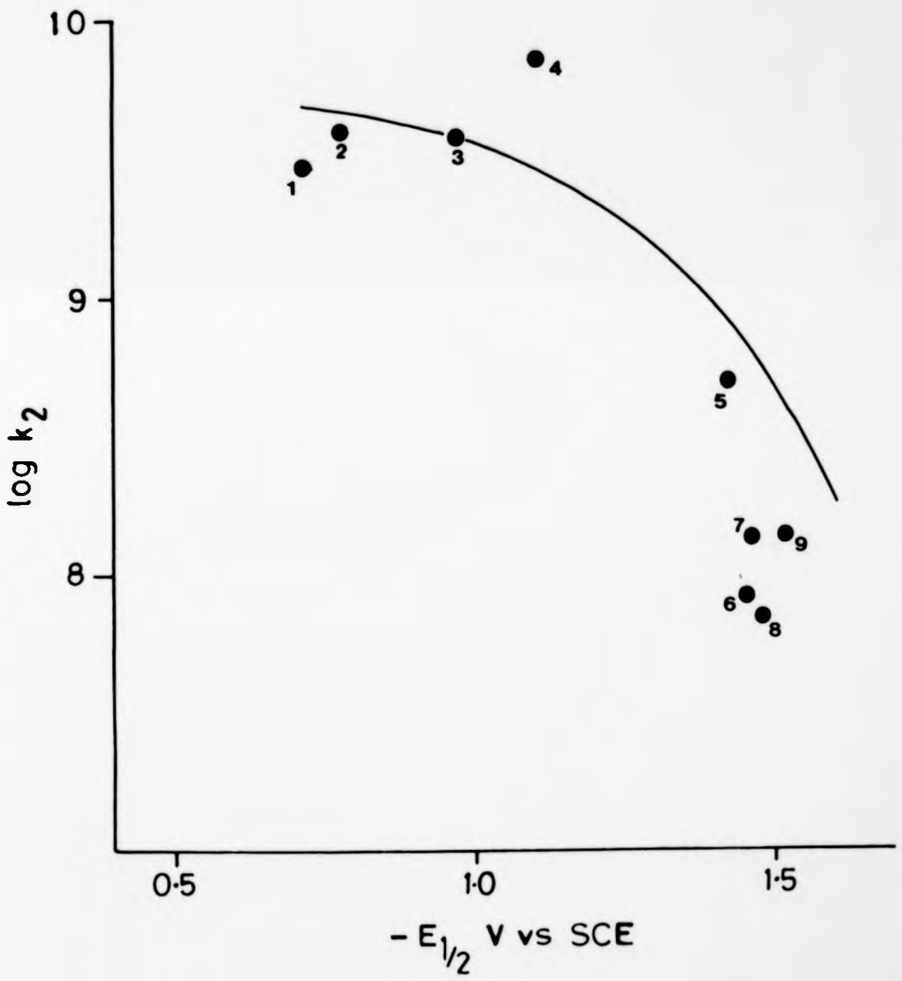

Figure 3.14 Correlation of log k_2 with reduction potential in MeCN for the quenching of triplet excited thymidine by electron acceptors. Full line - theoretical curve derived from Rehm-Weller equation using the parameters: $E^0(D/D^+)$ = 1.55 ± 0.2 V *versus* SCE and $\Delta G^{\ddagger}_{2s}$ (O) = 19.46 kJ mol^{-1}.

3.7 Discussion and conclusion

The results in this chapter indicate that triplet excited pyrimidine bases are quenched by radiosensitizing drugs *via* an electron transfer mechanism. However, the damage induced in DNA, which can ultimately lead to cellular destruction *via* this alternative direct action model, still needs to be elucidated.

Very recently, Schulte-Frohlinde,[180a] using conductivity methods, has shown that high energy laser irradiation, λ_{248} nm, of anoxic aqueous solutions of polyuridylic acid (poly U) results in biphotonic photoionisation of uracil moieties. The ejection of an electron from a uracil moiety of the poly U leads to a sequence of reactions resulting in single strand breakage (ssb) of the poly U chain. This nucleotide chain breakage *via* the DNA base radical cation strongly suggests that an electron transfer process from an excited triplet base to an electron affinic radiosensitizing drug can result in ssb of DNA.

The reaction sequence leading to the poly U ssb is as yet not fully understood. However, the kinetics of the photoionisation ssb are very similar to the kinetics observed for ·OH radical-initiated ssb, indicating that the chemical pathways for both reactions are the same. This implies that whilst the "indirect" and "direct" mechanisms are initiated differently, they ultimately lead to ssb through a common chemical pathway.

The ultimate site for strand breakage in DNA induced by ·OH has been shown to be heterolytic cleavage of one of the phosphoric acid ester bonds, mainly *via* the C-4' sugar moiety radicals,[180b] and for poly U both the C-2' and C-4' radicals have been implicated.[180c] The mode of decay for the radical cation based on the uracil moiety may well be by H-abstraction from the sugar moiety, but other possible

pathways are by proton dissociation from N-3, or by the addition of water across the C=C double bond. The similarity of the kinetics in both cases favours H-abstraction from the sugar moiety. The ssb of poly U by photoionisation was inhibited in the presence of H-donors, *e.g.*, dithiothreitol and glutathione.

The characterisation of the mode of action of radiosensitizing drugs is far from being finalised. According to the redox hypothesis of radiation modification, the molecular mechanism of electron affinic radiosensitization involves an oxidative interaction of the sensitizer with reactive, potentially damaging target radicals, which competes with reductive processes which restore the target to its undamaged state. Greenstock *et al.*, [180d] have recently found that there is a threshold redox potential for the radiosensitizers below which no sensitization occurs. This threshold value corresponds to the oxidation potential of the target bioradical involved, and comparisons indicate that it is the sugar phosphate backbone of DNA and not the heterocyclic base which is the DNA target site for radiosensitizers. The proposal that the action of radiosensitizing drugs mimics that of oxygen at the molecular level, based on the charge-sequestration model[32,132,133] has recently met with some reappraisal.

Following γ-irradiation of calf-thymus DNA in aqueous glasses at 77 K, Symons *et al.*,[46] observed the usual $T^{\bar{\cdot}}$ and $G^{+}_{\cdot}$ radicals, but in the presence of metronidazole and misonidazole found a reduction in the yield of $T^{\bar{\cdot}}$. An increase in the yield of $G^{+}_{\cdot}$ was <u>not</u> observed, in contrast with the earlier results of Gräslund[35] on DNA fibres. Further, metronidazole significantly reduced the number of strand breaks, indicating that the drugs protect DNA itself from the effects of ionising radiation. If both $G^{+}_{\cdot}$ and $T^{\bar{\cdot}}$ centres can lead to strand breakage, the

capture of an electron from $T^{\cdot}$ by the sensitizer would indeed be expected to decrease the yield of strand breakages. Symons *et al.* [35] reported earlier that the presence of oxygen causes a small increase in damage to DNA, which indicates that in Symons' system, oxygen and the radiosensitizing drugs are acting differently; these effects of oxygen and the nitroimidazoles upon DNA were found to be opposite and approximately additive. It has also been reported elsewhere that high concentrations of radiosensitizer may actually protect against radiation damage[180e] by scavenging the principal damaging species, ·OH, to form less reactive intermediates.

The fate of the sensitizer anion is unknown. Reduction of misonidazole has been performed electrolytically at pH 7 in the presence of DNA.[181] Results indicate that the reduced misonidazole destabilises the DNA helix by a process of strand breakage.

With regard to the "indirect" model, γ-irradiation of thymine in the presence of a wide range of radiosensitizers was found to increase the yield of thymine glycol (3.I).[182] In explanation, it was proposed that

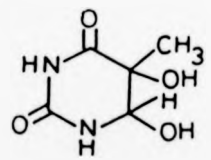

(3.I)

the sensitizer(s) oxidises an intermediate hydroxythymyl radical, producing the hydroxythymine cation which then undergoes solvolytic substitution, Scheme (3.1).

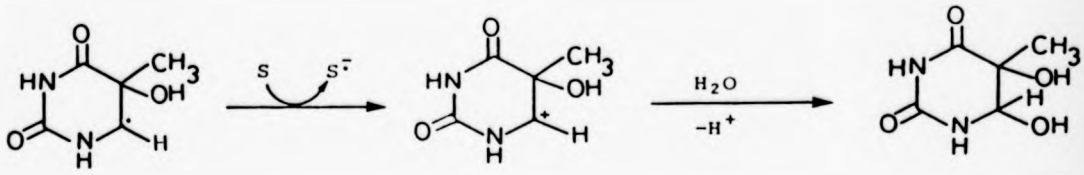

Scheme 3.1

This hypothesis was supported by observation of an increase in the yields of thymine hydrates and other dimeric products obtained in the absence of sensitizer.

Recently a misonidazole metabolite, a hydroxylamine, has been found to react with guanosine giving (3.II):[183]

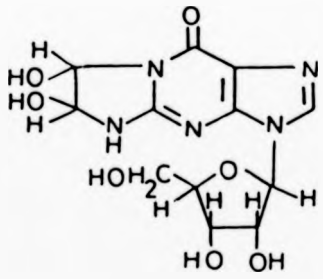

(3.II)

but so far, the biological consequences of such a reaction can only be speculative.

The many aspects of radiosensitization by electron affinic nitroaryl compounds and the problems in correlating their radiobiological

effects with chemical models for radiosensitization phenomena have been reviewed by Wardman.[183a]

While the contribution of the direct action model for the radiosensitizing effect of the proven drugs metronidazole and misonidazole remains an open question, what is certain from our results is that subsequent to excitation, electron transfer from thymine and uracil to the drugs occurs *in vitro* and may occur *in vivo*. We also note that the Rehm-Weller treatment has been applied very largely to singlet quenching studies and in rather few cases to triplets,[184] and the present results provide a useful confirmation of its successful generalisation to triplet state electron transfer.

CHAPTER 4

An Investigation of the Triplet and Ground State Properties of Metronidazole and Misonidazole by Laser Flash Photolysis and other Methods

4. Laser Flash Photolysis of Metronidazole and Misonidazole

While the biological role of the electroaffinic drugs metronidazole (MET) and misonidazole (MIS) may depend on their ability to capture electrons (in the charge-sequestration model) or to act in the forms of their radical anions, in the process of exciting cells with high-energy radiation, the possibility of involvement of electronic excited states of these molecules, if only in part, cannot be ruled out. The triplet excited states of the sensitizing drugs *p*-nitroacetophenone[50] and methylnaphthoquinone[54,55] and their interaction with various DNA bases is known. Kemp and Martins have characterised the triplet states of the nitroheteroaromatic molecules, 5-nitrofuroic acid,[185] 2-nitrothiophen[186] and *N*-(*n*-butyl)-5-nitro-2-furamide,[187] but little is known about the heteroaromatic nitroimidazoles. We therefore made an examination, principally by laser flash photolysis, of solutions of MET and MIS as follows.

Laser pulsing (347 nm, 50 ns) of aqueous, acetone and acetonitrile solutions of both MET and MIS failed to produce any transient absorption in the spectral range 400 to 700 nm.

This lack of T-T absorption may be due to:-

(i) the triplet state being very short-lived;

(ii) a low yield of ϕ_{isc} from excited singlet to triplet;

(iii) a low T-T absorption extinction coefficient.

Triplet states of molecules containing the nitro group are usually short-lived, because of the efficient vibrational relaxation decay pathway through the nitro group. The lifetimes of various nitroaromatic compounds are given in Table (4.1), and vary from the microsecond to picosecond time

Table 4.1 Lifetimes of various triplet nitroaromatic compounds

Compound	Lifetime /s	Solvent	Reference
Nitrobenzene	770×10^{-12}	THF	164
2-Nitrotoluene	690×10^{-12}	THF	164
1-Ethyl-2-nitrobenzene	450×10^{-12}	THF	164
2-Nitrothiophen	300×10^{-9}	CH_3CN	186
5-Nitro-2-furoic acid	290×10^{-9}	CH_3CN	185
N-(*n*-butyl)-5-nitro-2-furamide	260×10^{-9}	CH_3CN	187
1-Nitronaphthalene	4.9×10^{-6}	EtOH	188

range. Interestingly, laser flash photolysis of another nitrogen-containing heteroaromatic, 2-nitropyrrole, in both water and organic solvents also failed to yield any transients within the spectral range 390 to 700 nm.[187] It is suggested that the high photostability of 2-nitropyrrole in the presence of nucleophiles, such as CN^-, CNO^-, OCH_3^- and H_2O,[189] is due to the triplet state lifetime being exceedingly short.

4.1 Triplet State Energy of Metronidazole

The lifetimes of various excited triplet states were found to decrease in the presence of MET. The second order quenching rate constants of these triplets, along with their triplet energies, are given in Table (4.2). These quenching data were found to fit the general treatment of energy transfer, due to Balzani *et al.*[129] by an exchange (collisional) mechanism, equation (1.36), relating the triplet energy of the excited state donor/acceptor with the second order quenching rate constant, see section (1.9.8.) for a full explanation of this approach.

From optimum fitting of the data by a computer program developed by us (Appendix A), the following parameters were obtained: $k_{en}^0 = 2 \times 10^{10}$ s^{-1}, $\Delta G_2^{\ddagger}(0) = 6.12$ kJ mol^{-1} and $E_T = 245$ (±3) kJ mol^{-1}. k_{-d} was calculated from equation (4.1).[192]

Table (4.2) Quenching by metronidazole of triplet state donors in solution

Donor	Numbering	k_2 /10^9 dm^3 mol^{-1} s^{-1}	E_T^D [a] /kJ mol^{-1}
Benzophenone	1	6.40 (±0.39)	288
Thioxanthanone	2	11.84 (±0.79)	272
5,6-Benzoquinoline	3	5.80 (±0.09)	262
Phenanthrene [b]	4	3.30 (±0.11)	259
Naphthalene [b]	5	6.69 (±0.12)	254.8
2-Bromonaphthalene [b]	6	3.67 (±0.17)	251.9
1-Bromonaphthalene [b]	7	2.06 (±0.13)	247.7
2-Acetonaphthone	8	1.42 (±0.047)	247.69
1-Phenylnaphthalene [b]	9	0.62 (±0.035)	246
p-Terphenyl [c]	10	0.761 (±0.016)	244.4
1-Nitronaphthalene	11	0.265 (±0.018)	229.7
$[Cr(phen)_3]^{3+}$	12	0.063 (±0.0054)	163 [d]
$[Cr(bipy)_3]^{3+}$	13	0.017 (±0.0007)	163 [d]

[a] From reference 190.

[b] Sensitized by benzophenone.

[c] Solvent Me_2CO.

[d] From reference 191.

$$k_{-d} = k_d \left(\frac{3000}{Nr^3 4\pi}\right) \qquad (4.1)$$

where k_d was taken as 1.88×10^{10} dm^3 mol^{-1} s^{-1} and r was assumed to be 0.7 nm. The values for the derived parameters are in close agreement with those obtained for triplet states of other nitroheteroaromatic compounds.[129,186] The data from Table (4.2) are plotted in Figure (4.1).

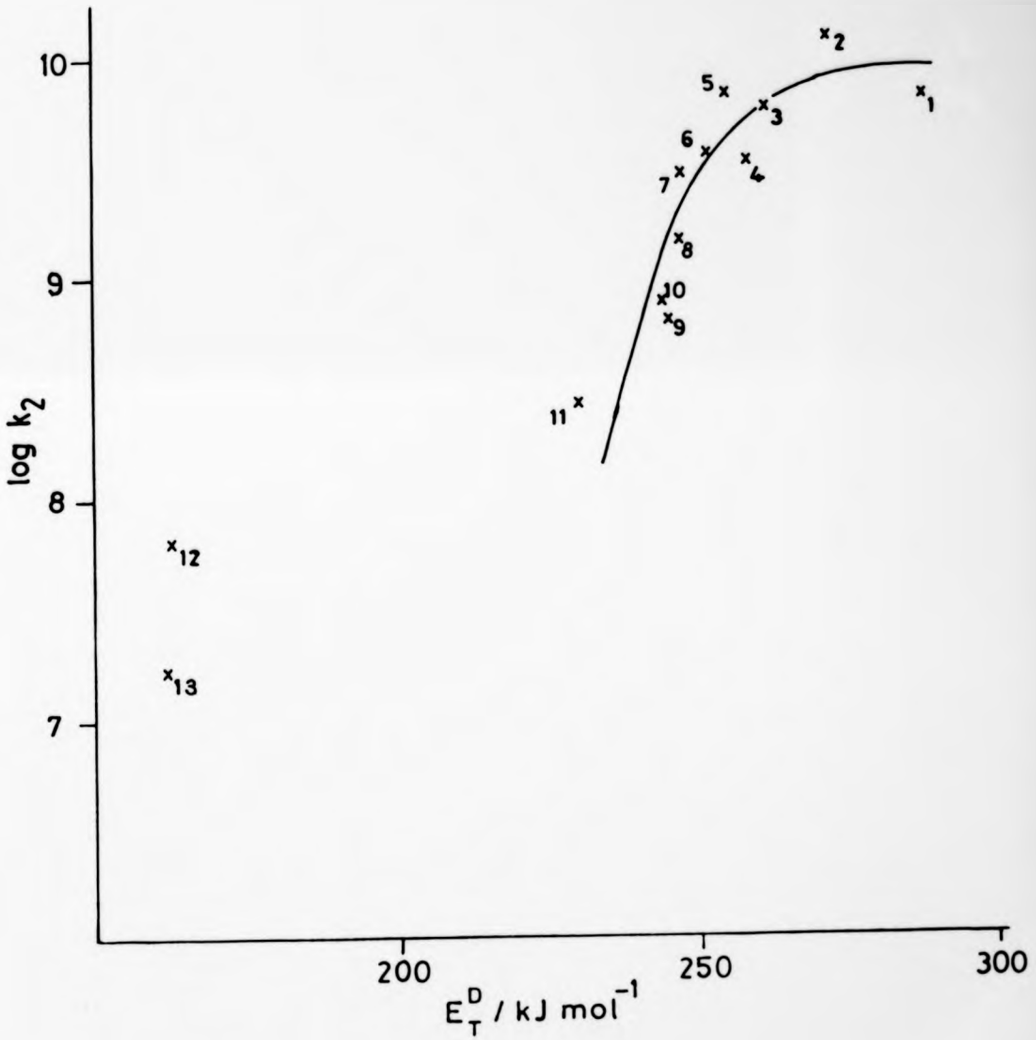

Figure 4.1 Correlation of log k_2 with donor triplet energy for the quenching of various triplet donors by metronidazole in MeCN or Me_2CO. Line-computer-fitted results using the parameters $k_{en}^0 = 2 \times 10^{10}$ s^{-1}, $\Delta G_{23}^{\ddagger}(0) = 6.12$ kJ mol^{-1} and $E_T = 245$ kJ mol^{-1}, (excluding the compounds 12 and 13).

The excited states of two inorganic compounds, namely tris-phenanthrolinechromium(III), $[Cr(phen)_3]^{3+}$, and trisbipyridylchromium(III), $[Cr(bipy)_3]^{3+}$, were also found to be quenched by MET, but were not included in the iterative determination of the triplet energy because of expected differences between the intrinsic energy parameters for inorganic and organic excited states, *cf* Balzani *et al.*[129] and references therein.

4.2 Triplet Detection Using 2,3-Diphenylindenone Oxide

2,3-Diphenylindenone oxide (DPIO) has been used successfully as a detector for short-lived triplet states having energies below 268 kJ mol^{-1}.[193,194]

DPIO (4.I) gives the bright red (ε_{544} = 26750 dm^3 mol^{-1} cm^{-1}) diphenylbenzopyrylium oxide, DPBO, (4.II) both by direct absorption of light and indirectly following energy transfer from sensitizers having triplet energies greater than 268 kJ mol^{-1}.

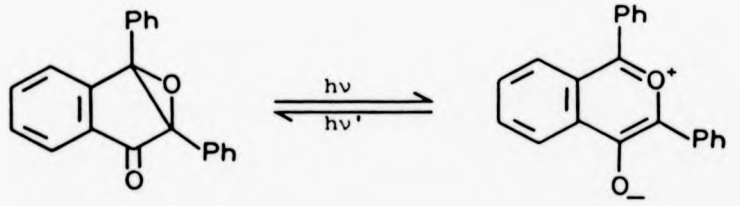

4.I (DPIO) 4.II (DPBO)

On the other hand, when a compound is excited having a triplet state of less than 268 kJ mol^{-1}, then sensitized oxidation of DPBO (also produced by direct absorption of light) takes place, depleting the red colouration of DPBO [equation (4.2)].

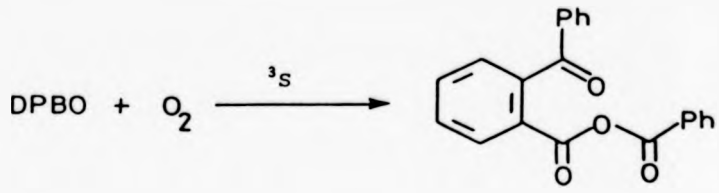

(4.2)

The concentrations of DPIO (3.7×10^{-4} mol dm^{-3}) and triplet sensitizer ($^3\Delta E_{O_2O}$ <268 mol^{-1}) are arranged so that 95% of the incident 364 nm light is absorbed by the sensitizer. The concentration of the test molecule is generally *ca.* 10^{-5} mol dm^{-3} and its absorbance is usually negligible at 364 nm.

If the test molecule (TM) quenches the triplet sensitizer by energy transfer, then the result is a <u>decreased</u> yield of photo-oxidation of DBPO, which induces an increase in absorbance at 544 nm compared with the comparator solution not containing the test molecule. This overall, rather convoluted, argument is depicted in Scheme (4.1).

The method is effective only for very short-lived triplet states, since ^{3}TM must disappear before it, too, can function like ^{3}S. By systematically varying the energy of ^{3}S, it is possible to establish the triplet energy of TM.

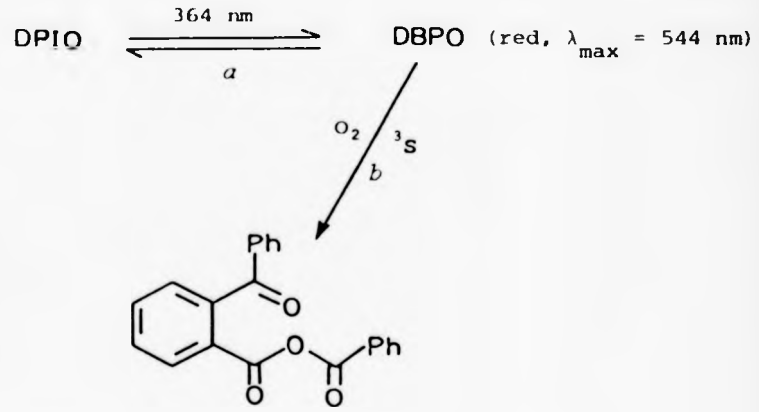

[a] Conversion only by direct absorption, since all "sensitizers" have E_T < 268 kJ mol^{-1}.

[b] Sensitized photo-oxidation by known triplets which are quenched by test compounds; TM, $^3S + TM \rightarrow {}^3TM + S$

Scheme (4.1)

The results obtained for the various sensitizers and DPIO solutions in the presence of the quenchers MIS and MET are given in Table (4.3). The colour change is termed 'positive' when there is an increase in red colouration in going from (DPIO + Sensitizer) to (DPIO, Sensitizer + Nitroimidazole) solutions.

Neither MET nor MIS quench any of the sensitizers of lowest triplet energy. However, above this, the smooth transition to the expected increase in colour due to triplet quenching of sensitizer as the triplet energy becomes greater than metronidazole and misonidazole is not observed.

Table 4.3 Quenching of sensitizer triplets by misonidazole and metronidazole

Sensitizer	$^3\Delta E_{o,o}$ [a] /kJ mol^{-1}	Observed increase in DPBO [absorption (544 nm)] Metronidazole	Misonidazole
Anthaquinone	259	+	+
4-Phenylbenzophenone	253.97	} Net reaction, %T went above 100%	
2-Naphthaldehyde	250.2		
2'-Acetonaphthalene	248.1	-	-
2,3-Benzofluorene	241.0	+	+
Chrysene	239.7	-	-
Coronene	228	-	-
9-Fluorenone	223	-	-
1,2,3,4-Dibenzanthracene	213	-	-

[a] From reference 190.

The data indicate the triplet energies of both MET and MIS to be *ca.* 245 kJ mol^{-1}, but closer 'bracketing' of the value is not possible by this method. This figure is in agreement with the value obtained in section (4.1) for MET. The effects evidenced in Table (4.3) may well be due to distortion within the excited states involved, introducing an intrinsic energy barrier to the energy transfer process, which would be expected to cause a decrease in the rate of energy transfer.[129]

4.3 Electron-Transfer Processes

The reduction of triplet heteroaromatics by both inorganic and organic molecules has been widely studied.[185-187] The laser flash photolysis of acetone solutions of MET and MIS containing such inorganic ions as Br^-, I^- and SCN^- led only to the one-electron oxidation of SCN^-: the transient spectrum obtained for the laser flash photolysis (347 nm) of an acetone

solution of MET (2.3×10^{-4} mol dm^{-3}) and KCNS (0.19 mol dm^{-3}) is given in Figure (4.2). The spectrum agrees precisely with the literature spectrum of $(SCN)_2^{\bullet-}$.[195] Reduction of the triplet state by organic electron donors proved unsuccessful in the case of the readily ionised triphenylamine and *N,N,N',N'*-tetramethyl-*p*-phenylenediamine.

4.3.1 Determination of the Reduction Potentials of Metronidazole and Misonidazole in Acetonitrile

Three approaches were used here, namely (i) conversion of known values of E_7^1 using a correlation diagram, (ii) interpolation into a figure showing the dependence of the rate of quenching of $^*[Ru(bipy)_3]^{2+}$ by electron acceptors, and (iii) when very shortly before completion of this work a cyclic voltammeter became available in this department by courtesy of Dr. Phillip Bartlett, by cyclic voltammetry.

(i) Using known E_7^1 values

The one-electron reduction potentials in water at pH 7.0 for MET and MIS are respectively -0.486 V and -0.389 V *versus* NHE.[196] The corresponding values for $E_{\frac{1}{2}}$ (red) in acetonitrile solutions would be expected to be somewhat different from these E_7^1 values because of solvation effects, *etc.*

Table (4.4) gives the values for both E_7^1 *versus* NHE and $E_{\frac{1}{2}}$ (red) *versus* SCE in acetonitrile for various quinones and nitroaromatic compounds. A plot of E_7^1 against $E_{\frac{1}{2}}$ (red), Figure (4.3), gives a reasonably good straight line of slope 1.074 ± 0.077, the $E_{\frac{1}{2}}$ (red) value being given by equation (4.3) with an estimated error of 7%.

$$E_{\frac{1}{2}} \text{ (red)} = 1.074\ E_7^1 - 0.545 \qquad (4.3)$$

Using equation (4.3) gives $E_{\frac{1}{2}}$ (red) for MET as -1.07 ± 0.08 V *versus* SCE and for MIS as -0.96 ± 0.07 V *versus* SCE.

Table 4.4 $E_{\frac{1}{2}}$ (red) in acetonitrile and E_7^1 for quinones and nitro-aromatic compounds

Compound	Number	$-E_{\frac{1}{2}}$ [a]	$-E_7^1$ [b]
		V *versus* SCE	V *versus* NHE
1,4-Benzoquinone	1	0.51	0.009
2,5-Dimethyl-1,4-benzoquinone	2	0.67	−0.065
1,4-Dinitrobenzene	3	0.70	0.257
2-Methyl-1,4-naphthoquinone	4	0.77	0.203
1,2-Dinitrobenzene	5	0.83	0.287
Duroquinone	6	0.84	0.235
1,3-Dinitrobenzene	7	0.91	0.345
4-Nitroacetophenone	8	0.925	0.358
3-Nitroacetophenone	9	1.042	0.437
Nitrobenzene	10	1.147	0.486
Nitromesitylene	11	1.442	0.86

[a] From reference 158.
[b] From reference 196.

(ii) Quenching of $^*[Ru(bipy)_3]^{2+}$

The luminescence of $^*[Ru(bipy)_3]^{2+}$ is quenched by both MET [k_2 = (1.15 ± 0.19) x 10^8 dm^3 mol^{-1} s^{-1}] and MIS [k_2 = (5.39 ± 0.046) x 10^8 dm^3 mol^{-1} s^{-1}], see Figure (4.4). Using the second order quenching rate constants for the quenching of $^*[Ru(bipy)_3]^{2+}$ by aromatic nitro-compounds,[172] which fit the Weller equation[53] very well, see section [3.2(iv)], the $E_{\frac{1}{2}}$ (red) values are calculated to be: MET -1.09 ± 0.01 V *versus* SCE, and MIS -1.03 ± 0.01 V *versus* SCE.

Considering both methods, the mean values for $E_{\frac{1}{2}}$ (red) in acetonitrile are for metronidazole, -1.08 ± 0.01 V *versus* SCE and for misonidazole -0.99 ± 0.04 V *versus* SCE.

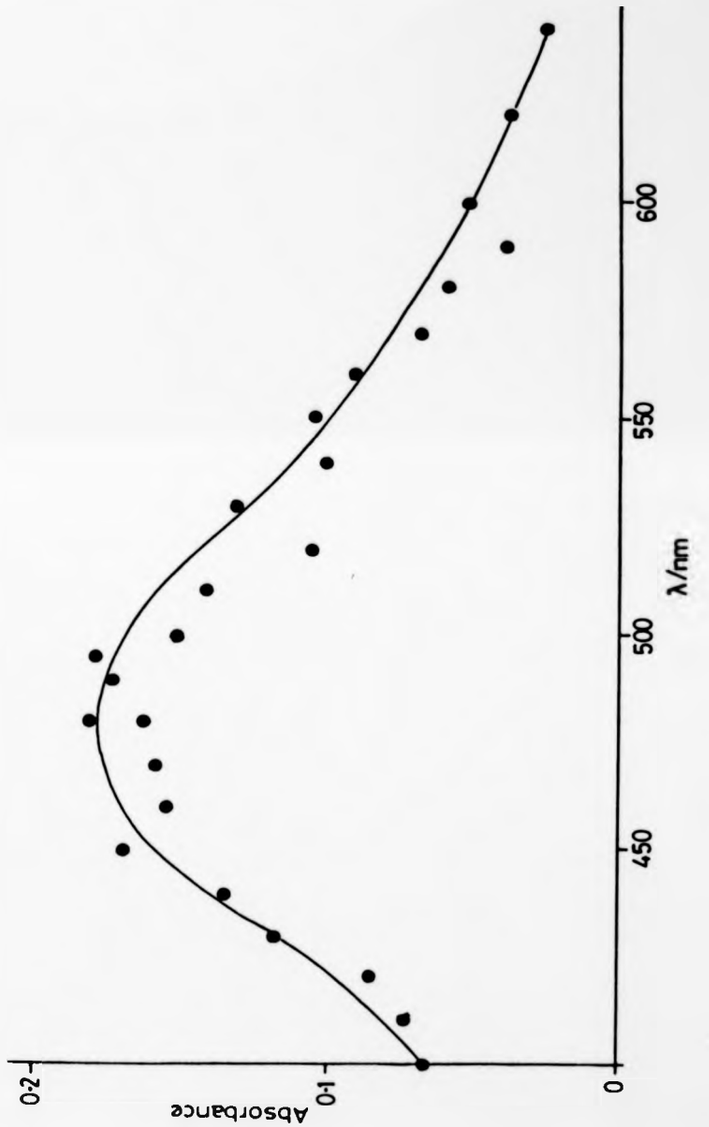

Figure 4.2 -●, spectrum of the transient formed on laser flash photolysis (347 nm) of a deaerated solution of MET (2.3×10^{-4} mol dm^{-3}) and KCNS (0.194 mol dm^{-3}) in acetone, measured 500 ns after the end of the pulse. The solid line is that obtained from reference 195.

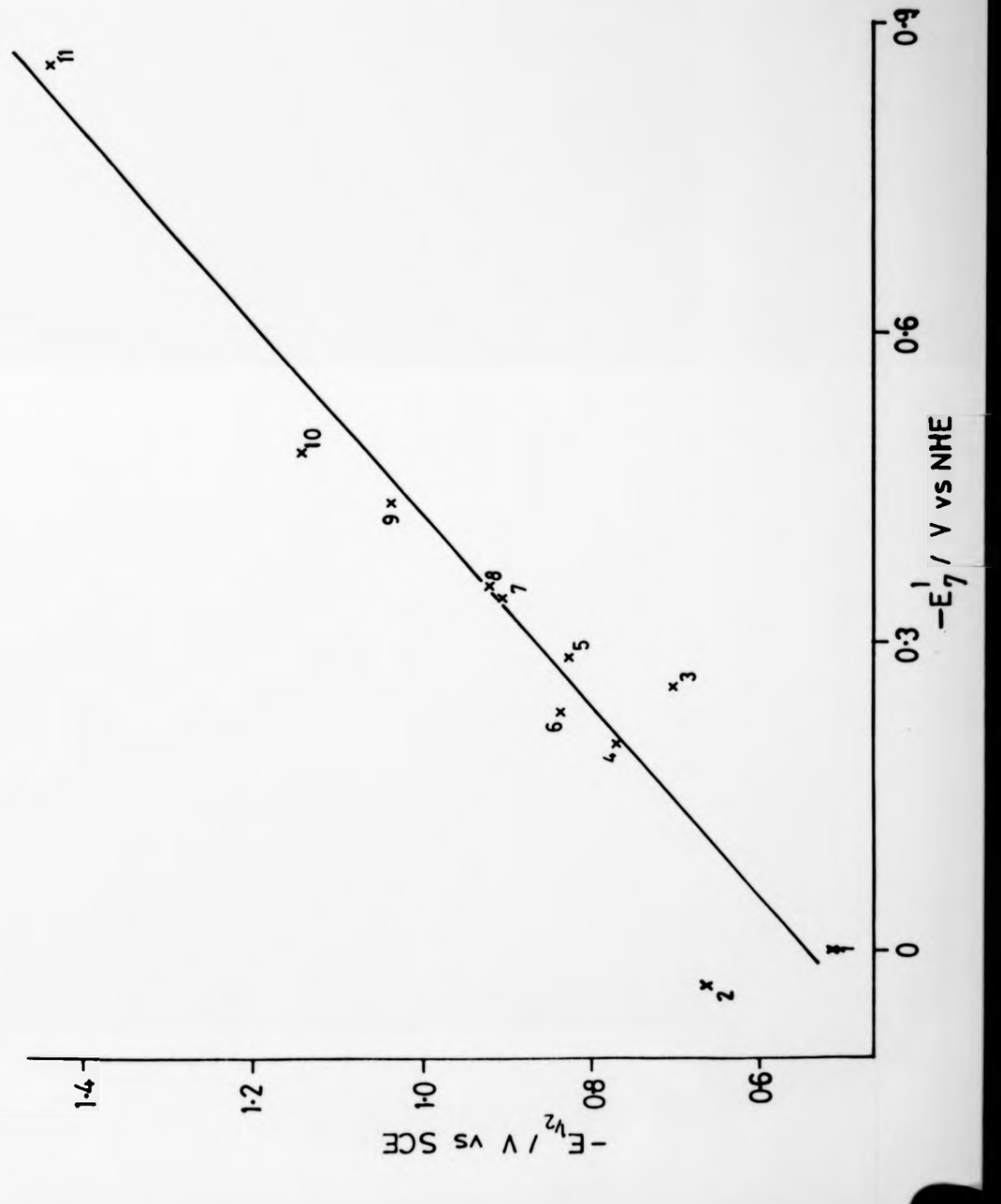

Figure 4.3 Correlation of E_7^1 *versus* NHE in water and $E_{\frac{1}{2}}$ (red) *versus* SCE in acetonitrile for various quinone and nitroaromatic compounds; the numbering refers to Table (4.4)

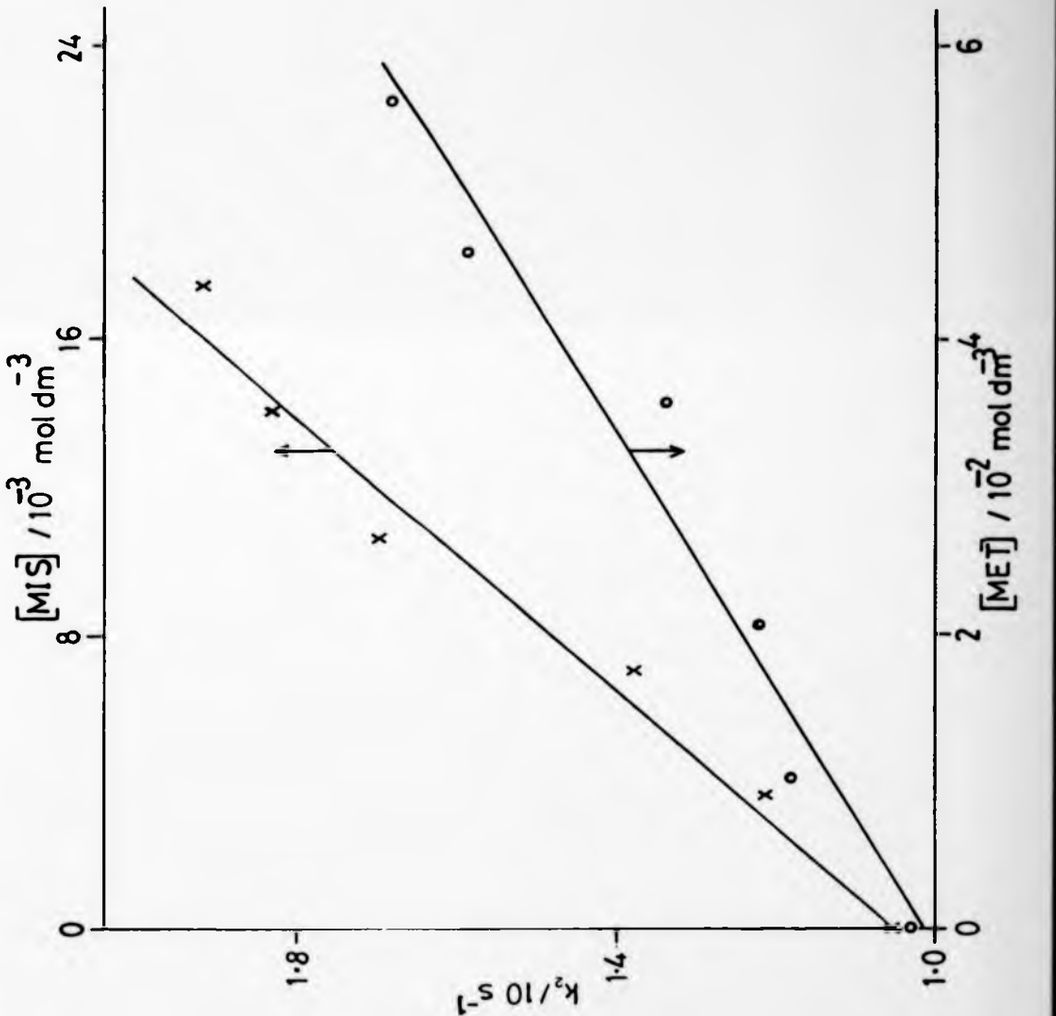

Figure 4.4 Quenching of $^{*}[Ru(bipy)_3]^{2+}$ (2.2×10^{-4} mol dm^{-3}) by MET and MIS in deaerated acetonitrile solutions

(iii) Direct electrochemical measurement

The cyclic voltammograms, at various sweep rates, for deoxygenated acetonitrile solutions of the two nitroimidazoles are illustrated in Figure (4.5). Table (4.5) lists the calculated value of $E_{\frac{1}{2}}$ (red) derived from these plots from the various sweep rates; the average values are MET -1.125 ± 0.005 V and MIS -0.970 ± 0.014 V *versus* SCE.

Table 4.5 $E_{\frac{1}{2}}$ (red) determinations for MET and MIS from the cyclic voltammograms illustrated in Figure (4.5)

	Sweep rate /mV s^{-1}	$-E_{peak\ cathodic}$ /V	$-E_{peak\ anodic}$ /V	$-\Sigma E/2$ /V
MET	50	1.22	1.02	1.12
	100	1.26	1.0	1.13
	200	1.31	0.94	1.125
MIS	50	1.12	0.85	0.986
	100	1.17	0.762	0.966
	200	1.2	0.718	0.959

Both these reduction potentials are in very good agreement with those determined in sections (ii) and (iii). All values are summarised in Table (4.6). [I wish to thank Dr. P.N. Bartlett (Warwick University) for his help in obtaining these measurements.]

Table 4.6 Summary of all $E_{\frac{1}{2}}$ (red) values for metronidazole and misonidazole

Method	$-E_{\frac{1}{2}}$ (red)/V *versus* SCE in MeCN	
	MET	MIS
(i) Using E^1_7	1.07 (±0.08)	0.96 (±0.07)
(ii) $^*[Ru(bipy)_3]^{2+}$ quenching	1.09 (±0.01)	1.03 (±0.01)
(iii) Cyclic voltammetry	1.125 (±0.005)	0.970 (±0.015)

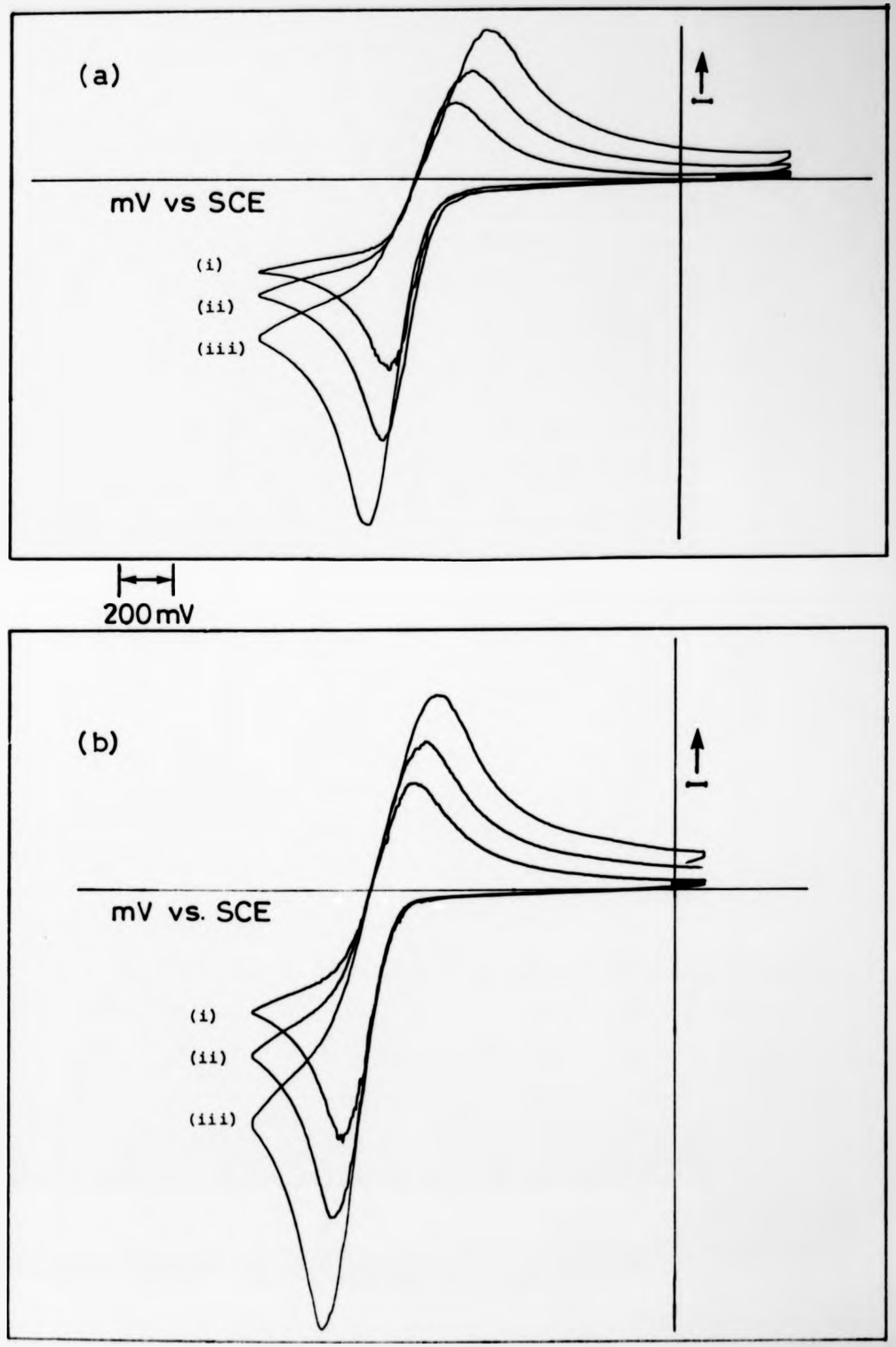

Figure 4.5 Cyclic voltammograms for deoxygenated acetonitrile solutions of (a) misonidazole (3.27×10^{-3} mol dm^{-3}) and (b) metronidazole (2.31×10^{-3} mol dm^{-3}), background electrolyte tetrabutylammonium chloride (0.1 mol dm^{-3}).
Measurements made using stationary Pt disc, standard three-electrode cell and purpose-built potentiostat. The counterelectrode was a large area Pt gauze and the reference electrode was aqueous saturated calomel. Sweep rates (i) 50; (ii) 100; and (iii) 200 mV s^{-1}.

4.4 Measurement of Intracellular Concentrations of Radiosensitizers

A number of fluorescent probes have been used to determine the intracellular oxygen concentration for various cells. The ideal fluorescent probe should have the following properties:

(i) a long-lived excited state, *i.e.*, > 100 ns;

(ii) high quantum efficiency of fluorescence;

(iii) localised in a well-defined region within the cell;

(iv) a wavelength of excitation which should be longer than the absorption bands of the cell, so that specific excitation can occur.

Two examples of such probes are pyrene and 1-pyrenebutanoic acid (4.III).[197,198]

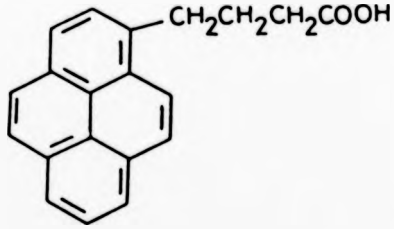

(4.III)

A probe which could be used to determine cellular concentrations of radiosensitizing drugs such as metronidazole and misonidazole, would be of great interest. This section deals with evaluation of the potential of such probes from kinetic quenching measurements *in vitro*.

4.4.1 Quenching of Ruthenium Complexes

Ruthenium polypyridyl complexes are known to have good luminescence properties and are quenched with varying degrees of efficiency by nitro-aromatic compounds, depending on their reduction potentials.[172] The results for the quenching of $[Ru(bipy)_3]^{2+}$ in aqueous solutions, buffered to pH 7.0, by various known sensitizers, are given in Table (4.7). All the compounds

Table 4.7 Quenching of the luminescence of $^*[Ru(bipy)_3]^{2+}$ (7.3×10^{-5} mol dm^{-3}) by various radiosensitizing drugs, laser flash photolysis (347 nm) of aqueous solutions buffered to pH 7.0

Radiosensitizer[a]	k_2 /10^{-9} dm^3 mol^{-1} s^{-1} (±)	E_7^1 /mV *versus* NHE
p-Nitroacetophenone	3.18 (0.035)	-355
Misonidazole	3.23 (0.02)	-389
Metronidazole	2.71 (0.12)	-486
5-Chloro-1-methyl-4-nitroimadazole	3.56 (0.062)	-534

[a] Solutions buffered to pH 7 using KH_2PO_4 (0.025 mol dm^{-3}) and anhydrous Na_2HPO_4 (0.025 mol dm^{-3}).

quench at near-diffusion controlled rates, which would seem to promise well for their use *in vivo*. However, attempts to incorporate $[Ru(bipy)_3]^{2+}$ into cells failed,[200] which may be due to repulsion of the dipositive complex ion by the hydrophobic membrane cell wall. In an attempt to overcome such an effect, the neutral complex *cis*-dicyanobis(2,2'-bipyridine)ruthenium(II) was prepared, and its excited state was also found to be quenched by metronidazole at a similar rate [$k_2 = (3.24 \pm 0.21) \times 10^9$ dm^3 mol^{-1} s^{-1}] as for the quenching of $^*[Ru(bipy)_3]^{2+}$. Again, unfortunately, this ruthenium complex was also unable to diffuse through the cell wall,[200] indicating that perhaps the sheer bulk of the complex is prohibitive.

Recently, Turro *et al.*[201] have studied the binding of three ruthenium complexes, $[Ru(bipy)_3]Cl_2$, $[Ru(phen)_3]Cl_2$ and $[Ru(DIP)_3]Cl_2$ (where DIP = 4,7-diphenyl-1,10-phenanthroline) to calf thymus DNA. The luminescence of both $[Ru(phen)_3]^{2+}$ and $[Ru(DIP)_3]^{2+}$ is increased in the presence of DNA, whilst for $[Ru(bipy)_3]^{2+}$ no enhancement is observed. These results indicate that binding takes place between DNA and the metal complexes $[Ru(phen)_3]^{2+}$ and $[Ru(DIP)_3]^{2+}$. Further, in the presence of ferrocyanide, only the luminescence from the $[Ru(bipy)_3]^{2+}$ is quenched, indicating also that this compound is not closely bound to DNA, while for $[Ru(phen)_3]^{2+}$ and $[Ru(DIP)_3]^{2+}$ biphasic Stern-Volmer plots are found, indicating protection of their excited states by DNA from ferrocyanide. Two binding modes are postulated, one of which is electrostatic: at this site the complexes are quenched by ferrocyanide. The other site is regarded as intercalative, and is not quenched by ferrocyanide. The binding of $[Ru(DIP)_3]^{2+}$ was also found to be stereoselective, with only the Δ-isomer binding to the helical asymmetric DNA.

These results indicate that ruthenium complexes may assist in the design of site- and conformation-specific drugs for *in vitro* studies. However, ultimate *in vivo* studies may not be possible, due to such difficulties as we have encountered in incorporating such complexes into the cell.

4.4.2 Quenching of 1-Pyrenebutanoic Acid

Both MET and MIS quench the time-resolved fluorescence of 1-pyrenebutanoic acid (PBA). The second order rate constants obtained from 351 nm, Xe/F_2 excimer laser flash photolysis of water/ethanol (9:1) solutions of PBA are: metronidazole, $(0.296 \pm 0.035) \times 10^{10}$ dm^3 mol^{-1} s^{-1} and misonidazole, $(0.588 \pm 0.026) \times 10^{10}$ dm^3 mol^{-1} s^{-1}.

Attempts to obtain a Stern-Volmer plot for the quenching of PBA by MET and MIS were frustrated by the powerful inner filter effects of MET and MIS at the excitation wavelength of 351 nm. Accordingly, such plots showed slight positive curvature. Correction would have been of the order of >50% and was not attempted. However, effects are in agreement with those obtained before.[202]

The kinetic rates obtained from the time resolved fluorescence study show that the intracellular concentrations of both MET and MIS can be monitored using PBA as a kinetic fluorescence probe.

4.5 Conclusions

The triplet energy of MET has been determined as 245 kJ mol^{-1} using the approach of Balzani *et al.* to energy transfer. The ability of MET to quench known triplet states is strong evidence for the existence of triplet MET. Whilst DPIO gives complementary results for the triplet energy, the inconsistency in the fitting of donor and acceptor energies between two particular energy levels [see Table (4.3)] indicates that this method is less effective.

The two indirect methods used to determine the reduction potentials of the drugs give consistent values which compare well with those obtained from cyclic voltammetry {in particular the quenching of $*[Ru(bipy)_3]^{2+}$ by aromatic nitro- compounds may be relied upon due to the excellent fitting of their quenching rates to the Weller equation}.

For an intracellular fluorescent probe, Ru^{II} compounds as candidates have been shown to be unacceptable because of their inability to penetrate the cell wall. Further, time-resolved work on ^{1}PBA indicates that the drugs quench at diffusion controlled rates. However, steady state methods to determine unknown concentrations of these drugs using cell fluorescence microscopy would be inhibited because of strong inner-

filter effects.

Returning to the question of whether the drug triplet states are involved in sensitizing effects, the inability to observe the triplet states by flash photolysis, combined with the general lack of production of inorganic anions (*i.e.*, $Br_2^{\bullet-}$ and $I_2^{\bullet-}$), indicates that the triplet states are extremely short lived. This being so, drug triplet states would not be expected to live long enough to react with DNA unless some intercalation occurs, binding the drugs to DNA.

CHAPTER 5

Quenching of Excited Uranyl Ion and Triplet Benzophenone by Nucleic Acid Bases

5. Quenching of Excited Uranyl Ion by Nucleic Acid Bases

The excited state of the uranyl ion, $[UO_2^{2+}]^*$, is quenched by many types of organic molecules covering a wide variety of processes, including energy transfer, electron transfer, heavy atom effects and chemical quenching.[203-206] Excited uranyl ion may be monitored by its intense green luminescence, λ_{max} *ca.* 510 nm, by both steady state and time-resolved flash photolysis, or by observing the lowest excited state absorbance, λ_{max} *ca.* 590 nm.[203] Both of these wavelengths are dependent upon pH and solvent.[206] There has been some controversy as to whether the first electronically excited state of $[UO_2^{2+}]^*$ is a singlet or a triplet,[203] but the current view is that spin-orbit coupling is so great that purely spin labels are inappropriate.[206]

Although the interaction of many types of organic molecule (alcohols, thioethers, ethers, aldehydes, carboxylic acids, esters, aromatics and alkenes) with $[UO_2^{2+}]^*$ have been studied by steady-state methods, fluorimetry, cryogenic e.s.r. and μs and ns flash photolysis, no previous kinetic study has been reported of any interaction with pyrimidines or purines, although excited uranyl acetate is known to kill *Escherichia coli* K-12[210] and $[U^{VI}]^*$ can cleave thymidine dimers.[211]

We found the decay rate of the excited uranyl ion in water (pH 2.2) is accelerated by nucleic acid bases. The second-order quenching rate constants which are given in Table (5.1) were obtained from both time-resolved laser flash photolysis (347 nm, 50 ns, 70 m J) and steady-state luminescence measurements using the Stern-Volmer technique. The Stern-Volmer constants were converted into second-order rate constants by measuring the lifetime of $[UO_2^{2+}]^*$ in the absence of quencher, τ_0, as 3.41×10^{-6} s.

Table 5.1 Quenching of $[UO_2^{2+}]^*$ in water (pH 2.2) by nucleic acid bases. Uranyl nitrate (0.068 mol dm^{-3})

Base	Stern-Volmer constant /dm^3 mol^{-1}	k_{sv} /10^8 dm^3 mol^{-1} s^{-1}	k_2 (laser 347 nm) /10^8 dm^3 mol^{-1} s^{-1}
Guanosine	4850 ± 33	14.2	17.7 ± 0.7
Thymine	4247 ± 32	12.4	16.4 ± 1.0
Uracil	3313 ± 17	9.7	12.0 ± 0.4
Adenosine	1061 ± 19	3.1	3.5 ± 0.4
Cytosine	-	-	3.4 ± 0.3

The values obtained from both methods are in fairly good agreement, bearing in mind that the second-order rate constants calculated from Stern-Volmer constants are critically dependent upon the value taken for τ_0. The possible mechanisms for this quenching will now be discussed.

(i) Energy transfer

This process, [equation (5.1)], can be ruled out because of the positioning of the excited state energies of the nucleic acid bases $^3\Delta E_{o,o}$ 300 kJ mol^{-1}, [see section (1.7.4)], which is much higher than that of $[UO_2^{2+}]^*$, *ca.* 250 kJ mol^{-1}.[203-206] For such a highly endothermic process energy transfer would not occur.[106]

$$[UO_2^{2+}]^* + B \not\longrightarrow [UO_2^{2+}] + B^* \qquad (5.1)$$

(ii) Chemical quenching

Excited uranyl ion is known to be quenched by alcohols and carboxylic acids through chemical interaction.[203,205] There are two possible mechanisms for this, *i.e.*, (i) hydrogen atom abstraction [equation (5.2)], or (ii) hydride-ion transfer [equation (5.3)].

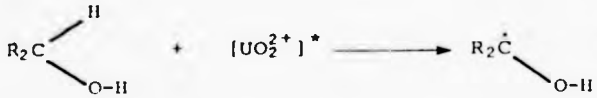

(5.2)

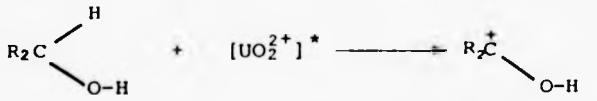

(5.3)

Equation (5.2) is generally accepted for alcohols because the resulting alcohol radical has been identified by e.s.r. in both a solid state matrix at 77 K[210] and in solution both directly[211] and by spin-trapping.[212] However, the second-order rate constants for this process are of the order of 10^6 dm^3 mol^{-1} s^{-1}, while the rate constants given in Table (5.1) are three orders of magnitude greater than this, indicating such a mechanism to be unlikely.

Further evidence against this mode of quenching is that irradiation for 2 hours of aqueous uranyl nitrate (2.71×10^{-3} mol dm^{-3}) and the bases, *e.g.*, thymine (0.011 mol dm^{-3}), using a Xenon arc-lamp (200 W) and a 401 nm metal bandpass filter, failed to produce any sizeable concentrations of U^{IV} as measured at 648 nm, ε_{648} *ca.* 58 dm^3 mol^{-1} cm^{-1},[203] (formation of U^{IV} is brought about by disproportionation of the reduced U^{V} species to U^{IV} and U^{VI}).[213] The absorbance change was <0.01, which gives a quantum yield of <0.02 based upon ferrioxalate actinometry.[214]

(iii) Intermolecular electron transfer (exciplex formation)

Aromatic hydrocarbons quench uranyl luminescence very efficiently at rates near diffusion control *via* the formation of an excited state π-complex, or exciplex.[215] Spectral evidence for exciplex formation has been obtained by Tokumura[216] for the quenching of $[UO_2^{2+}]^*$ by benzene, who observed novel, weak absorption and emission spectra following the decay

of $[UO_2^{2+}]^*$: these new bands were assigned to the exciplex $(U^{\delta-}O_2^{2+}---Ar^{\delta+}H)^*$ with a weak charge-transfer interaction. The overall quenching process is:

$$[UO_2^{2+}]^* + ArH \rightleftharpoons [U^{\delta-}O_2^{2+}---Ar^{\delta+}H]^* \longrightarrow [UO_2^{2+}] + ArH + heat$$

High rate constants have also been obtained for quenching of $[UO_2^{2+}]^*$ by alkenes,[205] both conjugated and nonconjugated; again, no U^{IV} was produced and the mode of quenching was attributed to charge transfer, or exciplex quenching.

Our evidence strongly favours a mechanism of quenching of excited uranyl ion by nucleic acid bases *via* exciplex formation. The fact that there is no net photochemical reaction leading to products implies that if there is intermolecular charge transfer, then it is totally reversible.

5.1 Quenching of Triplet Benzophenone by Nucleic Acid Bases

Benzophenone, along with acetophenone and acetone, is known to photosensitize the dimerisation of the pyrimidine bases, thymine, uracil and orotic acid, by means of triplet-triplet energy transfer.[217] The efficiency for the benzophenone sensitization increases in the order uracil << thymine < orotic acid, which is expected, in view of the triplet energies of the bases. Efficient triplet-triplet energy transfer occurs when the sensitizer energy is greater than that of the acceptor; the efficiency increases with the size of the energy gap.[106]

Triplet acetone generated by KrF laser pulsing of aqueous buffered (pH 7.1) solutions of acetone was found to be quenched by thymine (k_2 = 7.0×10^9 dm^3 mol^{-1} s^{-1}).[218] A transient absorption spectrum was produced which is very similar to the T-T absorption spectrum of thymine,[75] indicating that the quenching mechanism is energy transfer. However, the

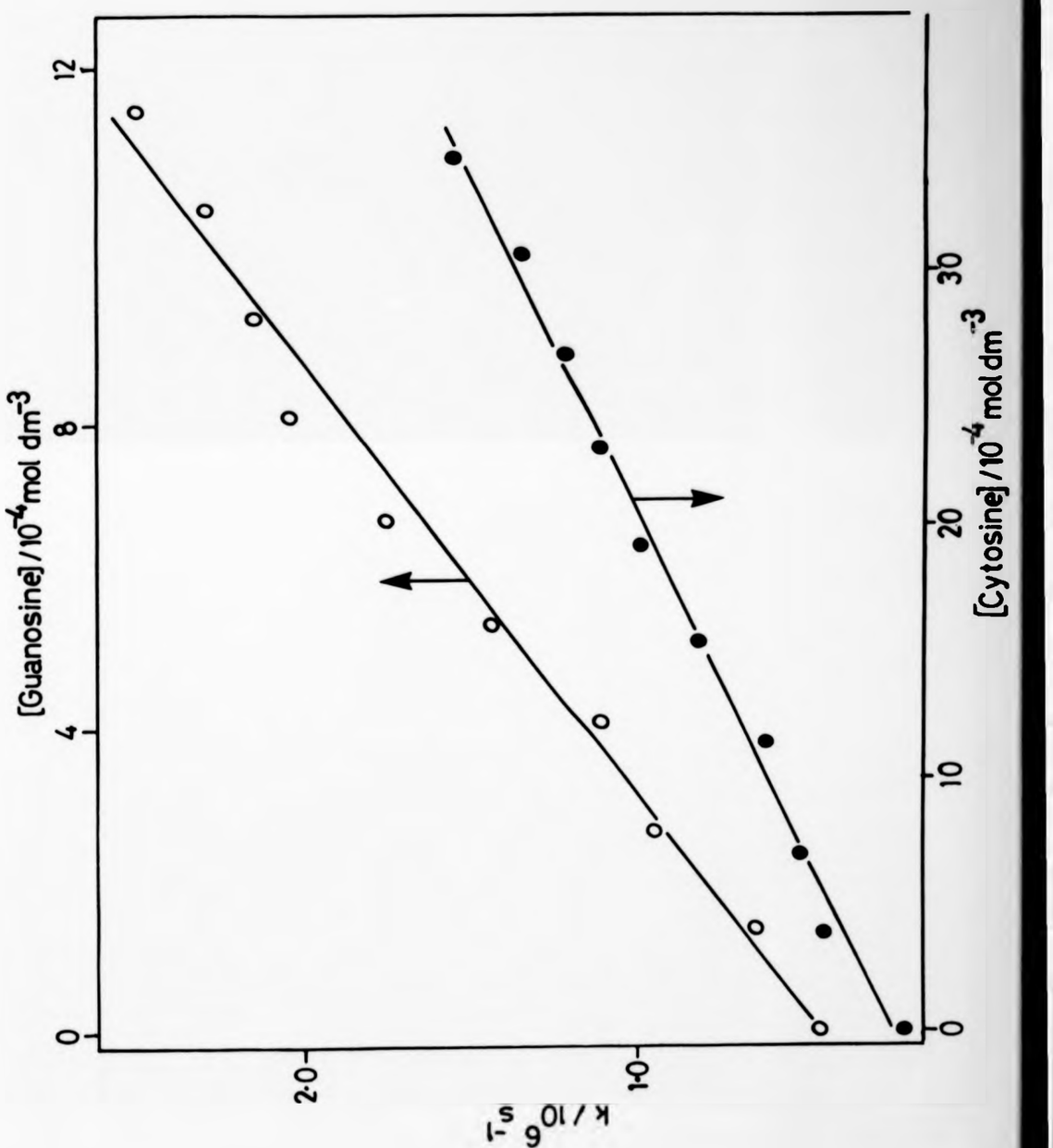

Figure 5.1 Typical plots for the second-order rate constants, determined by laser flash photolysis (347 nm), for the quenching of uranyl ion in water (pH 2.2) by cytosine (●) and guanosine (○). Uranyl nitrate (0.068 mol dm^{-3}).

sensitized yield of triplet thymine formation was only 0.2-0.3, and it was suggested that there is a photoadduct formation similar to that which has been observed by benzophenone,[72] see section (1.7.2b).

Recently, Das *et al.*,[219] have found the triplet states of benzophenone, acetophenone and various substituted derivatives are quenched by methyl viologen (MV^{2+}), *via* electron transfer from the excited ketone. The reactions for benzophenone, $Ph_2C{=}O$, are:

$$Ph_2C{=}O \xrightarrow{h\nu} {}^1(Ph_2C{=}O)$$

$${}^1(Ph_2C{=}O) \xrightarrow{isc} {}^3(Ph_2C{=}O)$$

$${}^3(Ph_2C{=}O) + MV^{2+} \xrightarrow[\text{electron transfer}]{} [Ph_2C{=}O]^{\ddagger} + MV^{\ddagger}$$

The quenching rate constants in deaerated water:acetonitrile (1:9) solutions are all near diffusion controlled. The growth of $MV^{\ddagger}$ was observed from its intense spectral absorbance at 610-615 nm.[220]

Our study made an attempt to extend the work of Charlier and Helene[72] on the quenching of triplet benzophenone by purine and pyrimidine bases. Excitation of benzophenone in water produces two transient species which have overlapping absorption spectra, namely the triplet state (λ_{max} 525 nm) and the ketyl radical (λ_{max} 540 nm). The ketyl radical is formed by reaction of triplet-state benzophenone with water, *i.e.*:

$${}^3(Ph_2C{=}O) + H_2O \longrightarrow Ph_2\dot{C}{-}OH + \cdot OH$$

Charlier and Helene[72] observed both ${}^3Ph_2C{=}O$ and $Ph_2\dot{C}OH$ using microsecond flash photolysis in absorption mode and obtained the second-order rate constants for the quenching of triplet benzophenone and the ketyl radical

by the pyrimidine bases. However, the rate constants for quenching by the purine bases could not be obtained. This was due to the ketyl radical concentration being very much higher in these systems than it was for the pyrimidine base systems, with the result that the triplet state was unobservable in the former. The relative enhancement of the ketyl radical was attributed to ready hydrogen abstraction from the C-8 atom of the purine ring. Evidence for this was[72] (i) if abstraction was from the amine group, cytidine would have given a similar reaction, and (ii) the reaction is not observed with pyrimidine nucleosides, and hence it does not involve hydrogen abstraction from the sugar moiety.

These problems have been overcome by using a pulsed, frequency doubled, ruby laser (347 nm, 50 ns, 70 m J) and monitoring of the benzophenone triplet by observing its time-resolved phosphorescence decay, (λ_{max} = 415 nm). This procedure overcomes the problems encountered in observing the triplet in absorption due to spectral overlap with the ketyl radical.

Unfortunately, the solubility of benzophenone in water is too low to yield a reasonable absorbance (*i.e.*, $O.D._{347}$ = 0.7) of the laser pulse, and an acetone:water mixture (6:4) was chosen as the solvent. The second-order rate constants for the quenching of triplet benzophenone by both purines and pyrimidines, or their corresponding nucleoside/nucleotide, are given in Table (5.2); the values obtained by Charlier and Helene[72] for the quenching of the pyrimdine bases in water are also given. The emission trace of triplet benzophenone in the absence of quencher did not fit first-order decay kinetics, but upon addition of quencher, good fits were obtained. This observation is in agreement with Bhattacharyya and Das[121] who monitored the triplet using T-T absorption.

Table 5.2 Quenching of triplet benzophenone by pyrimidine and purine nucleic acid bases. Benzophenone (8.9×10^{-3} mol dm^{-3}), solvent acetone:water (6:4)

Base or corresponding nucleoside/nucleotide	k_2 /10^8 dm^3 mol^{-1} s^{-1}	k_2[a] /10^9 dm^3 mol^{-1} s^{-1}
Guanosine monophosphate	5.59 (±0.80)	-
Thymine	3.00 (±0.17)	2.0
Adenosine	0.95 (±0.047)	-
Cytosine	0.51 (±0.050)	0.4
Uridine	0.21 (±0.02)	0.6

[a] From ref.,[72] using water as solvent.

There is disagreement between the two sets of data for k_2 given in Table (5.2), those for the pyrimidine bases differing by a factor of ten.

Charlier and Helene[72] calculated the quantum yields for the dimerisation of the pyrimidines using their obtained values for the appropriate second-order rate constants. For orotic acid, good agreement was found, but for thymine and uracil, values differed by two and three orders of magnitude respectively from the literature values determined directly. The triplet energy levels of the pyrimidine bases are usually placed[60] above that of benzophenones, see section (1.7.4), which makes triplet-triplet energy transfer an endothermic process (the difference being made up by vibrational energy contributions[106] for the sensitized dimerisation), and hence the quenching mechanism must be *via* an electron transfer or chemical quenching process.

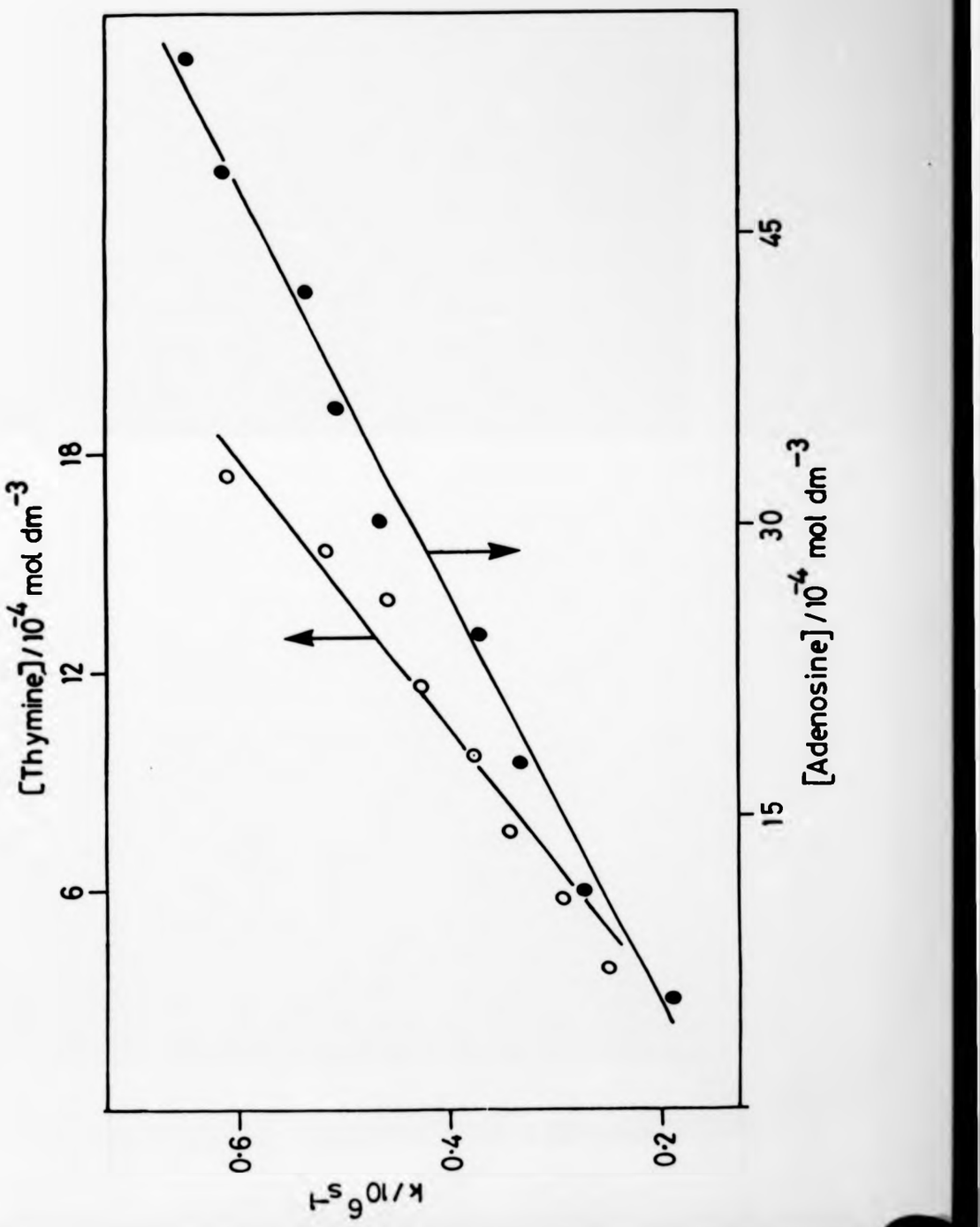

Figure 5.2 Typical plots for the second-order rate constants, determined by laser flash photolysis (347 nm), for the quenching of triplet benzophenone in acetone:water (6:4), by thymine (o) and adenosine (●). Benzophenone (8.9×10^{-3} mol dm^{-3}).

Das *et al.*,[221] have recently found amino acids, aminocarboxylic acids and their metal complexes reduce triplet benzophenone. The quenching rate constants obtained range from near diffusion-controlled to four orders of magnitude lower at pH 7.0, while increasing the pH to 9.5 makes the rates a factor of ten times faster. Under these conditions, the amino acids change from their cationic (zwitterionic) forms to their anionic forms, allowing reaction of the free amino group.

The mode of quenching for the pyrimidine bases may be electron transfer followed by proton transfer or by direct H-atom abstraction to form the ketyl radical. Taking the reduction potential of benzophenone $E^0(A^{\bullet-}/A)$ as -1.55 V *versus* SCE,[222] measured in 50% aqueous ethanol buffered to pH 12.65, its triplet energy as 3.0 eV[60] and the oxidation potential of the pyrimidine bases $E^0(D/D^{\bullet+})$ as >1.75 V *versus* SCE (see Chapter 3) and substituting these values into equation (5.4),[53] while taking the coulombic term as 0.06 eV, gives $\Delta G^0_{2,3}$ = +23.2 kJ mol^{-1}.

$$\Delta G^0_{2,3} = E^0(D/D^{\bullet+}) - E^0(A^{\bullet-}/A) - {}^3\Delta E_{0,0} + 0.06 \qquad (5.4)$$

This value makes electron transfer very unfavourable and we regard hydrogen atom abstraction as the likely quenching process.

APPENDICES

APPENDIX A

A. Video Camera Interface System for the Analysis of Oscilloscope Decay Traces

This system allows an image displayed on a storage oscilloscope to be captured into the screen addressing ram of a microcomputer. This captured image, in our case an excited state decay trace, is displayed digitally onto the monitor screen of the computer, where it may be manipulated to provide information such as decay constants.

A block diagram of the complete video camera interface system is illustrated in Figure (A.1). The video camera was supplied by Rediffusion (UK) and incorporates an 11 cm television screen, which displays the viewed image; a close-up lens was fitted to the normal 30-70 mm zoom lens supplied with the camera. The printer is an Epson (Japan) RX-80 F/T, supplied software being compatible with this make of printer. The video interface, supplied by Dataharvest (Milton Keynes, UK) is connected *via* the user port to a BBC model B.

A.1 The Interface

At the heart of the system is the video camera interface, VCI, which is an analogue-to-digital (A-to-D) converter for the video camera output. A standard 1 volt (75 ohm) black and white video signal consists of 50 frame scans per second; this is referred to as the field scan rate, and each of these frames consists of 312 line scans. Alternate frame scans are interleaved, in an interlace mode, resulting in the familiar 625 line picture. The waveforms are illustrated in Figures (A.2) and (A.3).

The VCI [Figure(A.4)] consists of a synchronous separator, A-to-D converter and a programmable line synchronous delay. Inputs to the microcomputer are data from the A-to-D converter, a line (busy) to indicate

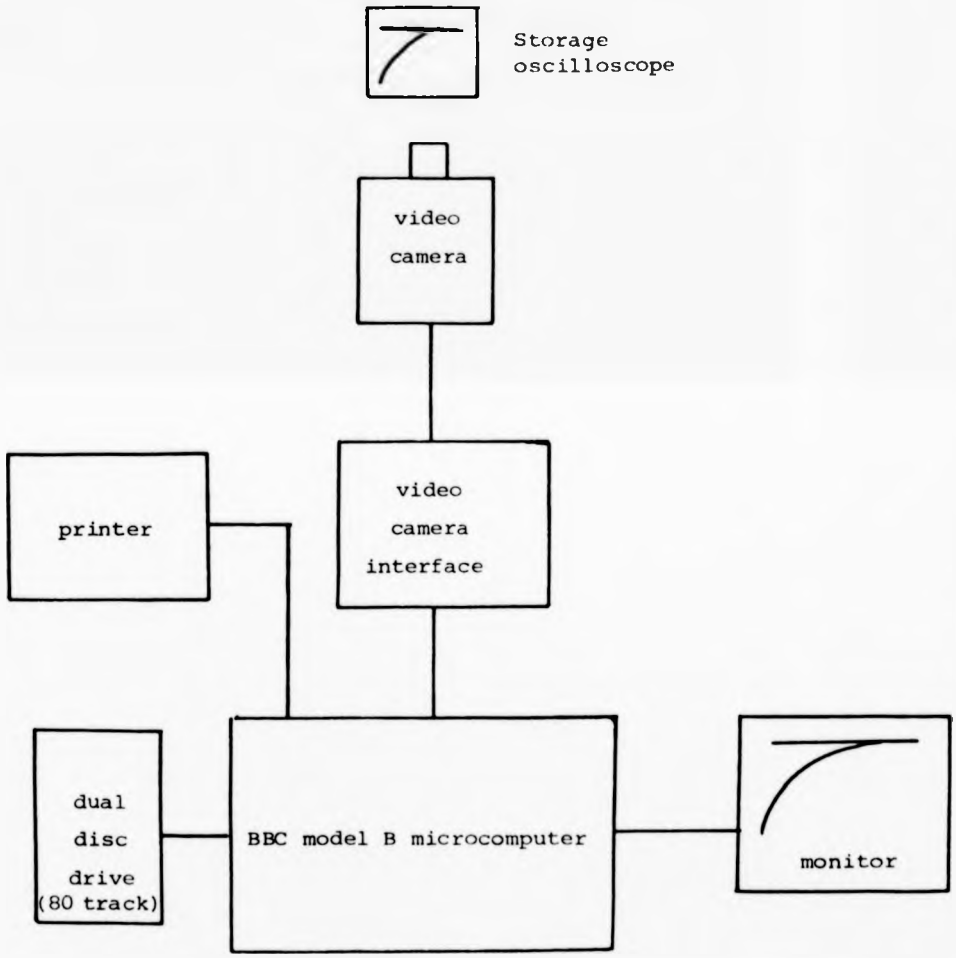

Figure A.1 Block diagram illustrating the various components for the video camera interface system.

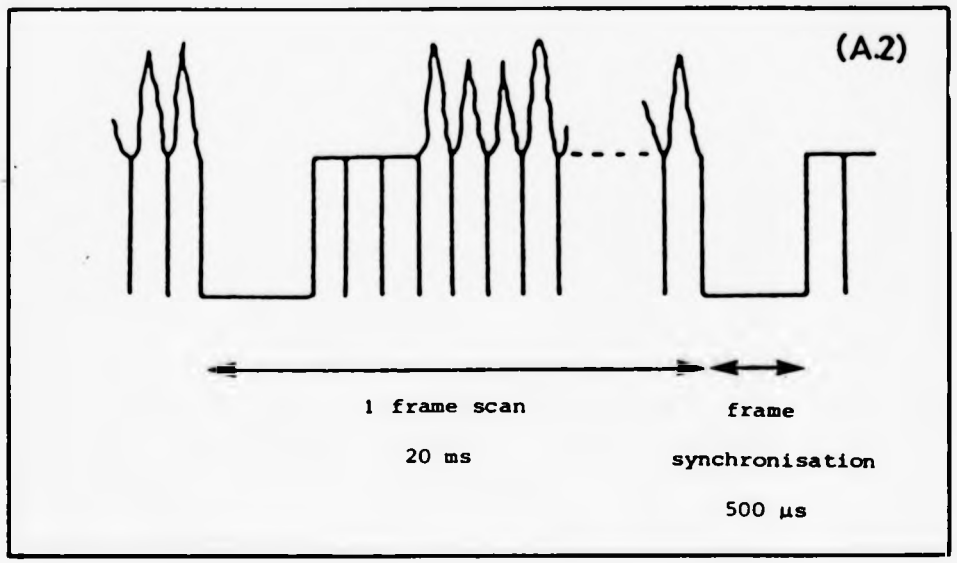

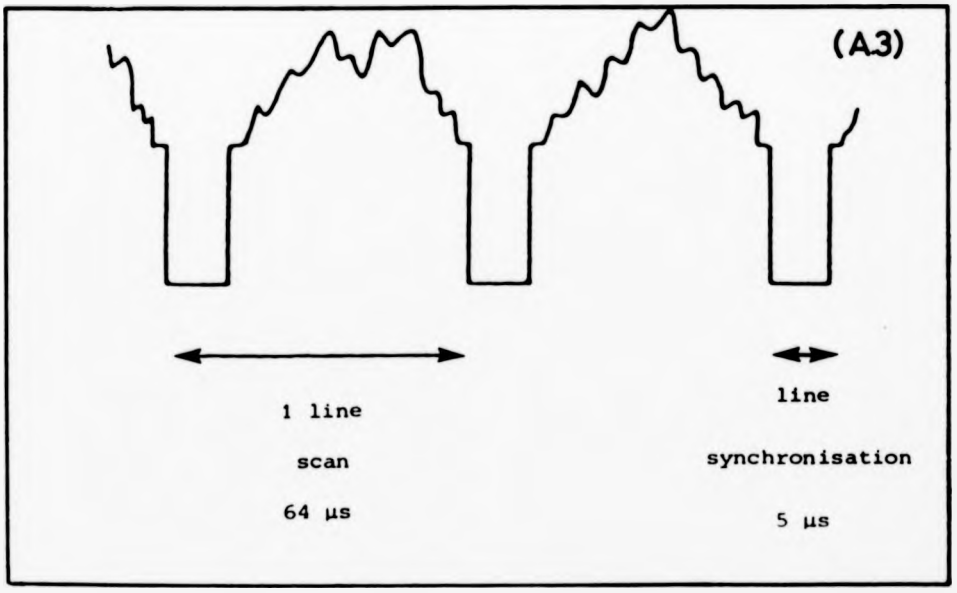

Figures A.2 and A.3 Representations of the waveforms for the frame scan signal, (A.2), and the line scan signal, (A.3) outputs from the video camera.

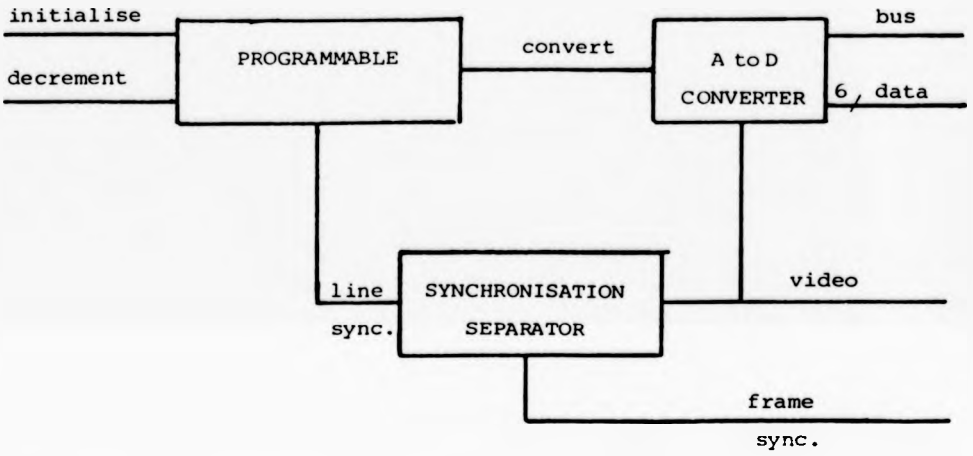

Figure A.4 Block diagram illustrating the working components of the video camera interface; diagram supplied by Dataharvest, U.K.

when these data are valid, and a frame synchronous signal. The microcomputer needs two output lines to the interface, one to initialise the programmable delay and one to decrement this delay during image capture.

The video camera signal is separated into line and frame synchronous signals, and is also fed directly to the A-to-D converter. Each line synchronous signal is subjected to a programmable time delay, before instructing the A-to-D converter to start. This programmable delay selects which part of each line scan is to be digitised. If this delay is large, then a position near the end (right) of each line scan will be digitised, and as the delay is decremented, the position to be digitised is moved nearer to the start position (towards the left). The interface converts a column of positions from each line scan during a single frame. Software detects the start of a frame scan signal, and can then decrement the delay when a new position is required. Thus the microcomputer initialises the counter to a maximum delay (near the right of the image), reads data from the A-to-D converter for each line in one frame scan, decrements the counter, and then reads data from the next frame scan. This cycle is repeated until the picture is complete, which takes approximately 4 seconds.

Each A-to-D conversion returns a digital value for the grey level at that point on the line. The interface provides 64 levels of grey, and conversion is to 8 bit accuracy.

A.2 Software

As already described above, the purpose of the software is to control the line synchronous delay. Additionally, the software must read the data from the A-to-D converter when valid, and process it. Most microcomputers, including the BBC model B, have insufficient memory available to store all the digital information received from a digitised image, insufficient speed to process data from one line scan and place it on the high resolution screen before the next line is received, and insufficient

screen resolution to use all available data. Thus, certain compromises between these factors must be made by the software program.

For the BBC microcomputer, memory is at a premium and so it is preferable to capture a few columns of data in the buffer and then plot them on the screen during the next few frame scans. Once all the buffer data have been plotted, the delay is decremented, data for a few more columns are read into the buffer and the process repeated until image capture is complete. The overall effect is that data capture and data plotting are interleaved, thereby increasing capture time, but saving memory.

The BBC graphic mode best suited to capturing the oscilloscope image is mode 2, which is a 16 colour mode with the graphics screen consisting of 160 horizontal points and 256 vertical points. The interface provides a maximum of 220 horizontal points and 312 vertical points, and thus only 160 of the 220 points possible for the horizontal pixels and 256 of the 312 points possible for the vertical pixels, are mapped.

The program V2.0 drives the supplied interface software for capturing of the image, screen dumps to printer, *etc.*

A second program PLOT is used to obtain the first-order rate constant from the oscilloscope trace image; there are two types, depending on whether an emission or absorption decay trace is being analysed.

In use, the video camera interface does not reproduce absolute colours, but assignment is based on light intensity levels within the picture. Originally we hoped that VCI would assign a completely different colour to the burnt phosphor decay curve compared with its assignment of the green phosphor background of the oscilloscope screen. This would have enabled the decay line to be "picked out" easily using colour

recognition algorithms, then, after scaling factors had converted each pixel into a unit of time and emission/absorption intensity, the constant could be calculated by the computer.

Unfortunately, this was not found to be so in use, for whilst the decay trace could be distinguished very easily by the human eye, some parts of the image background were of the same colour as the trace and *vice versa*. This was later found to be a property of the camera and not the interface. Whilst various algorithms are available, which enable image enhancement of the trace to be made, *e.g.*, in boundary detection and region analysis techniques, another alternative was used.

This required the movement of a flashing "X" cursor about the monitor picture with the operator selecting required points. Firstly, it is necessary to scale the screen, both vertically and horizontally for absorption traces, but only horizontally for emission traces, which is achieved by using the grid lines of the oscilloscope which are reproduced on the captured image. Once these points, two for each axis, have been entered with the time range and voltages covered, the cursor is directed onto the decay trace and analysis of the trace performed, and a flashing "X" is left at the places where points have been taken. Once enough points have been obtained, a linear regression analysis is performed on the data points, yielding the first-order rate constant.

VCI produces a slight horizontal distortion of the picture, as evidenced by oscilloscope grid squares being larger, horizontally, on the right-hand side than on the left-hand side of the captured image. This effect was completely corrected within the program PLOT, the correction being made at line 180. The X value of the co-ordinate is

corrected by 10.67; this figure was determined from an analysis of the distortion produced in a captured image of 1 cm squared graph paper.

A.3 Accuracy of the VCI System

This was firstly determined by analysis of a drawn, perfect, first-order decay trace; the decay rate determined by using PLOT agreed within 0.5% of the rates from which the simulated decay curves were drawn.

The accuracy of first-order rate constants for traces taken directly from the oscilloscope was the same as that obtained using the manual photographic enlargement technique [see section (2.1)].

A.4 Listings of the Programs written for the Video Camera Interface System

```
   10REM Program V2.0 By H.Douglas-Smith and adapted by A.W.Parker
   90*TV255
   95*L.MCRT0.3
   96*FX225,48
   97*FX4 1

99DIMC(7),S%(7):M2%=&18F0:FORI=0TO7:READS%(I),M2%?I:NEXT::ONERRORPROCe
rror:GOTO125
  110PROCinit:MODE7:HIMEM=&2C00
  125VDU22,7:*FX200
  130  PROCmenu:PROCg(48,58,48,58):ONA%GOTO160,170,180,190,230,240
  160PROCcapt:GOTO250
  170PROCk:PROCload:PROCl:GOTO250
  180PROCk:PROCsave:PROCl:GOTO250
  190*FX4,0
  191*DIR$
  192CHAIN"PLOT"
  230GOSUB31000:PROCdump:GOTO250
  240PROCquit:GOTO250
  250GOTO125
10000DEFPROCinit:@%=2:M%=2:*FX18
10050ENDPROC
11000DEFPROCmenu:PRINT" (1)  Capture Image"'" (2)  Load From
Disc"'" (3)  Save To Disc"
11060PRINT" (4)  Obtain Plot"'" (5)  Printer Dump"'" (6)  Quit
Digitiser"'"  ESCAPE for image   Space for
menu":VDU23;8202;0;0;0;:ENDPROC
12000DEFPROCg(L1,L2,L3,L4):*FX15,1
12020REPEAT:A%=GET:UNTIL(A%>L1ANDA%<L2)OR(A%>L3ANDA%<L4)OR(A%>(L1+128)
ANDA%<(L2+128))OR(A%>(L3+128)ANDA%<(L4+128)):IFA%>128A%=A%-128ELSEA%=A
%-48
12060ENDPROC
13000DEFPROCerror:IFERR=17PROCc(0):PROCcont:PROCc(7):GOTO130
13020VDU22,7:REPORT:PROCcont:ENDPROC
14000DEFPROCcont:*FX15,1
14020A%=GET:ENDPROC
15000DEFPROCcapt:VDU22,M%,23;8202;0;0;0;:FORX=0TO7:VDU19,X,M2%?X;0;:NE
XT
15020S&C00="/CODE"+STR$M%:X%=0:Y%=&C:CALL&FFF7:IF?&74=1PROCc(7):PRINT'
''TAB(5)" No camera sync detected.":PROCcont:GOTO15070
15030*FX200,1
15040S&CF0="TRACE":PROCsave2:PROCcont:PROCc(7)
15070ENDPROC
16000DEFPROCload:*FX200,1
16010CLS:PROCindex:IFA%>0PRINT''TAB(5)" Select Screen to Load"
16045PRINT''TAB(9)" (Space to
Exit)":PROCg(47,48+A%,31,33):IFA%<0GOTO16220
16180S&CF0="":FORO=0TO6:S&CF0=S&CF0+CHR$(?(&C01+A%*8+O)):NEXT:PROCc(0)
:S&C00="L."+STR$M%+"."+S&CF0:X%=0:Y%=&C:CALL&FFF7:PROCcont:PROCc(7)
16220ENDPROC
17000DEFPROCsave:CLS:PRINTTAB(10)"SAVE
SCREEN"':PROCindex:PRINT''"17070INPUT"" Enter
```

```
Filename..."$&CF0:IFLEN$&CF0>7PRINT" Too Long 7 Characters
only":GOTO17070
17082PROCsave2:ENDPROC
17085DEFPROCsave2:PROCc(0):IFM%>3GOTO17110
17100$&CF0="S."+STR$(M%)+"."+$&CF0+" 3000+5000":GOTO17120
17110$&CF0="S."+STR$(M%)+"."+$&CF0+" 5800+2800"
17120$&C00=S&CF0:X%=0:Y%=&C:CALL&FFF7:ENDPROC
22000DEFPROCdump:*FX200,1
22010PROCc(0):VDU2,1,27,1,64,1,13,1,10,1,10:*/DUMP
22020VDU2,1,13,1,10,1,10,1,27,1,64,3:ENDPROC
23000DEFPROCquit:VDU22,7:PRINTTAB(5,10)"QUIT FROM DIGITIZER (Y/N)
?":PROCg(77,79,88,90):IFA%=30ENDPROC
23080PRINTTAB(35,10)" Y":PRINTTAB(35,11)" Y":T=TIME:REPEATUNTILTIME>T+
50:CALL!-4
24000DEFPROCindex:IFM%<8PRINT"24020X%=0:Y%=&C:$&C00="DIR
"+CHR$(48+M%):CALL&FFF7:FORA%=&C00TO&CFFSTEP4:!A%=0:NEXT:A%=8:Y%=0:X%=
&70:?&70=M%+48:!&71=&C00:!&75=10:!&79=0:CALL&FFD1:$&CF0="":A%=0:REPEAT
:$&CF0="":B%=1:REPEAT:$&CF0=$&CF0+CHR$(?(&C00+A%*8+B%)):B%=B%+1:UNTILB
%=8OR?(&C00+A%*8+B%)=0:IFB%=2:$&CF0=""
24090IF$&CF0<>""PRINT" "A%")  ";$&CF0
24100A%=A%+1:UNTIL?(A%*8+&C00)=0:IFA%=1ANDS&CF0=""ANDM%<8PRINT'" No
Screens In Current Mode":A%=-1:ENDPROC
24140ENDPROC
25000DEFPROCc(A):IFA=0GOTO25050
25020A%=&7C:X%=4:Y%=&2C:CALL&900:VDU22,7:ENDPROC
25050IFA=7A=M%:M%=7
25060FORX%=0TO&B5:X%?&C03=X%?&CB3D:NEXT:X%?&C00=&60:!&C00=&8E0434AE:CA
LL&C00:IFM%=7:M%=A
25130A%=&2C:X%=4:Y%=&7C:CALL&900:VDU23;8202;0;0;0;:IFM%=5FORX=0TO3:VDU
19,X,M5%?X;0;:NEXT
25170IFM%=2FORX=0TO7:VDU19,X,M2%?X;0;:NEXT
25180ENDPROC
27000DEFPROCcol:P%=1:X=0:VDU24,0;0;1279;31;5
27020FORJ=0TOD%:FORI=0TOD%:IFC(I)<>C(J):B=I:F=J:I=8:J=8
27030NEXT:NEXT:GCOL0,X+128:CLG:GCOL0,(X+1)MOD 8:MOVEX*150,30:PRINT;X;
27070PROCg(135,140,31,33):IFA%=-16GOTO27160
27090IFA%=10ANDC(X)=0:VDU7:GOTO27070
27100IFA%=11ANDC(X)=7:VDU7:GOTO27070
27110IFA%=8ANDX>0X=X-1:GOTO27020
27120IFA%=9ANDX<D%X=X+1:GOTO27020
27130IFA%=11ANDC(X)<7C(X)=C(X)+1:VDU19,X,S%(C(X));0;:GOTO27020
27140IFA%=10ANDC(X)>0C(X)=C(X)-1:VDU19,X,S%(C(X));0;:GOTO27020
27150GOTO27020
27160IFD%=3:FORI=0TO3:M5%?I=S%(C(I)):NEXT:GOTO27180
27170FORI=0TO7:M2%?I=S%(C(I)):NEXT
27180ENDPROC
28000DATA0,0,4,4,1,1,5,5,2,2,6,6,3,3,7,7
29000DEFPROCk:$&C00="DR.1":X%=0:Y%=&C:CALL&FFF7:ENDPROC
30000DEFPROCl:$&C00="DR.0":X%=0:Y%=&C:CALL&FFF7:ENDPROC
31000INPUT"ENTER COMMENT-->"CO$
31010*FX15,0
31013*FX21,3
31015VDU2:PRINT''CO$:VDU3
31030RETURN
```

```
 1 REM Program PLOT for emission decay traces by A.W.Parker
10ONERRORPROCerror:REPORT:END
20DIM D(1,25)
30@%=&110608
40MODE7:PRINT''''" (1) TRACES AVAILABLE"''" (2) LAST
TRACE"'';TAB(7)"ENTER 1 OR 2 ":T=GET:IFT>50ORT<49GOTO40
42G$="TRACE":*DRIVE0
44IFT=49:PROCindex:INPUT'"NAME OF TRACE "G$
46MODE2:DIM V%30:$V%="*LOAD 2."+G$:X%=V%MOD256:Y%=V%DIV256:CALL&FFF7

50FORI=0TO7:READJ:VDU19,I,J;0;:NEXT:RESTORE
80VDU 28,4,31,19,29:N%=0
90 *FX 4,1
100X%=4:Y%=1000
110CLS:PRINT"BASELINE":GOSUB350:PX1=X%:PY1=Y%
130X%=1220:Y%=1000:PRINT" X2 ?":GOSUB350
140INPUT"TIME RANGE SCALE ";TS:TS=(X%-PX1)/TS
150INPUT"O.K. (Y/N)";Q$:IFQ$<>"Y"THENGOTO100
160CLS:PRINT"ENTER POINTS"
170GOSUB350:IFK%=70GOTO220
175IFY%>PY1 THENPRINT"NEGATIVE Y":SOUND 1,-15,80,10:GOTO170
180N%=N%+1:VDU30:PRINT"POINTS NOW ";N%:X=(X%-PX1+10.67)/TS
190Y=LN(PY1-Y%)
200D(0,N%)=X:D(1,N%)=Y

210SX2=SX2+(X*X):SY2=SY2+(Y*Y):SY=SY+Y:SXY=SXY+(X*Y):SX=SX+X:GOTO170
220SDXN=SQR((SX2-((SX*SX)/N%))/N%)
230SDYN=SQR((SY2-((SY*SY)/N%))/N%)
240M=(N%*SXY-(SX*SY))/(N%*SX2-(SX*SX))
250C=(SY-(M*SX))/N%
260SDM=SQR(((SDYN^2/SDXN^2)-M*M)/(N%-2))
270SDINT=SQR (SX2/(N%-2))*SDM
275CC=SDXN/SDYN*M
280MODE7:INPUT"ENTER COMMENT-->"CO$
295*FX21,3
300*FX4
305*FX15,0
307*FX6
308VDU2
310PRINT''CO$;''TAB(8)G$''':PRINTTAB(4)"TIME(s)";TAB(18)"LN If";''
320FORI%=1TON%
330PRINT;I%") "D(0,I%),TAB(16)D(1,I%):NEXT
335 PRINT';"S=";M'"(+/-)";SDM'"I=";C'"(+/-)";SDINT'"R=";CC
340VDU3:GOTO40
350COL%=15
360COL%=15
370OLDX%=X%:OLDY%=Y%
390OLDCOL%=COL%:COL%=POINT(OLDX%,OLDY%)+8
400GCOL 3,COL%
420XADD%=0:YADD%=0
430OLDX%=X%:OLDY%=Y%
440K%=GET
```

```
  450IF K%=139 THEN YADD%=4
  460IF K%=138THEN YADD%=-4
  470IF K%=136THEN XADD%=-8
  480IF K%=137THEN XADD%=8
  490IF K%=32 OR K%=70THEN GOSUB570:RETURN
  500IF XADD%=0 AND YADD%=0 THEN 440
  510X%=X%+XADD%:Y%=Y%+YADD%
  520PLOT 69,X%,Y%:PLOT 69,X%+8,Y%+4:PLOT 69,X%-8,Y%+4:PLOT
69,X%+8,Y%-4:PLOT 69,X%-8,Y%-4:PLOT 69,X%+16,Y%+8:PLOT
69,X%+16,Y%-8:PLOT 69,X%-16,Y%+8:PLOT 69,X%-16,Y%-8
  530GCOL 3,OLDCOL%
  540PLOT 69,OLDX%,OLDY%:PLOT 69,OLDX%+8,OLDY%+4:PLOT
69,OLDX%-8,OLDY%+4:PLOT 69,OLDX%+8,OLDY%-4:PLOT
69,OLDX%-8,OLDY%-4:PLOT 69,OLDX%+16,OLDY%+8:PLOT
69,OLDX%+16,OLDY%-8:PLOT 69,OLDX%-16,OLDY%+8:PLOT 69,OLDX%-16,OLDY%-8

  550GCOL3,COL%
  560GOTO390
  570PLOT 70,X%,Y%:PLOT 70,X%+8,Y%+4:PLOT 70,X%-8,Y%+4:PLOT
70,X%+8,Y%-4:PLOT 70,X%-8,Y%-4:PLOT 70,X%+16,Y%+8:PLOT
70,X%+16,Y%-8:PLOT 70,X%-16,Y%+8:PLOT 70,X%-16,Y%-8:RETURN
  580DEFPROCerror:*DIR$
  582INPUT"    COMMENT    ",C$:PRINTC$
  583*DRIVE0
  585IFERR=17 CHAIN"V2.0"
  590ENDPROC
  600DEFPROCindex:*DRIVE1
  610PRINT'TAB(3)"TITLES AVAILABLE :-"
  620X%=0:Y%=&C:$&C00="DIR
"+CHR$(48+M%):CALL&FFF7:FORA%=&C00TO&CFFSTEP4:!A%=0:NEXT:A%=8:Y%=0:X%=
&70:?&70=M%+48:!&71=&C00:!&75=10:!&79=0:CALL&FFD1:$&CF0="":A%=0:REPEAT
:$&CF0="":B%=1:REPEAT:$&CF0=$&CF0+CHR$(?(&C00+A%*8+B%)):B%=B%+1:UNTILB
%=8
  630IF$&CF0<>""PRINT" "A%")  ";$&CF0
  640A%=A%+1:UNTIL?(A%*8+&C00)=0:IFA%=1ANDS&CF0=""ANDM%<8PRINT'" No
Screens In Current Mode":A%=-1:ENDPROC
  650ENDPROC
  700DATA0,4,1,5,2,6,3,7
```

```
  1 REM Progam PLOT for absorption decay traces
 10ONERRORPROCerror:REPORT:END
 20DIMD(1,25)
 30@%=&110608
 40MODE7:PRINT''''" (1) TRACES AVAILABLE"''" (2) LAST
TRACE"'';TAB(7)"ENTER 1 OR 2 ":T=GET:IFT>50RT<49GOTO40
 42G$="TRACE":*DRIVE0
 44IFT=49:PROCindex:INPUT'"NAME OF TRACE "G$
 46MODE2:DIMV%30:$V%="*LOAD 2."+G$:X%=V%MOD256:Y%=V%DIV256:CALL&FFF7

 50FORI=0TO7:READJ:VDU19,I,J;0;:NEXT:RESTORE
 80VDU 28,4,1,19,0:N%=0
 90 *FX 4,1
100X%=4:Y%=140
110CLS:PRINT"BASELINE":GOSUB350:PX1=X%:PY1=Y%
120Y%=1000:PRINT" Y2 ?":GOSUB350:PY2=Y%
125INPUT"Y RANGE SCALE",YS:YS=(PY2-PY1)/YS
128INPUT" IO (mV)",IO
130X%=1220:Y%=PY1:PRINT" X2 ?":GOSUB350
140INPUT"TIME RANGE SCALE ";TS:TS=(X%-PX1)/TS
150INPUT"O.K. (Y/N)";Q$:IFQ$<>"Y"THENGOTO100
155Y%=1000:X%=4
160CLS:PRINT"ENTER POINTS"
170GOSUB350:IFK%=70GOTO220
175IFY%<PY1 THENCLS:PRINT"NEGATIVE Y":SOUND 1,-15,80,10:GOTO170
180N%=N%+1:VDU30:PRINT"POINTS NOW ";N%:X=(X%-PX1+10.67)/TS
190Y=(Y%-PY1)/YS:Y=LN(LOG(IO/(IO-Y)))
200D(0,N%)=X:D(1,N%)=Y

210SX2=SX2+(X*X):SY2=SY2+(Y*Y):SY=SY+Y:SXY=SXY+(X*Y):SX=SX+X:GOTO170
220SDXN=SQR((SX2-((SX*SX)/N%))/N%)
230SDYN=SQR((SY2-((SY*SY)/N%))/N%)
240M=(N%*SXY-(SX*SY))/(N%*SX2-(SX*SX))
250C=(SY-(M*SX))/N%
260SDM=SQR(((SDYN^2/SDXN^2)-M*M)/(N%-2))
270SDINT=SQR (SX2/(N%-2))*SDX
275CC=SDXN/SDYN*M
280MODE7:INPUT"ENTER COMMENT-->"CO$
295*FX21,3
300*FX4
305*FX15,0
307*FX6
308VDU2
310PRINT''CO$;''TAB(8)G$''':PRINTTAB(4)"TIME(s)";TAB(19)"LN ABS";''

320FORI%=1TON%
330PRINT;I%") "D(0,I%),TAB(16)D(1,I%):NEXT
335 PRINT';"M=";M'"(+/-)";SDM'"I=";C'"(+/-)";SDINT'"R=";CC
340VDU3:GOTO30
350COL%=15
360COL%=15
370OLDX%=X% :OLDY%=Y%
```

```
  390OLDCOL%=COL%:COL%=POINT(OLDX%,OLDY%)+8
  400GCOL 3,COL%
  420XADD%=0:YADD%=0
  430OLDX%=X%:OLDY%=Y%
  440K%=GET
  450IF K%=139 THEN YADD%=4
  460IF K%=138THEN YADD%=-4
  470IF K%=136THEN XADD%=-8
  480IF K%=137THEN XADD%=8
  490IF K%=32 OR K%=70THEN GOSUB570:RETURN
  500IF XADD%=0 AND YADD%=0 THEN 440
  510X%=X%+XADD%:Y%=Y%+YADD%
  520PLOT 69,X%,Y%:PLOT 69,X%+8,Y%+4:PLOT 69,X%-8,Y%+4:PLOT
69,X%+8,Y%-4:PLOT 69,X%-8,Y%-4:PLOT 69,X%+16,Y%+8:PLOT
69,X%+16,Y%-8:PLOT 69,X%-16,Y%+8:PLOT 69,X%-16,Y%-8
  530GCOL 3,OLDCOL%
  540PLOT 69,OLDX%,OLDY%:PLOT 69,OLDX%+8,OLDY%+4:PLOT
69,OLDX%-8,OLDY%+4:PLOT 69,OLDX%+8,OLDY%-4:PLOT
69,OLDX%-8,OLDY%-4:PLOT 69,OLDX%+16,OLDY%+8:PLOT
69,OLDX%+16,OLDY%-8:PLOT 69,OLDX%-16,OLDY%+8:PLOT 69,OLDX%-16,OLDY%-8

  550GCOL3,COL%
  560GOTO390
  570PLOT 70,X%,Y%:PLOT 70,X%+8,Y%+4:PLOT 70,X%-8,Y%+4:PLOT
70,X%+8,Y%-4:PLOT 70,X%-8,Y%-4:PLOT 70,X%+16,Y%+8:PLOT
70,X%+16,Y%-8:PLOT 70,X%-16,Y%+8:PLOT 70,X%-16,Y%-8:RETURN
  580DEFPROCerror:*DIR$
  582INPUT"    COMMENT   ?",C$:PRINTC$
  583*DRIVE0
  585IFERR=17 CHAIN"V2.0"
  590ENDPROC
  600DEFPROCindex:*DRIVE1
  610PRINT'TAB(3)"TITLES AVAILABLE :-"
  620X%=0:Y%=&C:$&C00="DIR
"+CHR$(48+N%):CALL&FFF7:FORA%=&C00TO&CFFSTEP4:!A%=0:NEXT:A%=8:Y%=0:X%=
&70:?&70=N%+48:!&71=&C00:!&75=10:!&79=0:CALL&FFD1:$&CF0="":A%=0:REPEAT
:$&CF0="":B%=1:REPEAT:$&CF0=$&CF0+CHR$(?(&C00+A%*8+B%)):B%=B%+1:UNTILB
%=8
  630IF$&CF0<>""PRINT" "A%")  ";$&CF0
  640A%=A%+1:UNTIL?(A%*8+&C00)=0:IFA%=1ANDN%&CF0=""ANDN%<8PRINT'" No
Screens In Current Mode":A%=-1:ENDPROC
  650ENDPROC
  700DATA0,4,1,5,2,6,3,7
```

APPENDIX B

The computer program WELLEREKQ (illustrated below) enables the optimum fitting of the kinetic results to the Weller equation of electron transfer when the ground state donor oxidation potential is unknown.

Both the donor oxidation potential and the intrinsic energy barrier, $\Delta G^{\ddagger}_{23}(0)$ are iterated between two preset values. The values which yield the minimum error of fit to the Weller equation are written to the data file DATA/WELLERFIT. Also sent to this file are the calculated ΔG^{0}_{23} values and the quenching rate constants for each quencher using the derived optimum values. The quenching data and reduction potentials of the quenchers are made into a file DATA/WELLER along with other parameters, as given in the comment statements at the beginning of the program WELLEREKQ.

The optimum fitting of energy transfer data uses a similar routine to WELLEREKQ. The iterated parameters are: the triplet energy of the acceptor (between 230-255 in increments of 1.0 kJ mol^{-1}), $\Delta G^{\ddagger}_{23}(0)$ (between 2.12-15.12 in increments of 0.05 kJ mol^{-1}), and the pre-exponential term, k^{0}_{en} (between 2×10^{9}-6×10^{10} increments of 0.1×10^{n}).

WELLERFKQ

```
1000      $RESET FREE
1010      C          WELLER DATA FITTING ROUTINE BY A.W.PARKER
1020      C       DATA IS READ FROM FILE "DATA/WELLER" WHICH HAS NO. OF DATA
1030      C       POINTS FIRST ,TRIPLET ENERGY (kcal/mol), THEN DATA AS E 1/2 eV,
1040      C       kQ. THE DATA CALCULATED IS WRITTEN TO FILE DATA/WELLERFIT.
1050      C
1060      FILE   4(KIND=DISK,TITLE="DATA/WELLER.",FILETYPE=7)
1070      FILE   60(KIND=DISK,TITLE="DATA/WELLERFIT",MAXRECSIZE=40,AREASIZE=60,
1080           1PROTECTION=SAVE);
1090            DIMENSIONDATA1(2,100)
1100            READ(4,/)N
1110            READ(4,/)TRIPEN
1120            SSKQ=1.0E35
1130            DO 50 ICOUNT=1,N
1140            READ(4,/)DATA1(1,ICOUNT),DATA1(2,ICOUNT)
1150       50   CONTINUE
1160            DIFF=1E10
1170            FDIFF=DIFF
1180       650  ELOW=.4
1190            EHIGH=2.5
1200            ALG0=1
1210            AMG0=9.5
1220       80   DO 400 E=ELOW,EHIGH,.05
1230            DO 100 G0=ALG0,AMG0,0.05
1240            SDKQ=0
1250            DO 75 ICOUNT=1,N
1260            X=23.06*(E-DATA1(1,ICOUNT)-.06)-TRIPEN
1270            CG23=X/2+SQRT(((X/2)*(X/2))+(G0*G0))
1280            KQ=DIFF/(1+(.25*(EXP(X/.593)+EXP(CG23/.593))))
1290            DKQ=(DATA1(2,ICOUNT)-KQ)*(DATA1(2,ICOUNT)-KQ)
1300            SDKQ=SDKQ+DKQ
1310       75   CONTINUE
1320            IF(SDKQ.GT.SSKQ)GO TO 100
1330            FOUNG0=G0
1340            FOUNE=E
1350            SSKQ=SDKQ
1360       100  CONTINUE
1370       88   CONTINUE
1380       400  CONTINUE
1390            WRITE(60,160)DIFF
1400       160  FORMAT(1X,"  DIFFUSION RATE FIXED AS ",E16.8,"  1/(M SEC) ")
1410            WRITE(60,150)FOUNG0
1420       150  FORMAT(///"  THE BEST G0 FOUND WAS ",F15.3)
1430            ABSDKQ=0
1440            SDATAKQ=0
1450            DO 200 ICOUNT=1,N
1460            X=23.06*(FOUNE-DATA1(1,ICOUNT)-.06)-TRIPEN
1470            CG23=X/2+SQRT(((X/2)*(X/2))+(FOUNG0*FOUNG0))
1480            KQ=FDIFF/(1+(.25*(EXP(X/.593)+EXP(CG23/.593))))
1490            WRITE(60,190)ICOUNT,DATA1(2,ICOUNT),KQ
1500       190  FORMAT(1X," KQ ",I4," EXP= ",E10.5,"  CALCD= ",E10.5)
1510            ABSDKQ=ABS(KQ-DATA1(2,ICOUNT))+ABSDKQ
1520            SDATAKQ=DATA1(2,ICOUNT)+SDATAKQ
1530            WRITE(60,800)X
1540       800  FORMAT(1X," DELTA G  ",F16.8)
1550       200  CONTINUE
1560            R=100*ABSDKQ/SDATAKQ
1570            WRITE(60,250)R
1580       250  FORMAT("  GOODNESS OF FIT FACTOR= ",F16.8,"  % ")
1590            WRITE(60,500)FOUNE
1600       500  FORMAT(1X," ESTIMATE E 1/2 AS ",E16.8,"  eV ")
1610            STOP
1620            END
```

APPENDIX C

MISCELLANEOUS STUDIES

C. Triplet State of 5-Nitroindole

Santos and Testa[223] recently reported electron transfer from chloride ion to the triplet state of 5-nitroindole, 5-NI, following observation by flash photolysis of the 5-NI protonated anion radical, see Scheme (C.1). In Chapter 4, the electron transfer reactions of excited nitro-heteroaromatic compounds with inorganic ions were discussed, and it was noted, in particular, that misonidazole and metronidazole reacted only with SCN^- to give the charge-separated species, $(SCN)_2^{\cdot-}$.

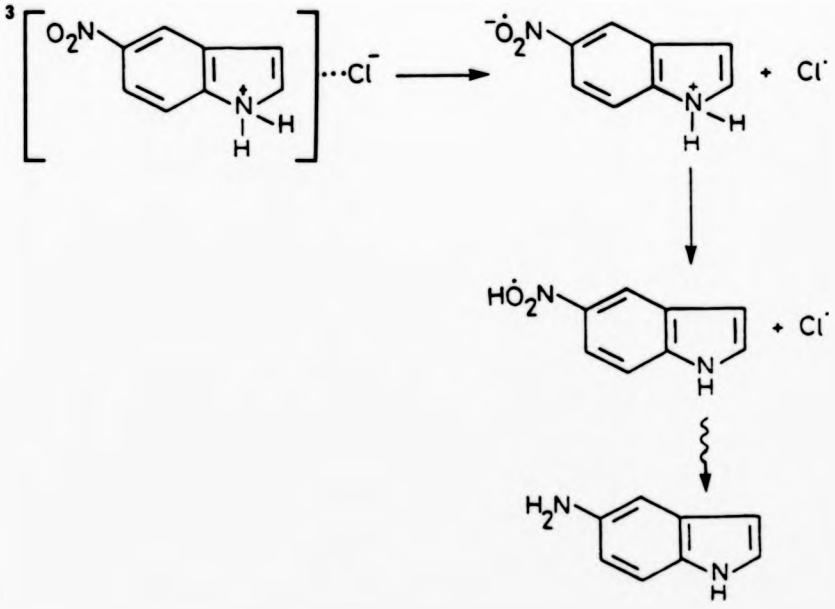

Scheme C.1

The transient absorption spectrum given in Figure (C.1) was obtained by laser pulsing ($\lambda_{249\,nm}$) deoxygenated acetonitrile solutions of 5-NI (1.26×10^{-4} mol dm^{-3}). Above 530 nm, the trace did not return to the base line within 20 μs and showed non-first-order kinetics, but above this wavelength the absorption decay trace gave a good fit to the pseudo first-order rate equation. The lifetime of this species was 2.4 μs and the spectrum attributed to the triplet state of 5-NI. This assignment is based upon the observation that the lifetime in non-deoxygenated acetonitrile solution was shortened to 0.36 μs. Assuming the concentration of oxygen in air-saturated acetonitrile is *ca.* 2.4×10^{-3} mol dm^{-3}, this lifetime yields $k_2 = 1 \times 10^9$ dm^3 mol^{-1} s^{-1} for the oxygen quenching of the 580 nm transient, *i.e.*, near the diffusion controlled rate.

The transient observed below 530 nm has still to be identified, but this is the spectral absorption region of the protonated radical anion.[223]

Attempts to observe the $(SCN)_2^-$ radical anion for solutions of 5-NI (1.26×10^{-4} mol dm^{-3}) and KCNS (0.2 mol dm^{-3}) following flash photolysis failed: this may be due to inner filter effects, which would be eliminated using 347 nm or 351 nm laser excitation.

C.1 Room Temperature Luminescence of Pyrimidine Bases

Enhanced room temperature phosphorescence from fluid solution has been obtained by Scypinski and Cline Love for many organic compounds, *e.g.*, polynuclear aromatic hydrocarbons[224] and nitrogen heterocyclic molecules,[225] using the monocyclic carbohydrate cyclodextrins as clathrating agents.

These compounds consist of six, seven, or eight glucose monomers, denoted alpha, beta and gamma cyclodextrin respectively, which are arranged in the form of a torus, see Figure (C.2). The cavity is hydrophobic and hence will expel water in order to enclose a less polar molecule which is of the correct size. This inclusion of a guest molecule restricts its vibronic motion, allowing enhancement of luminescence.

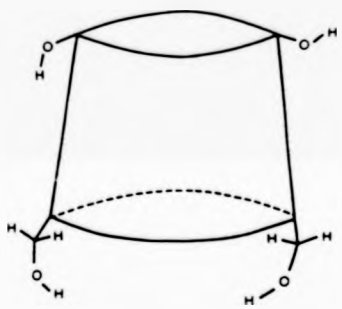

Figure C.2 Structural representation of the cyclodextrin molecule. The other primary and secondary hydroxyl groups have been eliminated for clarity, taken from ref. 226.

To achieve enhancement of phosphorescence, aqueous solutions of the cyclodextrin (0.01 mol dm^{-3}) are used with a suitable light-absorbing concentration of the organic molecule concerned, together with a heavy atom-containing molecule, such as 1,2-dibromoethane, to enhance singlet-to-triplet transitions. The cyclodextrin should be of the correct cavity size to allow enclosure of the organic molecule and the 1,2-dibromoethane.

Attempts to obtain room temperature luminescence from the pyrimidine bases (1.4×10^{-4} mol dm^{-3}) in aqueous deoxygenated solutions with 1,2-dibromoethane (0.58 mol dm^{-3}), using an excitation wavelength of 265 nm, failed for all types of cyclodextrins (0.01 mol dm^{-3}).

Figure C.1 *o*-Transient absorption spectrum obtained from laser pulsing (λ = 249 nm) deoxygenated acetonitrile solutions of 5-nitroindole (1.26×10^{-4} mol dm^{-3}). Measurements made immediately after the laser pulse.

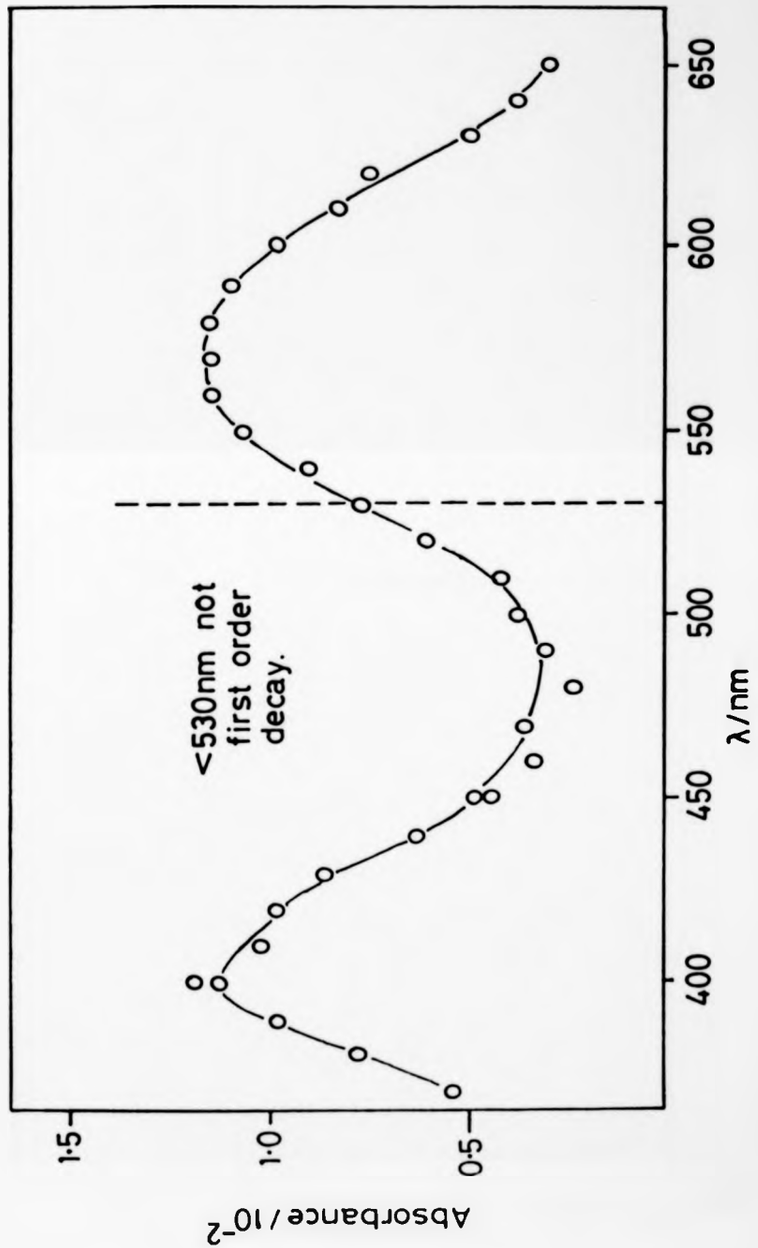

REFERENCES

REFERENCES

1 H.A. Schwarz, *J. Chem. Educt.*, 1981, 58, 101.

2 G. Scholes, *Br. J. Radiol.*, 1983, 56, 221.

3 L.H. Gray, A.D. Conger, M. Ebert, S. Hornsey, and O.C.A. Scott, *Br. J. Radiol.*, 1958, 26, 638.

4 T. Alper, 'Cellular Radiobiology', Cambridge University Press (Cambridge), 1979.

5 D.S. Grosch and L.E. Hopwood, 'Biological Effects of Radiations', 2nd Edition, Academic Press (New York), 1979.

6 R.H. Thomlinson and L.H. Gray, *Br. J. Cancer*, 1955, 9, 539.

7 B. Dixon, 'Cancer Topics and Radiobiology', Pitman (London), 1982, and references therein.

8 J.D. Chapman, *New Engl. J. Med.*, 1979, 301, 1429.

9 R.M. Sutherland and A.J. Franko, *Int. J. Radiat. Oncol. Biol. Phys.*, 1980, 6, 117.

10 J.E. Coggle, 'Biological Effects of Radiation', 2nd. Ed., Taylor and Francis (London), 1983.

11 G. Scholes, in 'Photochemistry and Photobiology of Nucleic Acids', Vol.1, (Ed.) S.Y. Wang, Academic Press (New York), 1976, P521.

12 J.F. Ward, *J. Chem. Educt.*, 1981, 58, 135 and references therein.

13 R.L. Willson, *Int. J. Radiat. Biol.*, 1970, 17, 349.

14 R. Latajet, B. Ekert, S. Apelgot and R. Reybeyrot, *J. Chem. Phys.*, 1961, 58, 1046.

15 J.E. Biaglow, *J. Chem. Educt.*, 1981, 58, 144 and references therein.

16 J. Hütterman, W. Kohnlein, R. Téoule, and A.J. Bertinchamps (Eds), 'Effects of Ionizing Radiation on DNA', Springer-Verlag (Heidelberg) 1978.

17 W.A. Bernhard, *Int. J. Radiat. Biol.*, 1981, 9, 199.

18 R.V. Bensasson, E.J. Land, and T.G. Truscott, 'Flash Photolysis and Pulse Radiolysis: Contributions to the Chemistry of Biology and Medicine', Pergamon Press (New York), 1983, P130.

19 A. Dulcić and J.N. Herak, *J. Chem. Phys.*, 1972, 57, 2537.

20 H. Zehner, W. Flossman, E. Westhof, and A. Muller, *Mol. Phys.*, 1976, 32, 869.

21 G. Nacifora, B. Smaller, R. Remko, and A.C. Avery, *Radiat. Res.*, 1972, 49, 96.

22 H.L. Lewis, D.R. Muhleman, and J.F. Ward, *Radiat. Res.*, 1978, 75, 305.

23 H. Lohman and M. Ebert, *Int. J. Radiat. Biol.*, 1970, 42, 255.

24 T. Henriksen and W. Snipes, *Radiat. Res.*, 1970, 42, 255.

25 G. Scholes and J. Weiss, *Cell Res.*, 1952, Suppl.2, 219.

26 R.L. Willson, P. Wardman, and K.D. Asmus, *Nature*, 1974, 252, 323.

27 C.L. Greenstock, G.E. Adams, and R.L. Willson, in 'Radiation Protection and Sensitization', (Eds) H.L. Moroson and M. Quintiliani, Taylor and Francis (London), 1970, P65.

28 D. Schulte-Frohlinde, 'Mechanisms of Strand Breaks in DNA induced by ·OH Radicals in Aqueous Soltuions', in "Proceedings of the Sixth Cong. Radiat. Res.", (Eds) S. Okuda, M. Imamura, T. Terasima, and H. Yamaguchi, Tappan Printing Company (Tokyo), 1979, P408.

29 C. Von Sonntag, U. Hagen, S. Schön-Bopp, and D. Schulte-Frohlinde, *Adv. Radiat. Res.*, 1981, 9, 109.

30 J.F. Ward, *Adv. Radiat. Biol.*, 1975, 5, 181.

31 G. Scholes, J.F. Ward, and J. Weiss, *J. Mol. Biol.*, 1960, 2, 379.

32 G.E. Adams and M.S. Cooke, *Int. J. Radiat. Biol.*, 1969, 15, 457.

33 J. Hüttermann, W. Kohnlein, R. Teoule, and A.J. Bertinchamps (Eds), 'Effects of Ionizing Radiation on DNA', Springer-Verlag (Heidelberg), 1978,118.

34 J. Hütterman, *Ultramicroscopy*, 1982, 10, 25.

35 A. Gräslund, A. Ehrenberg, and A. Rupprecht, *Int. J. Radiat. Biol.*, 1977, 31, 145.

36 S. Gregoli, M. Olast, and A. Bertinchamps, *Radiat. Res.*, 1982, 89, 238.

37 P.J. Boon, P.M. Cullis, M.C.R. Symons, and B.W. Wren, *J. Chem. Soc., Perkin Trans. 2*, 1984, 1393.

38 M.D. Sevilla, J.B. D'Arcy, K.M. Morehouse, and M.L. Engelhardt, *Photochem. Photobiol.*, 1979, 29, 37.

39 A. Ehrenberg, L. Ehrenberg, and G. Löfroth, *Nature*, 1963, 200, 376.

40 R. Salovey, R.G. Shulman, and W.M. Walsh, *J. Chem. Phys.*, 1963, 39, 839.

41 A.D. Lenherr and M.G. Ormerod, *Biochem. Biophys. Acta*, 1968, 166, 298.

42 R. Bergene, T.H. Johannessen, and T. Henrikson, *Int. J. Radiat. Biol.*, 1976, 29, 541.

43 S. Gregoli, M. Olast, and A. Bertinchamps, *Radiat. Res.*, 1979, 77, 417.

44 B. Rakvin and J.N. Herak, *Radiat. Phys. Chem.*, 1983, 22, 1043.

45 J. Hütterman, K. Voit, H. Oloff, W. Kohnlein, A. Gräslund, and A. Rupprecht, *Faraday Discuss. Chem. Soc.*, 1984, 78, 135.

46 P.J. Boon, P.M. Cullis, M.C.R. Symons, and B.W. Wren, *J. Chem. Soc., Perkin Trans. 2*, 1985, 1057.

47 M.C.R. Symons, personal communication.

48 A. Faucitano, A. Melo, A. Battafara, and F. Martinotti, *J. Chem. Soc., Perkin Trans. 2*, 1985, 329.

49 P.L. Altman and D. Katz, 'Volume and Dry Mass of Mammalian Cell Nuclei', in "Cell Biology", (Ed.) M.D. Bethesda, FASEB, 1976, P383.

50 G.J. Smith, *Int. J. Radiat. Biol.*, 1979, 35, 265.

51 G.J. Smith, *Radiat. Res.*, 1976, 68, 163.

52 A. Singh, *Radiat. Res. Rev.*, 1972, 4, 1.

53 D. Rehm and A. Weller, *Isr. J. Chem.*, 1970, 8, 259.

54 G.J. Fisher and E.J. Land, *Photochem. Photobiol.*, 1983, 37, 27.

55 J.R. Wagner, J. Cadet, and G.J. Fisher, *Photochem. Photobiol.*, 1984, 40, 589.

56 M. Daniels, in 'Photochemistry and Photobiology of Nucleic Acids', Vol.1, (Ed.) S.Y. Wang, Academic Press (New York), 1976, P23.

57 W.W. Hauswirth and M. Daniels, in 'Photochemistry and Photobiology of Nucleic Acids', Vol. 1, (Ed.) S.Y. Wang, Academic Press (New York), 1976, P109.

58 D.O. Cowan and R.L. Drisko, 'Elements of Organic Photochemistry', Plenum Press (New York), 1976.

59 D.W. Whillans and H.E. Johns, *Curr. Top. Radiat. Res. Quarterly*, 1973, 9, 119.

60 S.Y. Wang (Ed.), 'Photochemistry and Photobiology of Nucleic Acids', Vol. 1, Academic Press (New York), 1976.

61 L Satio, H. Sugiyama, and T. Matsuura, *Photochem. Photobiol.*, 1983, 38, 735.

62 M.I. Simon and H. Van Vunakis, *J. Mol. Biol.*, 1962, 4, 488.

63 J.D. Spikes, in 'The Science of Photochemistry', (Eds) J.D. Regan and J.A. Parrish, Plenum Press (New York), 1982, P113.

64 G.J. Fisher and H.E. Johns, in 'Photochemistry and Photobiology of Nucleic Acids', Vol. 1, (Ed.) S.Y. Wang, Academic Press (New York), 1976, P169.

65 C.L. Greenstock, I.H. Brown, J.W. Hunt, and H.E. Johns, *Biochem. Biophys. Res. Commun.*, 1967, 27, 431.

66 I.H. Brown and H.E. Johns, *Photochem. Photobiol.*, 1968, 8, 273.

67 C.L. Greenstock and H.E. Johns, *Biochem. Biophys. Res. Commun.*, 1968, 30, 21.

68 A. Garner and G. Scholes, *Photochem. Photobiol.*, 1985, 41, 259.

69 S.Y. Wang, *Nature (london)*, 1963, 200, 879.

70 A. Wacker, H. Dellweg, and D. Weinblum, *Naturwiss.*, 1960, 47, 477.

71 G.J. Fisher and H.E. Johns, in 'Photochemistry and Photobiology of Nucleic Acids', Vol. 1, (Ed.) S.Y. Wang, Academic Press (New York), 1976, 225.

72 M. Charlier and C. Helene, *Photochem. Photobiol.*, 1972, 15, 71 and references therein.

73 I. Saito, H. Sugiyama, and T. Matsuura, *J. Am. Chem. Soc.*, 1983, 105, 956.

74 R.V. Bensasson, E.J. Land, and T.G. Truscott, 'Flash Photolysis and Pulse Radiolysis: Contributions to the Chemistry of Biology and Medicine', Pergamon Press, 1983.

75 C. Salet and R.V. Bensasson, *Photochem. Photobiol.*, 1975, 22, 231.

76 C. Salet, R.V. Bensasson, and R.S. Becker, *Photochem. Photobiol.*, 1979, 30, 325.

77 G.J. Fisher, A.J. Varghese, and H.E. Johns, *Photochem. Photobiol.*, 1974, 20, 109.

78 R.S. Becker and G. Kogan, *Photochem. Photobiol.*, 1980, 31, 5.

79 E. Hayon, *J. Am. Chem. Soc.*, 1969, 91, 5397.

80 J.S. Connolly, *Diss. Abstr.*, 1969, 30B, 2629.

81 R. Arce, L.A. Jimenez, V. Riviera, and C. Torres, *Photochem. Photobiol.*, 1980, 32, 91.

82 A.G. Szabo, K.L. Wierzchowski, and K. Berens, *J. Lumin.*, 1975, 10, 331.

83 R. Arce, G. Rodríguez, and K. Singmaster, *Photochem. Photobiol.*, 1983, 38, 631.

84 V. Balzani, F. Bolletta, M.T. Gandolfi, and M. Maestri, *Top. Curr. Chem.*, 1978, 75, 1.

85 M. Julliard and M. Chanon, *Chem. Rev.*, 1983, 83, 425.

86 A.K. Chibisov, *Prog. React. Kinet.*, 1984, 13, 1.

87 R.A. Marcus, *J. Phys. Chem.*, 1963, 67, 853.

88 R.A. Marcus, *J. Chem. Phys.*, 1965, 43, 679.

89 R.A. Marcus, *Ann. Rev. Phys. Chem.*, 1964, 15, 155.

90 R.A. Marcus, *Electrochim. Acta*, 1968, 13, 995.

91 V. Balzani, F. Bolletta, M. Ciano, and M. Maestri, *J. Chem. Educt.*, 1983, 60, 447.

92 J.S. Littler, in 'International Review of Science, Organic Chemistry Series One. Free Radical Reactions', (Ed.) W.A. Waters, Butterworths (London), 1973, 10, 237.

93 L. Eberson, *Adv. Phys. Org. Chem.*, 1982, 18, 79.

94 R.A. Marcus, *J. Chem. Phys.*, 1956, 24, 966.

95 D. Rehm and A. Weller, *Ber. Bunsenges. Phys. Chem.*, 1969, 73, 834.

96 S. Glasstone, K.J. Laidler, and H. Erying, 'The Theory of Rate Processes', McGraw-Hill (New York), 1941.

97 N. Sutin and C. Creutz, *J. Chem. Educt.*, 1983, 60, 809.

98 F. Scandola, V. Balzani, and G.B. Schuster *J. Am. Chem. Soc.*, 1981, 103, 2519.

99 J.N. Brønsted and K. Pedersen, *Z. Phys. Chem.*, 1924, 108, 185.

100 J. Horiuchi and M. Polanyi, *Acta Physicochim. U.R.S.S.*, 1935, 2, 505.

101 N. Agmon and R.D. Levine, *Chem. Phys. Lett.*, 1977, 52, 197.

102 F. Wilkinson, 'Chemical Kinetics and Reaction Mechanisms', Ch.9, Van Nostrand Reinhold Company Ltd. (New York), 1980.

103 F. Scandola and V. Balzani, *J. Am. Chem. Soc.*, 1979, 101, 6140.

104 H. Shizuka, M. Nakamura, and T. Morita, *J. Phys. Chem.*, 1980, 84, 989.

105 H. Shizuka and H. Obuchi, *J. Phys. Chem.*, 1982, 86, 1297.

106 A.A. Lamola, *Photochem. Photobiol.*, 1968, 8, 601.

107 F. Wilkinson, *Pure Appl. Chem.*, 1975, 45, 661.

108 S. Speiser, *J. Photochem.*, 1983, 22, 195.

109 F. Scandola and V. Balzani, *J. Chem. Educt.*, 1983, 60, 814.

110 J. Barltrop and J.D. Coyle, 'Principles of Photochemistry', John Wiley and Sons (Chichester), 1978.

111 Th. Förster, *Faraday Discuss., Chem. Soc.*, 1959, 27, 7.

112 Th. Förster, in 'Modern Quantum Chemistry', (Ed.) O. Sinanoglu, Academic Press (New York), 1965, P3.

113 D.L. Dexter, *J. Chem. Phys.*, 1953, 21, 836.

114 J.T. Dubois and M. Cox, *J. Chem. Phys.*, 1963, 38, 2536.

115 F. Wilkinson and J.T. Dubois, *J. Chem. Phys.*, 1963, 39, 377.

116 A. Terenin and V.L. Ermolaev, *Trans. Faraday Soc.*, 1956, 52, 1042.

117 V.L. Ermolaev, *Soviet Phys.-Doklady*, 1962, 6, 600.

118 H.L.J. Bäckstrom and K. Sandros, *Acta Chem. Scand.*, 1958, 12, 823.

119 H.L.J. Bäckstrom and K. Sandros, *Acta Chem. Scand.*, 1960, 14, 48.

120 G. Porter and F. Wilkinson, *Proc. Roy. Soc., London, Ser. A*, 1961, 264, 1.

121 K. Sandros, *Acta Chem. Scand.*, 1964, 18, 2355.

122 V. Balzani, F. Bolletta, and F. Scandola, *J. Am. Chem. Soc.*, 1980, 102, 2152 and references therein.

123 G.S. Hammond and J. Saltiel, *J. Am. Chem. Soc.*, 1963, 85, 2516.

124 G.S. Hammond, J. Saltiel, A.A. Lamola, N.J. Turro, J.S. Bradshaw, D.O. Cowan, R.C. Counsell, V. Vogt, and C. Dalton, *J. Am. Chem. Soc.*, 1964, 86, 3197.

125 A. Bylina, *Chem. Phys. Lett.*, 1968, 1, 509.

126 P.J. Wagner and I. Kochevar, *J. Am. Chem. Soc.*, 1968, 90, 2232.

127 V. Balzani, L. Moggi, M.F. Manfrin, F.Bolletta and G.S. Laurence, *Co-ord. Chem. Rev.*, 1975, 15, 321.

128 F. Wilkinson and A. Farmilo, *J. Chem. Soc., Faraday Trans. 2*, 1976, 72, 604.

129 V. Balzani, F. Bolletta, and F. Scandola, *J. Am. Chem. Soc.*, 1980, 102, 2152.

130 A.R. Gutiérrez, T.J. Meyer, and D.G. Whitten, *Mol. Photochem.*, 1976, 7, 349.

131 F. Wilkinson and C. Tsiamis, *J. Am. Chem. Soc.*, 1983, 105, 767.

132 G.E. Adams and D. Jameson, *Radiat. Environ. Biophys.*, 1980, 17, 95.

133 Collected papers from 'Hypoxic Cell Sensitizers in Radiobiology and Radiotherapy', *Br. J. Cancer*, 1978, 37, Supp.III.

134 C.L. Greenstock, *Prog. React. Kinetics*, 1982, 11, 73.

135 G.E. Adams and D.L. Dewey, *Biochem. Biophys. Res. Commun.*, 1963, 12, 473.

136 G.E. Adams, I.R. Flockhart, C.E. Smithen, I.J. Stratford, P. Wardman, and M.E. Watts, *Radiat. Res.*, 1976, 67, 9.

137 G.E. Adams and P. Wardman, in 'Free Radicals in Biology', (Ed.) W.A. Prylor, Academic Press (New York), 1977, 3, 53.

138 P. Wardman and E.D. Clarke, *J. Chem. Soc., Faraday Trans. 1*, 1976, 72, 1377.

139 P. Wardman, 'Kombinierte Strahleund Chemotherapie', Symposium der Arbeitsgemeinschaften, 20/21 October, 1978.

140 P. Wardman, *Radiat. Phys. Chem.*, 1984, 24, 293.

141 G.E. Adams, *Curr. Top. Radiat. Res.*, 1967, 3, 35.

142 J.D. Zimbrick, J.F. Ward, and L.S. Myers, *Int. J. Radiat. Biol.*, 1969, 16, 505.

143 F. Hutchinson, *Quart. Rev. Biophys.*, 1973, 6, 201.

144 J.D. Regan and J.A. Parrish (Eds), 'The Science of Photomedicine'. Plenum Press (New York), 1982.

145 P.C. Beaumont, B.J. Parsons, S. Navaratnam, G.O. Phillips, and J.C. Allen, *Biochim. Biophys. Acta*, 1980, 608, 259.

146 S.T. Isaacs, C.J. Shen, J.E. Hearst, and H. Rapoport, *Biochemistry*, 1977, 16, 1058.

147 C. Salet, S.A.E. Melo, R.V. Bensasson, and E.J. Land, *Biochem. Biophys. Acta*, 1980, 607, 379.

148 B.H. Johnston, M.A. Johnson, C.B. Moore, and J.E. Hearst, *Science*, 1977, 197, 906.

149 R.V. Bensasson, C. Salet, E.J. Land, and F.A.P. Rushton, *Photchem. Photobiol.*, 1980, 31, 129.

150 B.H. Johnston, A.H. Kung, C.B. Moore, and J.E. Hearst, *Biochemistry*, 1981, 20, 735.

151 B.H. Johnston and J.E. Hearst, *Biochemistry*, 1981, 20, 739.

152 R.G.W. Norrish and G. Porter, *Nature (London)*, 1949, 164, 658.

153 E. Weitz and A. Scheffer, *Ber.*, 1921, 54, 2327.

154 J.N. Demas, T.F. Turner, and G.A. Crosby, *Inorganic Chem.*, 1969, 8, 674.

155 C.F. Liu, N.C. Liu, and J.C. Bailar, *Inorg. Chem.*, 1964, 3, 1197.

156 W.L.F. Armarego, D.R. Perrin, and D.D. Perrin, 'Purification of Laboratory Chemicals', 2nd Ed., Pergamon Press (Oxford), 1980.

157 J.N. Demas, 'Excited State Lifetime Measurements', Academic Press (New York), 1983.

158 L. Meites and P. Zuman, 'Handbook Series in Organic Electrochemistry', Vols I-IV, CRC Press (Cleveland, Ohio), 1977-79.

159 M.E. Peover, *J. Chem. Soc.*, 1962, 4540.

160 N. Weinberg, 'Techniques of Electro-organic Synthesis', Wiley Interscience (New York), 1975.

161 R.C. Weast (Ed.), 'CRC Handbook of Chemistry and Physics', 61st Ed., CRC Press Inc. (Boca Roton, Florida), 1980, P155.

162 G. Dryhurst, 'Electrochemistry of Biological Molecules', Academic Press (New York), 1977.

163 A. Kuboyama, *Bull. Chem. Soc. Japan*, 1978, 51, 2771.

164 R.W. Yip, D.K. Sharma, R. Giasson, and D. Gravel, *J. Phys. Chem.*, 1984, 88, 5770.

165 V.I. Slovetskii, T.A. Chenakik, and I.A. Abronin, *Acad. Sci., U.S.S.R., Chem. Sci. Bull.*, 1977, 289.

166 W. Rothman and D.R. Kearns, *Photochem. and Photobiol.*, 1967, 6, 775.

167 J. Eriksen and C.S. Foote, *J. Phys. Chem.*, 1978, 82, 2659.

168 K.A. Abdullah, PhD Dissertation, University of Warwick, 1985.

169 K.A. Abdullah and T.J. Kemp, *J. Photochem.*, 1985, 28, 61.

170 L.L. Miller, G.D. Nordblum, and E.A. Mayeda, *J. Org. Chem.*, 1972, 37, 916.

171 H.M. Roenstock, K. Draxl, B.W. Steiner, and J.T. Herron, 'Energetics of Gaseous Ions', J. Phys. Chem. Ref. Data, 1977, 6.

172 C.R. Bock, T.J. Meyer, and D.G. Whitten, *J. Am. Chem. Soc.*, 1975, 97, 2909.

173 C.R. Bock, A.J. Connor, A.R. Gutierrez, T.J. Meyer, D.G. Whitten, B.P. Sullivan, and J.K. Nagle, *J. Am. Chem. Soc.*, 1979, 101, 4815.

174 D.J. Glover, *Tetrahedron*, 1963, 19, Suppl. 1, 219.

175 C. Capellos and A.O. Allen, *J. Phys. Chem.*, 1970, 74, 840.

176 K.D. Asmus, A. Henglein, M. Ebert, and J.P. Keene, *Ber. Bunsenges. Physik. Chem.*, 1964, 68, 657.

177 J. Rabani, W.A. Mulac, and M.S. Matheson, *J. Phys. Chem.*, 1965, 69, 53.

178 V.S. Antonov, V.S. Letokhov, and A.N. Shibanov, *Soviet Physics J.E.T.P. Lett.*, 1980, 31, 441.

179 M.D. Sevilla, C. van Paemel, and C. Nichols, *J. Phys. Chem.*, 1972, 76, 3571.

180 J.D. Zimbrick, J.F. Ward, and L.S. Myers, *Int. J. Radiat. Biol.*, 1969, 16, 505.

180a D. Schulte-Frohlinde, J. Opitz, H. Görner, and E. Bothe, *Int. J. Radiat. Biol.*, 1985, 48, 397.

180b D. Schulte-Frohlinde, 'Radioprotectors and Anticarcinogens', (Eds) P.F. Nygaard and M.G. Simic, Academic Press (New York), 1983, p53.

180c E. Bothe and D. Schulte-Frohlinde, *Z. Naturforsch., Teil C*, 1982, 37, 1191.

180d C.L. Greenstock and R.P. Whitehouse, *Int. J. Radiat. Biol.*, 1985, 48, 701.

180e J.A. Raleigh, C.L. Greenstock, and W. Kremens, *Int. J. Radiat. Biol.*, 1973, 23, 457.

181 R.C. Knight, D.A. Rowley, I. Skolimowski, and D.I. Edwards, *Int. J. Radiat. Biol.*, 1979, 36, 367.

182 S. Nishimoto, H. Ide, T. Wada, and T. Kagiya, *Int. J. Radiat. Biol.*, 1983, 44, 585.

183 A.J. Varghese and G.F. Whitmore, *Radiat. Res.*, 1984, 97, 262.

183a P. Wardman, *Radiat. Phys. Chem.*, 1984, 24, 293.

184 E. Vogelmann, S. Schreiner, W. Rauscher, and H.E.A. Kramer, *Z. Phys. Chem. Neue Folge*, 1976, 101, 321; E. Vogelmann, W. Rauscher, R. Traber, and H.E.A. Kramer, *ibid.*, 1981, 124, 13.

185 T.J. Kemp and L.J.A. Martins, *J. Chem. Soc., Faraday Trans. 1*, 1981, 77, 1425.

186 L.J.A. Martins and T.J. Kemp, *J. Chem. Soc., Faraday Trans. 1*, 1982, 78, 519.

187 L.J.A. Martins and T.J. Kemp, *J. Chem. Soc., Faraday Trans. 1*, 1984, 80, 2509.

188 C. Capellos and G. Porter, *J. Chem. Soc., Faraday Trans. 2*, 1974, 70, 1159.

189 M.B. Groen and E. Havinga, *Mol. Photochem.*, 1974, 6, 9.

190 S.L. Murov, 'Handbook of Photochemistry', Dekker (New York), 1973.

191 N.A.P. Kane-Maguire and C.H. Langford, *Chem. Commun.*, 1971, 895.

192 M. Eigen, *Z. Phys. Chem. (Frankfurt am Main)*, 1954, 1, 176.

193 E.F. Ullman, *J. Am. Chem. Soc.*, 1964, 86, 5357.

194 E.F. Ullman and Wm. A. Henderson, *J. Am. Chem. Soc.*, 1967, 89, 4390.

195 G.E. Adams, J. Currant, and B.D. Michael, in 'Pulse Radiolysis', (Eds) M. Ebert, J.P. Keene, A.J. Swallow, and J.H. Baxendale, Academic Press (New York), 1965.

196 D. Meisel and P. Neta, *J. Am. Chem. Soc.*, 1975, 97, 5198; D. Meisel and R.W. Fessenden, *J. Am. Chem. Soc.*, 1976, 98, 7505.

197 J.R. Lakowicz and G. Weber, *Biochemistry*, 1973, 12, 4161.

198 M.A. O'Loughlin, D.W. Whillans, and J.W. Hunt, *Radiat. Res.*, 1980, 84, 477.

199 G.T. Podgorski, I.S. Longmuir, J.A. Knopp, and D.M. Benson, *J. Cell. Phys.*, 1981, 107, 329.

200 P. Wardman, personal communication.

201 C.V. Kumar, J.K. Barton, and N.J. Turro, *J. Am. Chem. Soc.*, 1985, 107, 5518.

202 P. Wardman and J.S. Wakeman, personal communication.

203 H.D. Burrows and T.J. Kemp, *Chem. Soc. Rev.*, 1974, 3, 139.

204 R. Matsushima and S. Skauraba, *J. Am. Chem. Soc.*, 1971, 93, 7143.

205 M. Ahmad, A. Cox, T.J. Kemp, and Q. Sultana, *J. Chem. Soc., Perkin Trans. 2*, 1975, 1867.

206 H. Güsten, in Gmelin 'Handbook of Inorganic Chemistry - Uranium', 8th Ed., Springer-Verlag (Berlin), Suppl. Vol.A6, 1983, Ch.3.

207 T. Rosenfeld-Grünwald and J. Rabani, *J. Phys. Chem.*, 1980, 84, 2981.

208 W.C. Neely, S.P. Ellis, and R.M. Cody, *Photochem. Photobiol.*, 1971, 13, 503.

209 A. Wacker, H. Dellweg, L. Träger, A. Kornhauser, E. Lodemann, G. Turck, R. Selzer, P. Chandra, and M. Ishimoto, *Photochem. Photobiol.*, 1964, 3, 369.

210 D. Greatorex, R. Hill, T.J. Kemp, and T.J. Stone, *J. Chem. Soc., Faraday Trans. 1*, 1972, 68, 2059.

211 D. Greatorex, R. Hill, T.J. Kemp, and T.J. Stone, *J. Chem. Soc., Faraday Trans. 1*, 1974, 70, 216.

212 A. Ledwith, P.J. Russell, and L.H. Sutcliffe, *Proc. Roy. Soc. London, Ser. A*, 1973, 332, 151.

213 L.J. Heidt, *J. Am. Chem. Soc.*, 1954, 76, 5962.

214 C.G. Hatchard and C.A. Parker, *Proc. Roy. Soc. London, Ser. A*, 1956, 235, 518.

215 R. Matsushima, *J. Am. Chem. Soc.*, 1972, 94, 6010.

216 K. Tokumra, XVth Informal Conference on Photochemistry, Mels Park, California, U.S.A., 1982.

217 C.L. Greenstock and H.E. Johns, *Biochem. Biophys. Res.*, 1968, 30, 21.

218 K. Kasama, A. Takematsu, and S. Arai, *J. Phys. Chem.*, 1982, 86, 2420.

219 S. Baral-Tosh, S.K. Chattopadhyay, and P.K. Das, *J. Phys. Chem.*, 1984, 88, 1404.

220 E.M. Kosower and J.L. Cotter, *J. Am. Chem. Soc.*, 1964, 86, 5524.

221 S.N. Bhattacharyya and P.K. Das, *J. Chem. Soc., Faraday Trans. 2*, 1984, 80, 1107.

222 A.J.G. Bamise, A.A. Gorman, R.L. Leyland, P.G. Smith, and M.A.J. Rodgers, *J. Am. Chem. Soc.*, 1978, 100, 1814.

223 O. Santos and A.C. Testa, *J. Photochem.*, 1985, 28, 131.

224 S. Scypinski and L.J. Cline Love, *Anal. Chem.*, 1984, 56, 322.

225 S. Scypinski and L.J. Cline Love, *Anal. Chem.*, 1984, 56, 331.

226 S. Scypinski and L.J. Cline Love, *Am. Lab.*, 1984, 16, 55.